B-cell phenotypes and BCR clonality in the human gut-liver axis: a tissue-specific analysis

Von der Medizinischen Fakultät der Rheinisch-Westfälischen Technischen Hochschule Aachen zur Erlangung des akademischen Grades einer Doktorin der Medizin genehmigte Dissertation

vorgelegt von

Monika Schütz
aus Waldbröl

Berichter: Universitätsprofessor Dr. rer. nat. Oliver Pabst
Universitätsprofessor Dr. med. Tony Bruns

Tag der mündlichen Prüfung: 14.10.2025

Abstract: B-cell phenotypes and BCR clonality in the human gut-liver axis: a tissue-specific analysis - Monika Schütz

The gastrointestinal tract is constantly exposed to enormous amounts of potentially harmful antigens through dietary intake and the microbiota. Therefore the immune response of the gut in precise coordination with the liver is critical to prevent pathogens from entering the systemic circulation. B-cells play an important role in this defense, and although the intestinal B-cell properties has been studied to some extent, only limited information is available on the human hepatic B-cell compartment. To obtain a complete picture, we performed an in-depth phenotypic and repertoire analysis of B-cells in the human gut-liver axis, both under normal conditions and in diseases known to involve interactions between these two organs. Our analysis revealed that the distribution of B-cell subsets and the expression of markers associated with cell migration, particularly CCR9 and integrin beta 1, differed in hepatic B-cells from their intestinal and blood counterparts. In addition, we found that plasma cells of the liver and intestine did not exhibit clonal sharing. By extending the analysis to non-alcoholic fatty liver disease (NAFLD), we observed no major differences in both the phenotype and repertoire of intestinal B-cells at different disease stages. Finally, we confirmed the impairment of the B-cell compartment with a reduction of memory B-cells in patients with liver cirrhosis. We extended these observations to the B-cells of the peritoneal cavity and demonstrated that these alterations were more pronounced in patients with poor clinical outcome. In addition, we found a decreased expression of the B-cell-activating factor receptor (BAFFR) in diseased patients. Our results thus provide new insights into B-cells in the human gut and liver. We suggest that hepatic plasma cells represent a small but tissue-specific population that potentially performs specific functions in the gut-liver axis. Although we showed that there is no significant phenotypic or repertoire difference in the different stages of NAFLD, our analysis cannot exclude the role of intestinal B-cells in the development and progression. Finally, we were able to confirm the alterations in the B-cell subsets in cirrhotic patients. Our observation of decreased expression of BAFFR could also help to determine the reason for the decreased memory B-cell population. In conclusion, our detailed characterization of B-cells in the human gut-liver axis contributes to a deeper understanding of the interaction of these two organs, both in a healthy immune response and under dysregulated conditions associated with chronic liver disease, and thus provides new approaches for further studies.

Zusammenfassung: Phänotyp und Rezeptor Klonalität von B-Zellen in der humanen Darm-Leber Achse: eine gewebsspezifische Analyse - Monika Schütz

Der Gastrointestinaltrakt ist durch die Nahrungsaufnahme enormen Mengen potenziell schädlicher Antigene ausgesetzt. Die Immunantwort des Darms in präziser Interaktion mit der Leber verhindert, dass Krankheitserreger in den systemischen Kreislauf gelangen. B-Zellen spielen bei dieser Abwehr eine wichtige Rolle. Obwohl B-Zellen im Darm ausgiebig untersucht worden sind, fehlen diese Untersuchungen für die hepatische B-Zell Population. Unser Ziel war daher, den Phänotyp und das Repertoire der B-Zellen in diesen beiden Organen, sowohl unter normalen als auch in erkrankten Bedingungen zu charakterisieren. Unsere Analyse ergab, dass hepatische B-Zellen sich sowohl in der Verteilung der Subtypen als auch in der Expression der Rezeptoren CCR9 und Integrin beta 1, welche mit der Zellmigration assoziiert sind, von denen in Darm und Blut unterscheiden. Interessanterweise stellten wir fest, dass Plasmazellen in Leber und Darm keine geteilten Klone aufweisen. Zudem konnten wir zeigen, dass es während der Progression der nicht-alkoholischen Fettlebererkrankung (NAFLD), keine wesentlichen Unterschiede im Phänotyp oder im Repertoire der B-Zellen im Darm gibt. Außerdem konnten wir den geringeren Anteil von Gedächtnis-B-Zellen bei Patienten mit Leberzirrhose bestätigen. Wir konnten diese Reduktion auch in der Bauchhöhle beobachten und wiesen nach, dass die Veränderungen bei Patienten mit schlechter Prognose stärker ausgeprägt waren. Wir beobachteten außerdem eine verminderte Expression des B-Zell-aktivierenden Faktor Rezeptors (BAFFR) bei erkrankten Patienten. Wir vermuten, dass hepatische Plasmazellen eine kleine, aber gewebespezifische Population darstellen, die möglicherweise spezielle Funktionen bei der Immunantwort in der Darm-Leber Achse ausübt. Obwohl wir gezeigt haben, dass es keine signifikanten Unterschiede im Phänotyp oder im Repertoire in den Stadien von NAFLD gibt, kann unsere Analyse die Rolle der intestinalen B-Zellen bei der Entwicklung und Progression nicht ausschließen. Schließlich konnten wir die veränderte Verteilung der B-Zell Subtypen bei Zirrhose-Patienten bestätigen. Unsere Beobachtung der verminderten Expression von BAFFR könnte dazu beitragen, den Grund für die Reduktion der Gedächtnis B-Zellen zu ermitteln. Zusammengefasst trägt unsere detaillierte Charakterisierung der B-Zellen in der menschlichen Darm-Leber-Achse zu einem tieferen Verständnis der Interaktion dieser beiden Organe bei und bietet daher neue Ansätze für weitere Studien.

Table of Contents

1 Introduction

1.1 Humoral immunity

Our living environment is rich in microorganisms, including a variety of pathogens and other potential threats. But not only external microorganisms, also pathologically altered endogenous cells can have severe consequences for health. The immune system, the defense mechanism of biological organisms, ensures protection against diseases caused by pathogens or endogenous factors. This protection is achieved by a finely coordinated interaction of lymphoid organs, immune cells (leukocytes), cytokines and humoral factors.

The immune system consists of two parts functioning together, an evolutionarily older component, the innate immune system, and a younger part, the adaptive immune system. Both are composed of humoral and cellular components, with innate immunity inducing a direct, nonspecific response with limited memory formation, whereas adaptive immunity leads to a delayed but highly specific response. A major difference from the innate immune system is also the ability to develop an antigen-specific immunological memory, which enables a faster immune response upon reinfection (Cooper & Alder, 2006).

Adaptive immunity comprises T and B-lymphocytes including the antibodies produced by B-cells. The production of specific antibodies (immunoglobulins) is the main function of B-cells, and therefore their contribution is referred to as humoral immunity. Antibodies have several different types of functions, depending on the tissue and the condition. These include binding to their specific antigen for neutralization, opsonization and activation of the complement system. Especially in the intestinal tract, antibodies are also involved in other regulatory functions essential for the symbiosis between the protective gut microbiota and immunity (Chen, Magri, Grasset, & Cerutti, 2020).

B-cells develop from a lymphoid precursor in the bone marrow, where also the further maturation and selection of the cells takes place. One of the most important steps in B-cell development is the formation of a unique, non-autoreactive B-cell receptor (BCR). After B-cells have completed their development in the bone marrow, they circulate through the blood or remain in secondary lymphoid organs, such as the spleen and lymph nodes, where they can bind to their specific antigen. Once they encounter their

specific antigen, they internalize it for presentation through the major histocompatibility complex class II receptor (MHC-II), which enables their activation by cognate T-helper (Th) cells. Subsequently, the activated cell proliferates and differentiates into either antibody-producing plasma cells (PCs) or memory B-cells (MBCs). Depending on their function, these cells can then be recruited to inflamed tissues or migrate to different organs. Proper B-cell development and response is crucial as B-cell compartment abnormalities can lead to diseases such as immunodeficiencies, autoimmunities and proliferative disorders (LeBien & Tedder, 2008).

1.1.1 The development of a diverse BCR repertoire

The ability to recognize a virtually unlimited number of different antigens is central to the adaptive immune system. This capacity is achieved through an enormously diverse adaptive immune repertoire and the process of clonal selection. Through various genetic mechanisms before and after antigen contact, the immune system establishes a wide range of antigen receptors to anticipate future antigen encounters. This diversity of different BCRs is referred to as the BCR repertoire. It is estimated that these mechanisms can lead to a theoretical diversity of $>10^{13}$ possible BCRs (Calis & Rosenberg, 2014). However, since the body does not contain that many B-cells, the actual BCR diversity in an individual is much lower. Until now, even after much research on the real repertoire diversity, only estimates can be made.

A BCR consists of a membrane-bound monomeric antibody. Upon binding of the specific antigen, signal transduction can be induced in combination with intracellular associated Igα- and Igβ-chains. In principle, a BCR can be expressed as an antibody of any class (IgM, IgD, IgG, IgA, IgE). However, due to the arrangement of the gene segments, IgD can only be expressed in combination with IgM. A monomeric antibody consists of 2 identical heavy chains and 2 identical light chains linked by disulfide bridges in a Y-shaped structure (see Figure 1). Each of these chains is composed of a variable and a constant part. The variable part of the chains, especially the complementarity-determining region 3 (CDR3), forms the antigen binding site. The genes encoding these two chains consist of variable (V), diverse (D), junctional (J) and constant (C) gene segments, each of which includes multiple loci. The CDR3 region spans the three gene segments V, D, J

and is the region with the greatest variability. D segments are found only in the heavy chain, whereas the light chain consists only of V and J segments.

The first two processes that contribute to the variability of BCRs, V(D)J recombination and stochastic modification of the junctions, occur during the B-cell development in the bone marrow. In both B and T-lymphocytes, the two processes are dependent on the proteins RAG 1 and RAG 2 (recombination activation gene). A defect or absence of these proteins results in the inability to develop mature lymphocytes, leading to a severe immunodeficiency (Delmonte, Schuetz, & Notarangelo, 2018).

In V(D)J recombination, loci of the individual segments are excised and joined, resulting in a combination of one of each V, (D) and J segments. Depending on the C segment to which this combination is linked, different isotypes are formed (see Figure 1). During the development of naive B-cells (NBCs), both Cγ and Cδ are retained and only at the RNA level one of the two is removed, so that NBCs express both IgM and IgD on their surface. In addition, RAG also causes double-strand breaks in DNA during the joining of the coding VDJ segments. Subsequent incorporation of random palindromic (P-) or nontemplate-encoded (N-) nucleotides further amplifies the BCR diversity (see Figure 1) (Helmink & Sleckman, 2012).

Activation of the enzyme AID (activation-induced cytidine deaminase) induces further changes in the BCR of mature B-cells in secondary lymphatic tissues. AID converts cytidine into uracil. This conversion leads to double-strand breaks in certain switch regions between the different C gene segments. Depending on the rejoined C segment, the immunoglobulin class can change from IgD/ IgM to IgA, IgG or IgE. The activation of AID and the resulting class switch is regulated by Th cells.

In addition to class switching, AID-induced conversion in variable segments of the heavy chain also leads to somatic hypermutation, which in combination with affinity selection results in affinity maturation of B-cells. Cellular repair mechanisms incorporate new bases at the altered sites, but with a significantly increased error rate. This leads to high mutation rates in the variable region, resulting in an altered antigen binding site (Di Noia & Neuberger, 2007). After somatic hypermutation, the modified B-cells undergo again selection in the germinal centers (GC), so that only B-cells with their BCR recognizing antigens equally or better continue to proliferate and differentiate. Depending on selection and proliferation, B-cells are generated that express the same BCR, thus forming a B-cell clone.

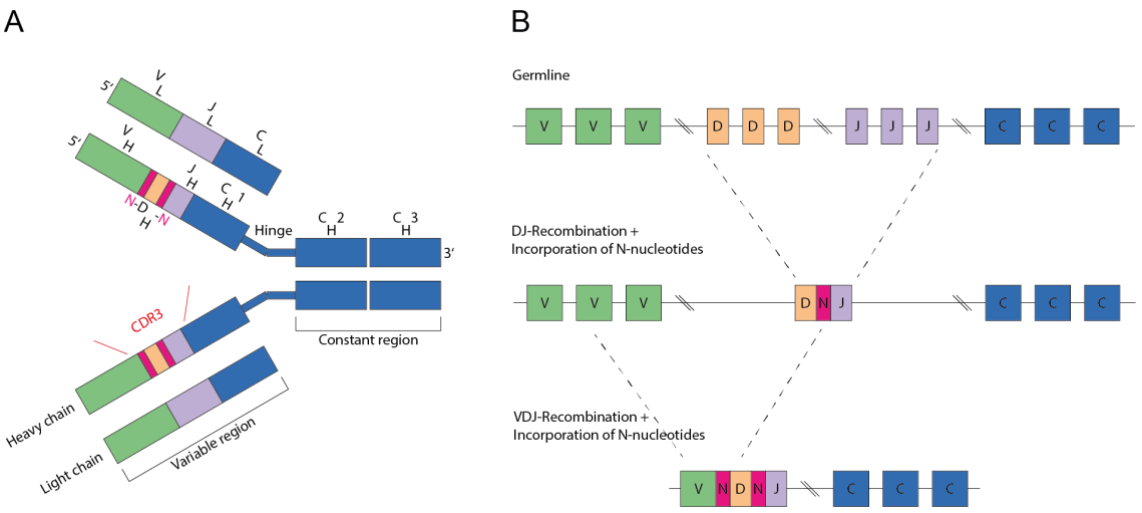

Figure 1: Formation of a diverse antibody structure by VDJ recombination and incorporation of nontemplate-encoded (N-) nucleotides during B-cell development. A: Schematic structure of an antibody with the constant and the variable regions of the two paired chains. Germline gene segments, the CDR-3 region and the nontemplate-encoded (N-) nucleotides are indicated. **B:** Illustration of the recombination of variable (V), diversity (D) and joining (J) gene segments, and the incorporation of random nontemplate-encoded (N-) nucleotides in the heavy chain. CDR-3: complementarity-determining region 3. Adapted from (Georgiou et al., 2014).

1.1.2 B-cell subsets and their functions

During the B-cell response, different subsets of B-cells are generated, which not only differ phenotypically, but also perform functionally distinct tasks. The B-cell phenotype is in general characterized by the pan-leukocyte marker CD45, the B-cell marker CD19, which regulates intracellular signal transduction by enhancing kinase activity, and CD20, which functions as a membrane-resident Ca^{2+} channel (LeBien & Tedder, 2008). Important B-cell subsets include naive B-cells (NBCs), memory B-cells (MBCs) and plasma cells (PCs).

After maturation and initial selection, B-cells leave the bone marrow as transitional B-cells, which undergo further maturation processes in the periphery. As many of the transitional B-cells are self-reactive, these processes are particularly important for the elimination of these autoreactive immature cells before they form the final BCR repertoire. Only a small number of cells that leave the bone marrow develop into mature B-cells (Y. Zhou et al., 2020). These mature NBCs express a functional IgD and IgM BCR and circulate through the blood or the secondary lymphoid tissues, where they are able to encounter their specific antigen (Loder et al., 1999). On contact with their specific antigen, the expression of certain chemokine receptors, CXCR5 and CCR7, changes on both NBCs and Th cells, resulting in their migration toward each other from areas that

are spatially separated. The NBC presents the processed antigen using its MHC-II receptor to the cognate Th cell. After binding of the MHC-II complex and the T-cell receptor (TCR), the NBC becomes activated by the Th cell through CD40-CD40L binding and cytokine signals. NBCs are characterized by the expression of CD45, CD19, IgD and IgM.

Upon activation, B-cells differentiate into either short-lived, mostly IgM-secreting PCs or form secondary follicles and GC where they further proliferate, mature and differentiate. At this point, B-cells are identified as germinal center B-cells. In the GC, MBCs and PCs are then produced as part of a T-cell dependent immune response (see Figure 2) (Stebegg et al., 2018).

In case of re-infection, MBCs are involved in the secondary immune response by faster expansion and differentiation into antibody-producing PCs. In addition, it is not yet fully understood how MBCs influence the secondary GC response, because although this is mainly initiated by NBCs (without prior GC exposure), some MBCs with prior antigen contact are also present in these secondary GCs. Interestingly, these MBCs are mainly cells from a limited number of clones, which could influence and potentially limit the diversity of the secondary immune response (Mesin et al., 2020). Recent studies have shown that MBCs have a longer lifespan than other B-cells, providing protection in the body for decades (Seifert & Küppers, 2016). CD27, a member of the TNF-receptor family, is considered the most important marker for distinguishing MBCs. This receptor interacts with its ligand CD70 on activated T-cells, leading to proliferation and differentiation of B-cells, therefore GC B-cells and PCs also express CD27. However, switched MBCs lacking CD27 expression have been found in healthy adults (Fecteau, Côté, & Néron, 2006). The reason for this altered expression is not yet known. One suggestion could be that these are aged, exhausted cells, as the population increases in elderly people (Colonna-Romano et al., 2009). MBCs can be further subdivided into the two subpopulations, class switched (IgA, IgG, IgE) and non-class switched (IgM, (IgD)).

Antibody-producing PCs are considered to be the most terminally differentiated effector cells of the B-cell lineage. These cells are morphologically, phenotypically and functionally distinct from other B-cell subsets. Morphologically, they appear as larger cells (approx. 14 to 20 µm) with a prominent endoplasmic reticulum due to high antibody production. PCs, similar to MBCs, can arise from a T-cell dependent GC reactions, but can also be generated by T-cell-independent activation by signals through

the binding of lipopolysaccharides and unmethylated CpG (Nutt, Hodgkin, Tarlinton, & Corcoran, 2015). PCs not only contribute to the acute immune response but, in combination with MBCs, are also responsible for the immune memory. As long-lived PCs, they can migrate into the bone marrow and produce antibodies continuously for decades, leading to a constant supply of the respective required antibodies (Brynjolfsson et al., 2018). PCs are mainly defined by the expression of CD38 and CD27. In blood, PCs, like other B-cell subsets, express CD45 and CD19, but recently it was found that there are PCs in the intestine that do not express these markers. It is suggested that these PCs may constitute a long-lived PC population in the gut (Landsverk et al., 2017). However, further studies are needed to prove this hypothesis. PCs can thus also be further subdivided based on their CD45/CD19 and isotype expression.

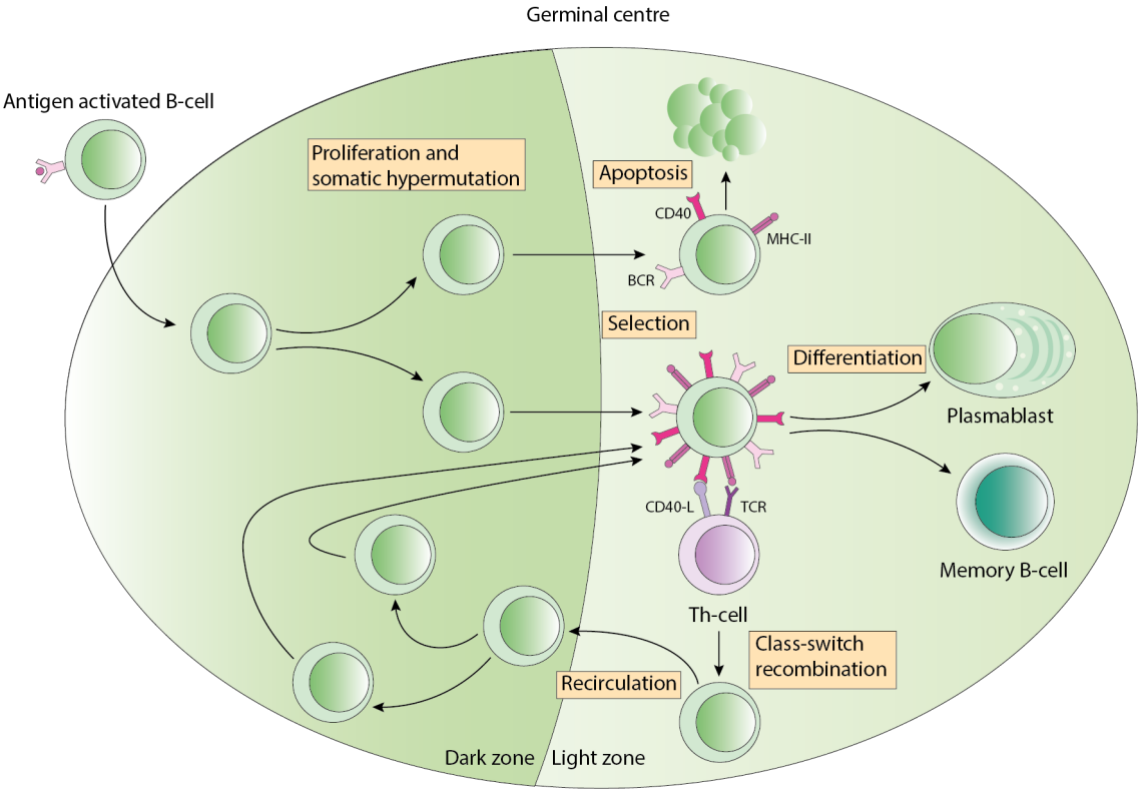

Figure 2: Schematic illustration of affinity maturation, class switch recombination and generation of the different B-cell subsets in the GC Representation of the reactions in a mature GC, which is characterized by the dark and the light zone. Somatic hypermutation and proliferation of antigen-activated B-cells occurs in the dark zone. Selection of the modified BCR for improved binding to the presented antigen is carried out, for instance, by the interaction with Th cells in the light zone. Some B-cells perform class switch recombination or re-enter the dark zone for further somatic hypermutation and proliferation. Newly generated B-cells that are not positively selected undergo apoptosis. Positive selected B-cells differentiate into either MBCs or plasma blasts. BCR: B-cell receptor; TCR: T-cell receptor; MHC-II: major histocompatibility complex class II; MBC: memory B-cell; Th cells: T-helper cells. Adapted from (De Silva & Klein, 2015).

1.1.3 Surface expression profile of B-cells

In addition to the previously mentioned key B-cell markers, many other proteins are expressed on their surface that mediate important cellular functions such as survival, activation, signal transduction and proliferation.

Since B-cells also function as professional antigen-presenting cells (APCs), a large proportion of them express MHC II/ HLA-DR. The expression of HLA-DR decreases during differentiation into PCs. While circulating, newly generated plasma blasts still show HLA-DR expression, it is downregulated in mature PCs (Sanz et al., 2019). PCs also differ in the expression of CD138, with CD138+ PCs thought to represent a more mature phenotype (Caraux et al., 2010).

Like other APCs, B-cells also express the B7 family molecules CD80 and CD86. These proteins bind to the surface markers CD28 and CTLA-4 and thus play a central role in the control of T-cell activation through costimulatory and co-inhibitory signaling (Gardner, Jeffery, & Sansom, 2014). Regarding the humoral immune response, the formation of GCs and the generation of antibodies also appear to be dependent on the interaction between CD80/CD86 and CD28 (Ferguson, Han, Kelsoe, & Thompson, 1996).

Peripheral B-cells require signals for survival regulated by the surface receptors BAFFR (B-cell activating factor receptor), TACI (transmembrane activator and calcium-modulator and cyclophilin ligand interactor) and BCMA (B-cell maturation factor). Monocytes, macrophages, dendritic cells, stromal cells and T-cells express their ligands BAFF and APRIL, with increased expression under proinflammatory conditions. While BAFF binds to all three receptors, APRIL only binds to TACI and BCMA. Receptor expression differs among the B-cell subsets. All human B-cells except PCs express BAFFR on their surface. In contrast, PC survival is regulated by expression of the receptors TACI and BCMA. Increased expression of TACI is also found on MBCs. Upon binding of BAFF to BAFFR, the extracellular part of the receptor is regulatory shed by the ADAM proteases 10 and 17. Co-expression of TACI is required for this shedding, and since TACI expression is increased on switched and marginal zone B-cells (spleen), these B-cell subsets are mainly affected by BAFFR shedding. The receptor TACI is also cleaved by the proteases ADAM 10 and 17, although unlike BAFFR, this occurs constitutively and without ligand binding. For this reason, the expression of TACI is generally lower than

the usually high expression of BAFFR. The blocking of BAFFR by injection of an anti-BAFF antibody revealed that switched MBCs and PCs can survive without BAFFR signaling (Smulski & Eibel, 2018).

Recent studies have shown that CD11c known for its expression on monocytes, granulocytes, macrophages and some dendritic cells, is also present on a subset of B-cells. This subset is observed in healthy donors as well as increased in some autoimmune-mediated diseases. Although CD11c is present in all previously mentioned B-cell subsets, it appears to be enriched in MBCs. However, the exact function in B-cells is not yet known (Golinski et al., 2020).

1.1.4 B-cell migration

The migration of B-cells to either the inflamed site or other compartments is regulated by various mechanisms, including the expression of adhesion molecules such as selectins, chemokine receptors, and integrins on the cell surface of leukocytes and the endothelium. Generally the extravasation of leukocytes takes place in sequential phases, starting with selectin binding and the subsequent "rolling" of the leukocytes on the blood vessel. The following binding of integrins leads to firmer cell contacts, necessary for cell migration. Integrins are heterodimeric transmembrane cell adhesion molecules that consist of an alpha and a beta chain and which not only initiate these cell-cell interactions but can also bind to the extracellular matrix. Binding of a chemokine receptor, which belongs to the G protein-coupled receptor family, to its chemokine ligand also induces various cellular changes including the activation of integrins that collectively enable the migration of the cell to the respective tissue. Depending on the tissue and inflammatory state, different adhesion molecules are expressed and thus enable regulated migration to the required location in the organism (Muller, 2002).

Both, integrin beta 7 and CCR9 expression, are associated with the migration of lymphocytes to intestinal tissues. Integrin beta 7 can pair with either the α4- or the αE-chain. Depending on the associated chain, migration can be regulated either by the interaction of integrin α4β7 with the endothelial-expressed MAdCAM-1 (Mucosal Addressin Cell Adhesion Molecule-1) or by the interaction of integrin αEβ7 with E-

cadherin on epithelial cells (Gorfu, Rivera-Nieves, & Ley, 2009). The chemokine receptor CCR9 is also involved in intestinal migration. Studies have shown that the chemokine CCL25, the ligand of CCR9, is constitutively expressed in the epithelium and vessels of the small intestine and thus directs CCR9 expressing B-cells into the small intestine (Pabst et al., 2004). Besides CCR9 and Integrin beta 7, IgA-positive plasma blasts express CCR10, which also plays an important role in the migration to mucosal tissue. CCL28, the ligand for CCR10, is produced by both intestinal and extra-intestinal mucosal tissue. This production has been shown to vary between intestinal compartments and is particularly high in the colon, resulting in the homing of plasma blasts to specific intestinal regions (Brandtzaeg & Johansen, 2005).

CXCR3 is expressed on various leukocytes including activated lymphocytes, dendritic cells and natural killer cells, but also on other cell types as fibroblasts, epithelial and endothelial cells. The chemokine receptor CXCR3 and its ligands CXCL9, CXCL10 and CXCL11 play an important role in regulating the migration of leukocytes to sites of inflammation, but are also associated with many other diseases such as cancer and autoimmunities (Lacotte, Brun, Muller, & Dumortier, 2009). Regarding CXCR3 expression in the gut-liver axis, studies have shown increased expression in inflammatory conditions involving ulcerative colitis (Hosomi et al., 2011) and hepatitis (Mizuochi et al., 2010).

Integrin beta 1 (CD29) also performs crucial function in the recruitment of B-cells and other leukocytes to various tissues that are not restricted to a specific one. (Sixt, Bauer, Lämmermann, & Fässler, 2006). Depending on the alpha subunit with which this integrin is non-covalently associated, it can form one of 12 different transmembrane molecules and, accordingly, bind to different ligands. The ligands mainly include extracellular matrix molecules such as collagen, laminin, fibronectin and in the case of α4β1, also known as VLA-4 (very late antigen-4), VCAM-1 (vascular cell adhesion molecule 1). As a result of intracellular signaling initiated by binding to the ligands, the functions of integrins include not only cell adhesion but also regulation of proliferation, survival, migration and gene expression (Brakebusch & Fässler, 2005).

1.2 Gut-liver axis

1.2.1 Interaction between gut and liver

Digestion and absorption of orally ingested nutrients takes place in the gut before being processed in the liver for controlled release into the bloodstream. Thus functions in gut and liver metabolism are tightly coordinated. Yet also additional functions of gut and liver such as the shielding from disseminating bacteria and immunity are shaped by the integrated functions of both organs. Anatomically gut and liver are connected through the portal vein and bile ducts. The portal vein transports nutrient-rich blood, including gut-derived products, absorbed from the gastrointestinal tract to the liver and also provides the main blood supply. Circulation through the portal vein ensures the metabolism of ingested nutrients such as glucose, fats and proteins and also the elimination of toxins. On the other hand, bile synthesized in the hepatocytes, which is needed for the digestion of fats as well as for the removal of bilirubin or steroids, is transported through the bile ducts into the small intestine (see Figure 3) (Tripathi et al., 2018).

But the gut and liver not only function together in the digestion and metabolism of nutrients, they are also responsible for tolerance to the commensal microbiota and defense against pathogens. The two organs together form several barriers that prevent pathogens from entering the systemic circulation. Beneath the epithelial layer, in the lamina propria of the intestine, many different immune cells, such as T-cells, PCs and macrophages, are located to defend against penetrating antigens by releasing cytokines, producing antibodies and performing non-inflammatory phagocytosis. However, if control at this stage is unsuccessful, they can enter the liver via the portal vein, where in turn a number of immune cells and barriers, such as specific liver resident macrophages called Kupffer cells, dendritic cells and T-cells, induce an immune response against them (Pabst et al., 2023). Conversely, bile produced in the liver, which contains bile acids, retinoids, and cholesterol metabolites, influences the small intestine by affecting the epithelium and enteric microbiota. For example, certain liver-derived bile acids have been shown to influence the development and composition of the newborn gut microbiome (van Best et al., 2020). This indicates that liver metabolism may have a

significant impact on the bacterial colonization of the gut and may be involved in the development of microbiota-associated diseases.

In addition to these examples, there are many other mechanisms that contribute to the interaction between the two organs and the regulation of homeostasis. Dysregulation of these mechanisms, particularly the integrity of the intestinal barrier, can lead to pathological conditions within this unit and to the development and progression of various liver diseases. Impairment of the intestinal barrier in the prevalent liver pathologies of non-alcoholic fatty liver disease (NAFLD) and alcohol-related liver disease causes increased and uncontrolled translocation of microbial products from the intestine to the liver, which can induce and exacerbate hepatic inflammation. For this reason, new therapeutic treatments are being developed that attempt to restore homeostasis by targeting the gut-liver axis (Bruneau, Hundertmark, Guillot, & Tacke, 2021).

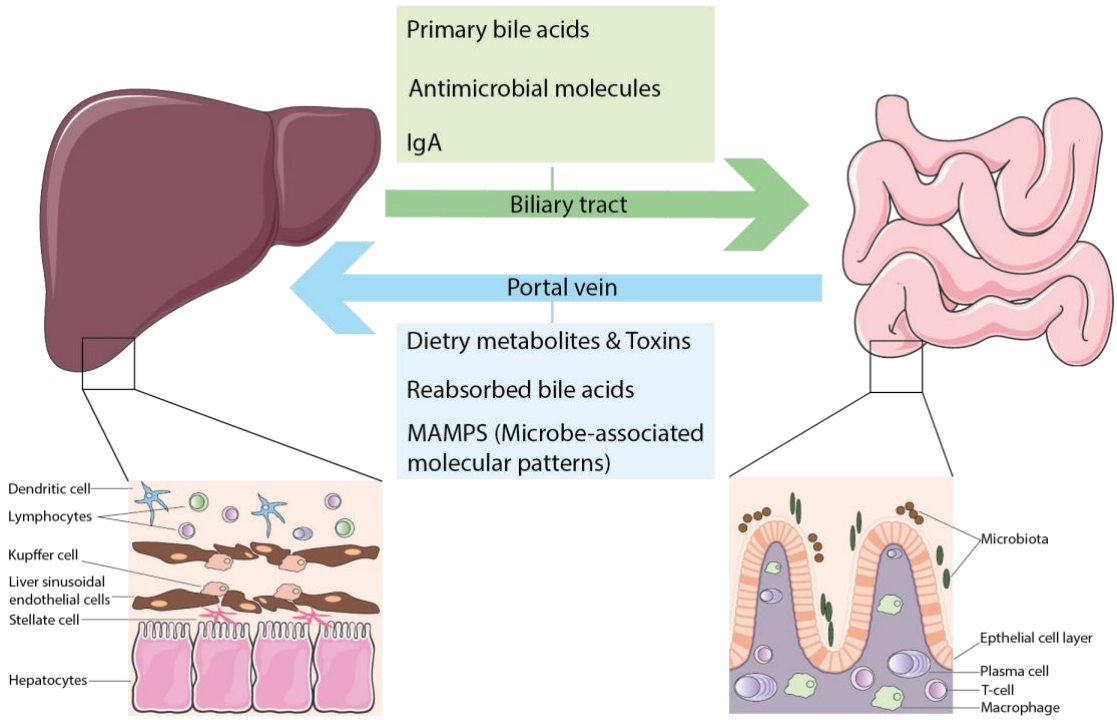

Figure 3: Interactions between gut and liver in homeostasis Anatomical connection between the liver and the gut through the biliary tract and portal vein. Transport of primary bile acids, antimicrobial products, and IgA through the bile into the intestine. Conversely, dietary metabolites, toxins, reabsorbed bile acids, and MAMPS are transported to the liver by the portal vein. Immune cells with different distribution patterns are found in both organs. MAMPS: Microbe-associated molecular patterns. Adapted from (Tripathi et al., 2018).

1.2.2 B-cells in the gut

The intestinal B-cell compartment can be divided into inductive and effector sites. Inductive sites are involved in the generation of immune responses and include the gut-associated lymphoid tissues (GALT) such as Peyer's patches, other small lymphoid follicles and, in humans, the appendix. In GALT, antigens from the intestinal lumen can be taken up to be presented to B- and T-cells, and the various steps of B-cell activation and maturation take place (Mörbe et al., 2021). This activation includes a specific T-cell-independent or T-cell-dependent response with formation of a germinal center. Within this GC reaction, class-switched and mutated MBCs and PCs may be generated. These cells can subsequently express the intestinal homing factors integrin beta 7, CCR9 or CCR10 on their surface and then re-migrate through the systemic circulation back to the intestine, where they localize to the lamina propria. The lamina propria is considered part of the B-cell effector compartment and harbors many different effector immune cells, but in particular a dense population of PCs that mainly produce IgA. This IgA is transported in dimeric form through the epithelium into the lumen by the polymeric immunoglobulin receptor (PIGR). After the release of IgA into the intestinal lumen, the IgA retains the secretory component of PIGR and becomes secretory IgA. IgA fulfills several functions in the intestinal lumen, such as defense against potential pathogens, protection of the mucosal surface from toxins, but also interaction with commensal bacteria of the microbiota to maintain homeostasis. But not only IgA is produced in the intestine and released into the lumen. IgM^+ PCs and MBCs are located in the lamina propria as well. IgM can also be secreted into the lumen via PIGR, where it binds to the commensal microbiota or other antigens (Spencer & Sollid, 2016). While IgA- and IgM-positive PCs and MBCs are found in the intestine of healthy individuals and are involved in maintaining homeostasis, IgG-positive PCs are particularly prevalent in inflammatory conditions such as inflammatory bowel disease (Spencer & Bemark, 2023).

1.2.3 B-cells in the liver

The liver is the largest metabolic organ in the human body and, accordingly, its main tasks are the metabolization of food, the elimination of toxins and the synthesis of

proteins. Nevertheless, the liver must also be considered as an immunological organ, since it is exposed to enormous amounts of dietary and bacterial products via the portal vein. In addition, the constant remodeling activity of the tissue also leads to constantly necessary immunological reactions. In contrast to the intestine, resident macrophages (Kupffer cells), dendritic cells and innate lymphocytes are the predominant cells of the liver immune population. Although adaptive lymphocytes are part of the resident immune component of a healthy liver, B-cells make up only about 8% of these lymphocytes in humans (M. W. Robinson, Harmon, & O'Farrelly, 2016). Despite of this low number, the B-cell compartment as well as the expression of individual receptors and the synthesis of antibodies have been found to be altered in patients with various liver diseases. Thus, patients with alcohol-related liver disease appeared to have fewer circulating B-cells in the peripheral blood in general, and the subsets of immature, memory and naive B-cells were particularly affected by this decrease (Almeida et al., 2015). Alteration of the hepatic B-cell compartment was also observed in patients with NAFLD, which was associated with disease severity driven by increased cytokine production as well as T-cell activation (F. Zhang et al., 2016). There is also evidence that B-cells may be involved in the development and progression of other diseases such as viral hepatitis, autoimmune hepatitis, primary sclerosing cholangitis and primary biliary cholangitis.

As PCs make up only a small proportion of the liver resident B-cells, not much is known about the quantity or function of this population. However, in humans with chronic inflammation and fibrosis, an accumulation of IgA-producing PCs has been found in the liver, which may promote the progression of hepatocellular carcinoma by suppressing tumor-regulating cytotoxic T-cells (Shalapour et al., 2017). In addition, consistent with the concept of shared functionality in the gut-liver axis, previous work suggests that some of the hepatic B-cells originate in the GALT, migrate to the liver and produce IgA as tissue-resident PCs. Together with IgA extracted from the serum, this would be secreted into the gastrointestinal tract via bile. The IgA produced in the liver could react with commensal bacteria and oral antigens and would thus be involved in the B-cell mediated intestinal immunity (Moro-Sibilot et al., 2016).

Since B-cells and PCs are associated with the pathogenesis of several diseases, it is essential to further study human B-cells in the healthy and diseased liver to better understand the pathophysiology and therapeutic options (Patel et al., 2021).

1.3 Phenotyping of human B-cells

1.3.1 Phenotypical analysis of B-cells in human tissues

By analyzing the phenotypic characteristics of B-cells, it is possible to obtain insights into their functionality in the individual tissues. Although immunophenotypic analysis of human B-cells has been a focus of immunological studies in recent years, in most cases B-cells from peripheral blood, tonsils or lymph nodes have been investigated as these are the most accessible sites. However, the phenotype and functionality of these cells may differ greatly to other tissue resident B-cells. Other studies that have analyzed and compared cells from different organs have often used samples from mice, and while these results can provide interesting findings, they are not directly applicable to the human body.

A study by Weisel et al. followed the approach of phenotypic and tissue-specific analysis of B-cells by including bone marrow, spleen and intestine in addition to blood, and was thus able to identify a gut-specific MBC subpopulation (Weisel et al., 2020). In another study, single-cell RNA sequencing was used to investigate the phenotype of various immune cells from different tissues, including intestine and liver, from organ donors. Through their tissue-specific approach, the authors were able to show that long-lived PCs previously only detected in bone marrow and strongly suspected in the intestine, may also be present in the human liver (Domínguez Conde et al., 2022). However, surface phenotypic analyses of the human B-cell compartment in the gut-liver axis and specifically of liver-resident B-cells are still rare to find in the literature. Using new techniques such as single-cell RNA sequencing and high-dimensional flow cytometry, it may be possible to gain more detailed information and new insights into the tissue-specific immunology.

1.3.2 Spectral flow cytometry

In recent years, the field of flow cytometry technology has expanded enormously. While conventional flow cytometry detects only part of the emission spectrum of a fluorochrome and works on the principle that one detector detects only one color, the technology of a spectral flow cytometer differs in that the entire emission spectrum of a fluorochrome is measured. The major limitation of conventional flow cytometry, the overlap of emission spectra of different fluorochromes and the resulting possible false-positive detection of signals, can be resolved by the spectral measurement. The detection principle of conventional flow cytometry has therefore limited the number of fluorochromes used and hence the number of cell markers to be analyzed (Sanders & Mourant, 2013). By analyzing the entire spectrum, it is possible to separately detect fluorochromes with similar emission spectra. Thus, both the overlap of the emission spectra of the fluorochromes and the respective intensity are no longer critical factors in the measurement. Therefore, spectral flow cytometry provides the significant advantage that more parameters can be measured simultaneously, allowing for more complex immunophenotypic analyses (J. P. Robinson, 2022).

1.3.3 High dimensional analysis

New technologies bring new challenges. The theoretical possibility of measuring up to 40-60 parameters simultaneously creates difficulties both in creating a complex multiparametric panel and in analyzing the high-dimensional data sets generated. To properly take advantage of the new method, these datasets need to be analyzed using innovative high-dimensional analysis. Thus, the traditional manual gating strategy is no longer sufficient to detect and depict the entirety of the data. Reducing the dimensionality of the data enables fast visualization and unbiased examination, allowing the detection of unknown cell subsets and their marker expressions. Dimensionality reduction analyses include t-distributed stochastic neighbor embedding (t-SNE), hierarchical stochastic neighbor embedding (h-SNE) and uniform manifold approximation and projection (UMAP). In addition to these analyses, there are other algorithms such as Flow Cytometry Self-Organizing Map (FlowSOM) and Spanning-tree Progression Analysis of Density-normalized Events (SPADE) that cluster the data,

allowing statistical comparisons between the individual clustered cell populations (den Braanker, Bongenaar, & Lubberts, 2021).

While t-SNE is mainly used for single cell RNA-Seq data analysis, the recently developed technique UMAP offers some significant advantages over t-SNE analysis, such as a faster generation of graphs and a better preservation of the global structure of the data. Although t-SNE and UMAP perform equally well in local clustering, that is for example the separation of different cell-subpopulations (e.g., MBCs, Th-cells), UMAP is better at integrating these subsets into global structures (e.g., B-cells and T-cells) than the t-SNE algorithm. However, it should be noted that both the size of the clusters and the distance between them do not give a direct indication of the relation between the respective populations. Although these analyses are very useful for visualization and initial understanding of the data, manual gating or automated clustering algorithms are still essential for statistical analysis (Andy Coenen).

1.4 Non-alcoholic fatty liver disease

1.4.1 NAFLD

Given its central metabolic and immunological function, it is not surprising that impaired gut-liver communication triggers and promotes various diseases such as alcoholic liver disease, NAFLD, primary sclerosing cholangitis and their shared end-stage liver cirrhosis (Tilg, Adolph, & Trauner, 2022). In particular, metabolic syndrome and the resulting common liver manifestation NAFLD have increased significantly in prevalence in recent decades due to the diet associated with today's lifestyle. In developed countries, about 25% of the population currently suffers from NAFLD, making it the most common chronic liver disease (Polyzos, Kountouras, & Mantzoros, 2019). The stages of the progressive disease can be divided into non-alcoholic fatty liver (NAFL), non-alcoholic steatohepatitis (NASH) and fatty liver cirrhosis. Initially, an unbalance of fats accumulated and metabolized leads to fatty liver, in which triglycerides are deposited in the hepatocytes. In about 20 percent of NAFL patients, the disease progresses to the second stage, fatty liver hepatitis, in which additional liver cell damage, inflammatory infiltrates, or fibrosis develop. When the entire structure of the inflamed liver begins to

show micro nodular changes with regenerative nodules, the patient is at the final stage of the disease, liver cirrhosis. This stage is associated with a significantly worse prognosis and an increased risk of complications such as liver failure and hepatocellular carcinoma (Parthasarathy, Revelo, & Malhi, 2020). However, the clinical course differs greatly among patients, and various factors such as environment, microbiome, comorbidities and genetic factors seem to play a crucial role in the progression. Although a very large proportion of the population is affected by this disease, the clinical factors for its development and progression are not yet clearly understood. Medical care for these patients, including early detection, diagnosis and treatment options, is also limited to date. For example, a definite diagnosis of NASH can only be made by liver biopsy, which is an invasive procedure associated with high costs and risks. In addition, no drugs have been approved for treatment so far. The only therapeutic option is lifestyle and dietary modifications with weight loss, but this is highly dependent on the patients' compliance (Friedman, Neuschwander-Tetri, Rinella, & Sanyal, 2018). Further research and a deeper understanding of the pathogenesis and progression of NAFLD are needed to minimize the impact on affected individuals and public health.

1.4.2 Role of the gut-liver axis in NAFLD

As mentioned above, the pathophysiological events leading to the development and progression of NAFLD are not yet fully understood. In recent years, however, it has been shown that a dysfunctional gut-liver axis might be an important progression factor, as it leads to a disturbed balance between immune tolerance and activation (Barrow et al., 2021). In addition to multifactorial causes such as nutritional conditions, genetic factors and insulin resistance, alterations in the gut microbiota, have been identified as drivers of the pathogenesis. Due to certain dietary habits, the intestinal contents can influence the gut microbiota and alter its composition as well as its functions and biological activities. This in turn can lead to an impairment of the intestinal barrier, resulting in an increased translocation of dietary products, but also of pathogenic antigens to the liver. The increased influx of pathogenic antigens, in addition to the already existing lipid accumulation in hepatocytes, can result in an excessive immune response along with a chronic inflammatory condition (Martín-Mateos & Albillos, 2021).

The gut microbiota consists of a total of 500-1000 species of microorganisms, most of which are bacteria that colonize the gut and exist in symbiosis with their host. These microorganisms not only have functions such as metabolizing dietary components and bile acids, synthesizing vitamins, regulating epithelial growth and immune responses, but are also responsible for preventing pathogen invasion and colonization (Fianchi, Liguori, Gasbarrini, Grieco, & Miele, 2021). Regarding the composition of the gut microbiota, significant changes were observed in the presence of NAFLD in both mouse and human studies. For example, Boursier et al. examined the composition of the gut microbiota in patients with different stages of NAFLD and found that in the advanced stages, the abundance of Bacteroides increased, whereas that of Prevotella decreased. In addition, a correlation between the abundance of Ruminococcus and the severity of fibrosis was found (Boursier et al., 2016) . Although these observations varied from study to study and did not show absolutely consistent results, an overall alteration in the composition of the microbiota was found.

This dysbiosis can lead to an impairment of the integrity of the intestinal barrier, which consists of mucus, intestinal epithelium and vascular endothelium and prevents the passage of pathogen-associated molecular patterns (PAMPs) into the bloodstream in healthy individuals. Miele L. et al. found increased elimination of 51Cr-ethylenediaminetetraacetate (51Cr-EDTA) in the urine of patients with NAFLD compared to healthy individuals. Also within the different stages, increased intestinal permeability was observed in patients in moderate to severe stages compared to mild stages. At the same time, the group found reduced immunohistochemically expression of zona occludens-1 in duodenal biopsies from NAFLD patients compared with healthy individuals (Miele et al., 2009). These findings support the theory that a disruption of tight junctions leads to a leaky gut, which promotes the development and progression of the disorder.

Given the above reasons for the influence of the gut-liver axis in the setting of chronic liver diseases, various therapies specifically targeting this entity have been investigated in the attempt to restore the balance. These include the use of antibiotics, probiotics and prebiotics, as well as bariatric surgery. However, transplantation of the fecal microbiota has been particularly promising and has therefore been the focus of multiple studies on mice and humans. These studies also showed partially differing results. For

example, a study by Vrieze et al. showed relatively promising findings that fecal transfer of gut microbiota from lean donors to patients with metabolic syndrome could increase their insulin sensitivity (Vrieze et al., 2012). In contrast, the study by Craven L. et al. demonstrated that fecal transfer restored the intestinal barrier but had no effect on insulin sensitivity or fat accumulation in the liver (Craven et al., 2020). In conclusion, an altered gut microbiota is found in patients with NAFLD and has been associated with both development and progression of the disease. However, the exact pathophysiological mechanisms and potential therapeutic approaches are not yet completely defined and require further research.

1.4.3 Role of B-cells in NAFLD

The progression of NAFLD is driven to a large extent by the innate immune system. In particular, activation of Kupffer cells, neutrophils, monocytes and natural killer cells leads to a pro-inflammatory state through the release of cytokines, chemokines and other substances (Arrese, Cabrera, Kalergis, & Feldstein, 2016). However, not only the innate immune system but also lymphocytes seem to have a major impact on the progression of NAFL to the more severe stages of NASH and cirrhosis. Histological studies of NASH livers, showed marked infiltration of lymphocytes with the formation of aggregates that correlated with the grade of inflammation and fibrosis. Interestingly, the authors additionally demonstrated that mice with NASH exhibited an increased hepatic expression of the B-cell-activating factor (BAFF) (Bruzzì et al., 2018). Studies with human samples similarly found that the amount of BAFF circulating systemically correlated with the disease progression stage (Miyake et al., 2013). Equally, the increased serum IgA level in NASH patients compared with patients with milder disease is an indication of the involvement of B-cells in the progression of NAFLD (McPherson, Henderson, Burt, Day, & Anstee, 2014).

Moreover, not only hepatic B-cells can trigger progression, but also B-cells outside the liver, such as in adipose tissue, can play a role. For example, B-cells of the adipose tissue between the intestine and the liver in mice can produce cytokines and free fatty acids, which can enter the liver via the portal vein and thus influence the inflammatory response (Wu et al., 2019).

Based on these results, modulation of the activity of the adaptive immune system seemed to be a good therapeutic approach for the treatment of the disease. Regarding B-cells, Bruzzì et al. also investigated whether treatment with a BAFF-neutralizing antibody would have an effect on disease progression, and indeed treated mice showed an improvement in their NASH condition (Bruzzì et al., 2018). These and other therapeutic approaches could represent interesting possibilities for the development of a targeted treatment, but a more detailed understanding of the pathophysiology is needed for this purpose. Since B-cells outside the liver can also have an impact on the inflammatory state, it could also be of interest to clarify the association of B-cells in other tissues of the gut-liver axis with the development and progression of NAFLD.

1.5 Liver cirrhosis

1.5.1 Liver cirrhosis and its consequences

Liver cirrhosis is the irreversible end stage of many chronic progressive liver diseases such as alcoholic and non-alcoholic fatty liver disease and chronic viral hepatitis. The normal lobular and vascular structure is destroyed over years by the underlying disease, leading to the formation of regenerative nodules and a complete remodeling of the connective tissue. The destruction is mainly caused by the increased cell necrosis-induced inflammation and activation of hepatic stellate cells with subsequent fibrogenesis and angiogenesis. Thus, connective tissue septa and regenerator nodules form, resulting in a complete alteration of the normal liver lobule structure (W. C. Zhou, Zhang, & Qiao, 2014).

The consequences of this conversion are mainly a disturbed metabolic process and an increase in the blood flow resistance. This increased resistance results in higher portal vein pressure, which in turn causes blood stasis. Portal hypertension with blood stasis then leads to further complications such as the formation of portosystemic collateral pathways, the development of splenomegaly and the progression to ascites. In addition to the complications resulting from portal hypertension, other consequences of cirrhosis include liver failure, bleeding tendency, hepatic encephalopathy, hepatorenal syndrome and hepatocellular carcinoma (Tsochatzis, Bosch, & Burroughs, 2014).

Ascites is defined as free fluid accumulating in the abdominal cavity. In the case of liver cirrhosis and portal hypertension as the underlying cause of ascites, the free fluid is a transudate, a non-inflammatory leakage of fluid from the vessels. However, about 5-25 % of all ascites patients develop spontaneous bacterial peritonitis as a complication. This is an inflammation of the peritoneum that may develop as a result of hematogenous infection or bacterial penetration of the intestine and is defined as > 250 neutrophil granulocytes per mm^3 of ascites. Spontaneous bacterial peritonitis has a relatively high mortality even at the first onset. The risk of recurrence is also high, and recurrences themselves increase mortality significantly (Mattos et al., 2020).

The prognosis varies greatly and depends strongly on the stage of the disease. Nevertheless, cirrhosis accounts for 3-5 % of the deaths worldwide. Therapeutic management is mainly limited to treatment of the underlying disease, complications and avoidance of hepatotoxic substances. To date, liver transplantation is considered the only curative treatment option (Ginès et al., 2021).

1.5.2 Immune dysfunction and B-cell alterations in cirrhotic patients

Liver cirrhosis represents a systemic disease with numerous consequences rather than a local, organ-specific disorder. One of these complications is the compromise of the immune system, causing a condition that is known as cirrhosis-associated immune dysfunction. This dysfunction is associated with a significant alteration of the immune cell compartments, with systemic inflammation on the one hand and immunodeficiency on the other. It is a dynamic process that worsens depending on the stage, ranging from an increased production of pro-inflammatory cytokines to a complete impairment of the immune system. The more severely the immune system is affected, the greater its influence on the course of the disease can be (Noor & Manoria, 2017). Systemic inflammation exacerbates the situation in acute-on-chronic liver failure by increasing peripheral vasodilation, portal hypertension and cardiac dysfunction, thus contributing to the pathogenesis of organ failure and affecting the prognosis. This inflammation mainly results from an excessive immune response to the increased appearance of PAMPS and damage-associated molecular patterns (DAMPS), by the influx of intestinal-derived pathogens and cell destruction of hepatocytes (Martin-Mateos, Alvarez-Mon, &

Albillos, 2019). Immune dysfunction, on the other hand, is caused by the changing structure of the liver parenchyma and the impairment of effector immune cells. For instance, restructuring of the parenchyma induces the formation of intrahepatic shunts, which then prevent the access of gut-derived PAMPS to Kupffer cells. Additionally, the destruction of hepatocytes by the underlying disease leads to a defective synthesis of important immune proteins. But not only intrahepatic immune abnormalities, also changes in circulating immune cells of the innate and adaptive immune system cause a compromised defense against pathogens and especially bacteria (Albillos et al., 2022).

Regarding the B-cell compartment, some studies have shown that there are distributional and functional differences between circulating B-cells from healthy subjects and patients with cirrhosis (Cardoso et al., 2021). The distribution seemed to be altered mainly by a lower proportion of MBCs and in particular by the reduction of non-switched IgM^+ MBCs in cirrhotic patients. This decrease appeared to be independent of etiology and occurred in cirrhosis due to viral hepatitis as well as due to alcohol and non-alcoholic liver disease (Doi et al., 2012). The authors additionally demonstrated functional impairment of circulating B-cells by measurements of CD70 upregulation, together with TNFβ and IgG production. With this study, they have shown that B-cells from cirrhotic patients were less responsive to CD40/TLR9 activation, which was additionally accompanied by a reduced ability to stimulate $CD4^+$ T-cells. Thus, the impairment of B-cells could be a possible explanation for the low reactivity to vaccination and bacterial infections in cirrhotic patients (Doi et al., 2012).

In patients suffering from hepatocellular carcinoma, a possible complication of liver cirrhosis, the same changes in the distribution of circulating B-cells were observed. Interestingly, B-cells from these patients expressed less BAFF-R than their counterparts in healthy patients (Khlaiphuengsin et al., 2020). However, whether the altered composition of the B-cell population is related to the altered BAFF-R expression remains unclear until now.

1.5.3 B-cells in the peritoneal cavity and ascites

The peritoneal cavity is the part of the abdominal cavity that contains most of the abdominal organs. It is a fluid filled space between the two serous membranes of the peritoneum lining the abdominal wall (parietal peritoneum) on the one hand and the organs (visceral peritoneum) on the other. The peritoneal cavity contains about 50-70 ml of peritoneal fluid, which ensures a smooth movement of the organs. The peritoneum also covers the omentum, an adipose tissue that hangs from the great curvature of the stomach and the transverse colon over the ventral side of the abdominal organs (M. Liu, Silva-Sanchez, Randall, & Meza-Perez, 2021). This omentum contains accumulations of immune cells, such as macrophages and lymphocytes, which are known as milky spots or fat-associated lymphoid clusters (FALCs). In addition, the omentum harbors local stromal cells that provide the necessary signals for leukocyte proliferation, activation and survival. The leukocytes in these milky spots can induce an appropriate immune response to antigens and pathogens that are present in the peritoneal cavity, thus protecting against peritonitis and sustain peritoneal homeostasis. Under normal, healthy conditions, macrophages represent the predominant immune cells (Okabe, 2024).

B-cells also exist in the peritoneal cavity, but are more abundant and better characterized in mice than in humans. Mouse peritoneal cavity B-cells can be divided into B1 and B2 cells, with B1 cells reflecting an innate-like phenotype with the production of natural antibodies, whereas B2 cells produce specific antibodies as a result of a T cell-dependent immune response (Suchanek & Clatworthy, 2023). To date, the existence and identity of B1 cells in humans have not been precisely defined. Some human peritoneal B-cells also appear to continuously produce antibodies similar to their mouse counterparts, and therefore have comparable biological functionality. However, further studies are needed to prove their actual existence, define the exact phenotype, and provide a more accurate characterization of this and the entire B-cell population in the peritoneal cavity in humans (Descatoire, Weill, Reynaud, & Weller, 2011).

2 Aims

B-cells have mostly been studied in mice or in human blood. Our primary aim was to extend information on human B-cells in gut and liver. Therefore, we sought to perform an in-depth phenotypic analysis using spectral flow cytometry and high-dimensional analysis methods.

In addition, the presence and the origin of liver-resident PCs is not well understood. Previous work suggests that liver resident PCs originate from gut-associated lymphoid tissue and that the antibodies produced by these cells react similarly to those produced by intestinal PCs to the microbiota and oral antigens (Moro-Sibilot et al., 2016). For this reason, we hypothesized that IgA^+ PCs from liver and gut might be clonally related. To investigate this, we performed RNA sequencing of IgA^+ PCs from gut and liver of the same individual.

Moreover, we were interested in whether and how the phenotypic or repertoire characteristics of B-cells are altered in liver diseases related to the gut-liver axis, such as NAFLD and liver cirrhosis. Since changes in the microbiota and intestinal barrier are known to be present during the development and progression of NAFLD (Martín-Mateos & Albillos, 2021), we wanted to investigate whether these changes also affect intestinal B-cells. Liver cirrhosis, which is the end stage of many liver diseases, can also have an enormous impact on the immune system. On the one hand, changes in the B-cell compartment may be involved in the development of many liver diseases leading to cirrhosis, and on the other hand, cirrhosis itself may lead to changes in the entire immune system, which are referred to as cirrhosis-associated immune dysfunction (Albillos et al., 2022). Since the exact changes within the B-cell compartment in this context have not yet been clearly determined, our final aim was to identify these in more detail by phenotypic analysis.

3 Materials and methods

3.1 Materials

3.1.1 Antibodies

Table 1: Materials - Antibodies

(Conjugated)-Antibodies	Company	Catalog no.
BAFFR (CD268) - BUV563	BD	748443
CCR9 (CD199) - BV421	Biolegend	358914
CD11c - BUV661	BD	612967
CD138 - BV711	Biolegend	356521
CD14 - AF700	Biolegend	301822
CD14 - Biotin	Biolegend	325623
CD14 - PerCP	Biolegend	325631
CD16 - APC-Cy7	Biolegend	302018
CD16 - Biotin	Biolegend	302004
CD16 - PerCP	Biolegend	302029
CD19 - eF450	ebioscience	48-0198-42
CD19 - Pe-Cy7	Biolegend	B254738
CD20 - BV570	Biolegend	302332
CD27 - BV750	Biolegend	302850
CD29 (Integrin β1) - AF700	Biolegend	303020
CD3 - AF700	Biolegend	300424
CD3 - Biotin	Biolegend	344820
CD3 - PerCP	Biolegend	344813
CD38 - APC	Biolegend	303510
CD38 - BUV496	BD	612947
CD45 - BUV395	Biolegend	563791
CD80 - BUV805	BD	751733
CXCR3 (CD183) - Pe-Cy5	BD	742048
HLA-DR - APC-Fire 810	Biolegend	307673
IgA - Horseradish Peroxidase	Jackson ImmunoResearch	109-035-011
IgA - PerCP Vio 700	Miltenyi Biotec	130-114-004
IgA - unconjugated	Santa Cruz	sc-51991
IgD - BV510	Biolegend	348219
IgG Fc - Pe-Cy7	Biolegend	410722
IgM - BV605	Biolegend	314524
Integrin β7 - FITC	Biolegend	321213
TACI (CD267) - Pe/ Dazzle 594	Biolegend	311907

3.1.2 Buffers, media and sera

Table 2: Materials - Buffer, media and sera

Buffer; medium; serum	Company	Catalog no.
CytoRich Red	Thermofisher scientific	B9990801
FCS	Gibco	10270106
HBSS	Gibco	14175-1292
L-Glutamine	Gibco	25030-024
Mouse serum	Sigma Aldrich	M5905
Pancoll human	Pan Biotech	P04-60500
PBS	Gibco	15140-122
Penicillin/Streptomycin	Gibco	15140-122
Recovery cell culture freezing medium	Gibco	12648010
RPMI	Gibco	31870025

3.1.3 Chemicals and enzymes

Table 3: Materials - Chemicals and enzymes

Chemical; enzyme	Company	Catalog no.
10% Tween 20	Bio-Rad	1662404
Amino-9-ethylcarbazole (AEC)	Sigma-Aldrich	6696
Anti-biotin microbeads ultrapure	Miltenyi Biotec	130-105-637
Collagenase A	Roche	10 103 586 001
Collagenase D	Roche	11 088 866 001
Collagenase VIII	Sigma-Aldrich	C2139-1G
DAPI	Carl-Roth	6843.1
Dimethylformamide (DMF)	Sigma-Aldrich	D4551
EDTA	Carl-Roth	8043.2
Ethanol, ≥99.8%	VWR	20821321
Hydrogene peroxide	Carl Roth	9683.1
KHCO3	Carl-Roth	P748.1
LE Agarose SeaKem, 500g	Lonza	50004
Live/Dead Blue viability stain	Thermofisher Scientific	L34961
Na-acetate	Carl-Roth	X891.1
NH4Cl	Carl-Roth	K298.2
PeqGREEN	Peqlab	37-5000
RNase AWAY	Thermofisher Scientific	7002 10666421
Roti Histokitt	Carl Roth	6638.2
Takara Ex Taq	Takara Clontech	RR001A
TrackIt 1 Kb Plus DNA Ladder	Invitrogen	10488-085
UltraComp eBeads	Thermofisher Scientific	01-2222-41

Xylene	Otto Fischar	27404
β-Mercaptoethanol	Carl-Roth	4227.3

3.1.4 Kits

Table 4: Materials - Kits

Kit	Company	Catalog no.
Mint-2 cDNA synthesis	Evrogen	SK005-EV
H&E fast staining kit	Carl Roth	9194.2
MinElute® PCR Purification Kit	Qiagen	28004
QIAquick PCR Purification Kit (250)	Qiagen	28106
RNeasy Plus Micro Kit (50)	Qiagen	74034
QIAquick PCR Purification Kit (1000)	Qiagen	28106x4
Template Switching RT Enzyme Mix 20 rxn	New england biolabs (NEB)	M0466S
MISeq Reagent Kit v3 600 cycles Kit	Illumina	MS-102-3003
Monarch® DNA Gel Extraction Kit (250)	New england biolabs (NEB)	T1020L

3.1.5 Primer

Primer	Sequence (5'-3')
SNNN, template switch adapter	AAGCAGUGGTAUCAACGCAGAGUNNNNUNNNNUNNNNUCTT(rG)5
Nested primer 1, human IgA heavy-chain	ATTGGGCAGCCCTGATTCAGCGGGAAGACCTTG
Step-out primer 1	CACTCTATCCGACAAGCAGTGGTATCAACGC
Nested primer 2, human IgA heavy-chain	ATTGGGCAGCCCTGATTCAGCGGGAAGACCTTG
Step-out primer 2	(N)2–4(XXXXX)CACTCTATCCGACAAGCA
Nested primer 3	ACATCTTTCCCTACAGAGCTCTTCCGATCTCAGTGGTATCAACGCAGAG
Illumina Multiplex Read Primer forward	ACACTCTTTCCCTACACGACGCTCTTCCGATCT
Illumina Multiplex Read Primer revers	GTGACTGGAGTTCAGACGTGTGCTCTTCCGATCT

3.1.6 Laboratory equipment

Table 5: Materials - Laboratory equipment

Equipment	Company	Catalog no.
5 ml polystyrene round-bottom tubes	Corning	352052

96-well microplate	Sarstedt	821583
Cell strainer 100 µm	VWR	734-0002
Disposable scalpel No. 10; No. 11	Feather	16400118; 16400119
Epredia shandon EZ single cytofunnel	Thermofisher scientific	12648166
Filtertips 2,5 µl	Biozym	69005
Filtertips 200 µl; 1000 µl	Starlab	S1120-8710; S1111-6701
MACS MultiStand	Miltenyi Biotec	130-042-303
Microcentrifuge tube 1,5 ml; 2 ml	Biotix	MTL-0150-BC; MTL-0200-BC
Microscope slides	R.Langenbrinck	03-0004
Mr. Frosty Freezing Container	Thermofisher scientific	5100-0001
MS Columns	Miltenyi Biotec	130-042-201
MultiScreen HTS 96-well plate	Merck	MSIPS4W10
Nylon mesh	Sefar	3A03-0048-102-00
OctoMACS Separator	Miltenyi Biotec	130-042-109
Pipette tips 10 µl; 200 µl; 1000µl	Starlab	S1111-3700; S1113-1700-C; S1111-6701
Stripettes 5 ml; 10 ml; 25 ml	Sigma-Aldrich	CLS4487-200EA; CLS4488-200EA; CLS4489-200EA

3.1.7 Devices, software, scripts

Table 6: Materials - Devices, software, scripts

Device; software; script	Name	Company; Source
Spectral flow cytometry analyzer	Cytek Aurora (5 Laser)	Cytek Biosciences
FACS Sorter	FACS Aria Fusion	BD
Automated cell counter	ViCELL XR Viability Analyzer	Beckman Coulter
Cytocentrifuge	Epredia Cytospin Cytocentrifuge	Thermofisher scientific
Flow cytometry analysis software	OMIQ	Dotmatics
Graphing and statistics software	GraphPad Prism (Version 9.1.1)	Dotmatics
Graphics software	Adobe Illustrator (version 26.5)	Adobe Inc.
Language for Statistical Computing	R (version 4.1.1.)	R Foundation for Statistical Computing
Pipeline for analysis of immune repertoire sequencing data	MiGEC: Molecular Identifier Guided Error Correction pipeline	https://github.com/mikesshh/migec
Software for analysis of immune repertoire sequencing data	MiXCR	https://github.com/milaboratory/mixcr

3.2 Tissue samples

3.2.1 Phenotypic analysis: Blood, small intestine and liver samples

Anonymized leukocyte reduction chambers from the Department of Transfusion Medicine, University Hospital Aachen were used to obtain peripheral blood mononuclear cells (PBMCs).

In collaboration with the Department of General Surgery, University Hospital Aachen, paired surgical samples of small intestine and liver were obtained from donors undergoing hemihepatectomy with biliary enteric anastomosis due to a malignant tumor. Liver samples were obtained from an area of the removed liver lobes that was not affected by the malignancy. Samples were processed, analyzed and sorted on the same day of surgery. In addition, small intestinal tissue was obtained from patients undergoing bariatric surgery for obesity. During the procedure, liver biopsies were routinely taken to rule out NAFLD. Retrospectively, patients diagnosed with NAFLD were classified into 3 stages based on their NAFLD activity score (NAS) (Kleiner et al., 2005) and compared to the other obtained small intestinal samples (chapter 3.2.1). Leukocytes were isolated from the small intestinal samples on the same day as surgery and stored at -156°C.

All samples were used for phenotypic analysis and for BCR repertoire analysis The study was approved by the institutional ethics committee (Medical Ethics Committee, RWTH Aachen University) with ethics vote EK 206/09, and all subjects signed an informed consent form before participation.

3.2.2 Cirrhosis: Ascites and blood samples

In collaboration with the Department of Gastroenterology, University Hospital Aachen, ascitic fluid was obtained from patients suffering from liver cirrhosis during diagnostic or therapeutic paracentesis. In addition, blood was drawn from the same patients, so that paired ascites and blood samples could be analyzed. Leukocytes were isolated on the same day as the procedure and then stored at -80°C until further analysis. The study was approved by the institutional ethics committee (Medical Ethics Committee, RWTH

Aachen University) with ethics vote EK 327/19, and all subjects signed an informed consent form before participation.

3.3 Preparation of single cell suspensions from human tissue

3.3.1 Isolation of peripheral blood mononuclear cells (PBMC)

The isolation of PBMCs from leukocyte reduction chambers (Leukotrap), using the density gradient separation procedure, was done by Nathalie Steinke and Silke Vaßen from the interdisciplinary center for clinical research (IZKF) - Flow Cytometry Facility.

The blood product was diluted 1:3 with PBS. 13 ml of the diluted blood was then carefully layered onto 30 ml of the lymphocyte separation medium Pancoll and centrifuged at room temperature for 30 min at 400 x g, using an acceleration of 6 and a break of 0. After cell separation, the PBMC layer was collected and washed 3 times with PBS at room temperature for 5 min at 300 x g. For red blood cell lysis, the pellet was resuspended in 9 ml of RBC lysis buffer (0,17 M NH4Cl, 10 mM KHCO3, 0,1 mM EDTA), incubated at 4°C for 10 min and washed again with PBS. Cell number was determined using an automatic cell counter (ViCell XR). 5-10^6 cells were resuspended in 1.5 ml of freezing medium (Recovery Cell Culture Freezing Medium) and frozen to -80°C overnight using a Mr. Frosty Freezing container. The following day, samples were transferred to a -152°C freezer for permanent storage.

3.3.2 Immune cell isolation from the small intestine

The small intestine sample, approximately 5 cm in length, was kept on ice before being cut open longitudinally along the surgical closure. Using a scalpel, the intestinal mucosa was separated from the muscular layer. The mucosa was then cut in 1x1 cm pieces and washed in HBSS + 3% FCS. For successful enzymatic digestion, the weight of each piece was controlled to be between 300 mg and 600 mg. These pieces were then cut very finely with scissors and incubated in pre-warmed HBSS + 2 mM EDTA at 37°C, for 30 min at 225 rpm. The tubes were shaken manually every 5 min. At the end of the incubation

period, the supernatant was discarded by filtering through a 50 µm nylon nitex mesh. The procedure was repeated with incubation in HBSS + 2 mM EDTA at 37°C, 225 rpm for another 15 min, manual shaking every few minutes and washing with HBSS. For enzymatic digestion, 8 ml of HBSS + 1 mg/ml collagenase VIII, 1.25 mg/ml collagenase D and 30 µg/ml DNase I were added to the remaining tissue. This was followed by incubation at 37°C, 225 rpm for 20 min. After digestion, the suspension was filtered through a 50 µm nylon nitex mesh, filled up with 4°C HBSS and centrifuged at 300 x g, 4°C for 10 min. The supernatant was discarded and the pellet was then resuspended in an appropriate volume of PBS/ 3% FCS for cell counting and further analysis.

3.3.3 Immune cell isolation from the liver

The liver sample was cut into small sections (between 800 and 1000 mg) and kept on ice. As a substitute for liver perfusion, these sections were dissect into very small pieces (approximately 2 x 2 mm) and washed in 20 ml PBS by shaking. PBS was removed by filtering through a 100 µm cell strainer. For digestion, the pieces were transferred to an enzyme solution consisting of 20 ml RPMI with 0.5 mg/ml collagenase A and 10 µg/ml DNase I. Subsequently this was incubated for 25 minutes at 37 °C and 225 rpm, and shaken manually every 5 minutes. The tubes were refilled with 20 ml PBS, filtered through a 100 µm cell strainer and centrifuged at 4 °C, 300 x g for 10 min. After the supernatant was discarded, the pellet was resuspended in 4 ml of RBC lysis buffer (0,17 M NH_4Cl, 10 mM $KHCO_3$, 0,1 mM EDTA) and incubated at 4 °C for 3 min. 20 ml of PBS was added and then centrifuged at 4°C, 300 x g for 10 min. The supernatant was discarded and the pellet was resuspended in an appropriate volume of PBS/ 3% FCS for cell counting and further analysis.

3.3.4 Immune cell isolation from ascites

For the analysis of B-cells in cirrhotic patients, leukocytes were isolated from paired ascites and blood samples using the density gradient separation method. This was performed by Dr. Oluwatomi Ibidapo-ob from the Hepatology Research Unit,

Department of Gastroenterology. Since the same method was used as described in 3.3.1, only a brief description of the approach is given here.

Ascites was centrifuged in separate 50 ml tubes and all pellets were together resuspended in 8 ml of ascitic fluid. The blood product as well as the 8 ml ascitic fluid were then carefully layered onto the Lympholyte Cell Separation Media. After the next centrifugation step the cell layer was collected and washed using PBS. The pellet was resuspended in PBS/ 3% FCS to obtain a single cell suspension. To ensure good flow cytometry staining and analysis of lymphocytes, cell isolation was followed by depletion of monocytes and macrophages. For this purpose, magnetic cell separation of CD14 and CD16 positive cells was performed. Cell number was determined and cells were resuspended in 1.5 ml of freezing medium and frozen to -80°C overnight. The following day, samples were transferred to a -152°C freezer for permanent storage.

3.3.5 Cell counting

After the cell isolation from different organs, cell number and viability were determined. In order to measure all the cell suspensions consistently, this was done with the help of an automatic cell counter (ViCELL XR Viability Analyzer). For this, a 1:10 dilution of the cell suspension in 500 µl was prepared. This was automatically diluted 1:1 by the instrument with 0.4% trypan blue, which is impermeable to the cell membrane. This results in only cells with a destroyed cell membrane (dead or dying cells) being stained, while living cells remain unstained. The cell counter then generated 50 images of the cell suspension, which were automatically evaluated by the ViCELL XR software.

3.4 Spectral flow cytometry

3.4.1 Multiparametric B-cell panel

In order to perform a deep immunophenotypic analysis of B-cells in the gut-liver axis, a multiparametric panel for the spectral flow cytometer was established by Dr. Ana Izcue from the Institute of Molecular Medicine.

The panel consisted of 23 surface markers specifically selected for the characterization of B-cell subsets in the intestine and liver. The panel also contained a viability dye and the markers CD3, CD14, CD16 for the exclusion of dead cells, T-cells, monocytes and macrophages, so that the B-cell population could be gated and analyzed more precisely. To determine the appropriate concentrations, all antibodies were titrated individually by staining in different dilutions. The panel was designed with the help of the Cytek spectrum viewer, to minimize interference between the conjugated fluorochromes. The remaining spectral overlap was unmixed on the Aurora, which required single stainings on Ultracomp eBeads. In addition, the compensation of all samples was manually corrected before each analysis using the software OMIQ. All fluorochrome-conjugated antibodies of the B-cell panel are listed in Table 7.

Table 7: Fluorochrome-conjugated antibodies used in the B-cell panel

Antibody and Fluorochrome	Dilution	Antibody and Fluorochrome	Dilution
CCR9 (CD199) - BV421	1:25	IgG Fc - Pe-Cy7	1:200
CD138 - BV711	1:50	CD27 - BV750	1:200
IgA - PerCP Vio 700	1:50	CD19 - eF450	1:200
TACI (CD267) - PE/ Dazzle 594	1:50	BAFFR (CD268) - BUV563	1:200
Integrin β1 (CD29) - AF700	1:50	CD45 - BUV395	1:200
CD11c - BUV661	1:50	HLA-DR - APC-Fire 810	1:200
CD14 - PerCP	1:100	CD80 - BUV805	1:200
CD16 - PerCP	1:100	Integrin β7 - FITC	1:200
CD3 - PerCP	1:100	CXCR3 (CD183) - Pe-Cy5	1:200
CD20 - BV570	1:100	IgM - BV605	1:400
IgD - BV510	1:100	Live/Dead Blue	1:1000
CD38 - BUV496	1:100		

3.4.2 Cell surface staining

For fluorescence-activated cell sorting (FACS) analysis and FACS cell sorting, cells were stained with fluorescently labeled antibodies, which are listed in Table 1. Depending on the experiment, a different number of cells were centrifuged at 4°C, 300 x g for 10 min

for staining preparation. First, an antibody mixture was prepared consisting of PBS/ 3% FCS/ 10% mouse serum + the required antibodies in their respective dilution factor. Cells were stained in this mixture on ice for 30 minutes in the dark. To exclude dead cells, viability staining was performed with either live/dead blue viability dye or 4',6-diamidino-2-phenylindole (DAPI). In the former case, cells were stained in 1:1.000 live/dead blue/PBS on ice in the dark for 15 min before the antibody staining. To stop the viability staining PBS was added and centrifuged at 4°C, 300 x g for 10 minutes. For the latter, the required amount of DAPI in PBS/ FCS 3%, which resulted in a total dilution of 1:10.000, was added for the last 2 minutes of the staining incubation time. After staining, the same volume of PBS/ 3% FCS was added and cells were washed by centrifugation at 4°C, 300 x g for 10 min. Depending on the cell number, the pellet was resuspended in an appropriate volume of PBS/ 3% FCS and filtered through a 50 µm nylon nitex mesh for further FACS analysis.

3.4.3 Flow cytometry analysis

Figures were created using Adobe Illustrator software (version 26.3.1). Figure 3 and Figure 14 modified with text and colors were partly generated using Servier Medical Art, provided by Servier, licensed under a Creative Commons Attribution 3.0 unported license.

Sample acquisitions were performed using the spectral flow cytometer Aurora (Cytek) and the data were then analyzed with the analysis software OMIQ. For UMAP analysis, the B-cell subsets and samples examined were combined and cell numbers were downsampled according to the number available in the subgroup so that each sample was represented in approximately equal proportions. All markers of the B-cell panel except the viability dye and the exclusion lineage marker were used for UMAP clustering.

Statistical analysis was performed using GraphPad Prism 9. For all data, the mean values and their corresponding standard deviations are reported and p-values ≤ 0.05 are considered significant. Comparisons of two groups were made using an ordinary unpaired t-test and multiple comparisons of three or more groups were calculated using one-way ANOVA (Analysis of variance) with Tuckey's multiple comparison test. For

paired sample comparisons, either a paired t-test or repeated measures one-way ANOVA with Sidak´s multiple comparison test was used, depending on the number of comparison groups. To test the frequencies of specific B-cell subsets between two experimental groups two way ANOVA followed by Sidak´s multiple comparison test was used. Significance is indicated as: * $P < 0.05$, ** $P < 0.01$, *** $P < 0.001$, **** $P < 0.0001$, ns: not significant.

3.5 Plasma cell isolation

PCs from small intestine and liver were isolated for further experiments such as Enzyme Linked Immuno Spot Assay (ELISpot), histological stainings and BCR bulk sequencing. Usually, this was performed by FACS sorting after cell isolation from organs. To avoid contamination with other cell types, samples were sorted at a maximum rate of 7.000-10.000 particles/sec. However, when the number of isolated cells exceeded the amount that could be sorted by FACS in a reasonable time, B-cells were enriched by magnetic negative depletion of T-cells, macrophages, and monocytes prior to FACS sorting.

3.5.1 Magnetic cell separation

For the enrichment, 10 x 10^6 cells of the isolated cell suspensions were centrifuged at 4°C, 300 x g for 10 min. Meanwhile, the preparation of the buffer containing PBS/ 0.5% FCS + 2mM EDTA was carried out. Cells were then blocked with 50 µl buffer + 10% mouse serum at 4°C for 10 min. To deplete T-cells, macrophages and monocytes, an antibody mixture of the biotin-labeled antibodies CD3, CD14 and CD16 at their respective dilutions in buffer/ 10% mouse serum was prepared. After blocking, 50 µl of this antibody mixture was added and the cells were incubated at 4°C for an additional 5 minutes. Washing was performed by centrifugation at 4°C, 300 x g for 10 min with 1 ml buffer. The cell pellet was then resuspended in buffer + 20% Anti-Biotin MicroBeads UltraPure (Miltenyi Biotec), incubated at 4°C for 15 min, and washed again with 1 ml buffer. In preparation for magnetic cell separation, MS columns (Miltenyi Biotec) were placed in the MACS separator (Miltenyi Biotec) and rinsed with

500 µl buffer. Cells resuspended in 500 µl buffer were then added to the columns and the flow-through was collected. Cells that bound beads remained in the column due to magnetic attraction. To collect all unbound cells, this step was repeated by rinsing again with 500 µl buffer. The collected flow through contained enriched B-cells, which were then used further for FACS sorting.

3.5.2 Fluorescence-activated cell sorting

FACS sorting was performed using the cell sorter FACSFusion (BD). Since this cell sorter is integrated into a laminar flow hood, it is suitable for sorting potentially infectious human samples.

For BCR bulk sequencing, a pure PC population from small intestine and liver was required. Therefore, surface staining of the cell suspensions was performed using the antibodies CD3, CD14, CD16, IgD, CD27, CD38 and DAPI as viability marker, as described in chapter 3.4.2. Depending on the number of stained cells, they were resuspended in an appropriate volume of PBS/ 3% FCS for sorting. The gating strategy for sorting was performed as described in Figure 4 A-C. Small intestinal samples were used to determine the purity after the sort. For this purpose, 10 µl of sorted cells were added to 300 µl PBS/ 3% FCS and then acquired and analyzed. Since the cells had to be lysed for RNA isolation of BCR bulk sequencing, they were sorted directly into 350 µl RLT buffer (RNeasy kit) supplemented with 1% β-mercaptoethanol and stored at -80°C.

To compare different CD45/ CD19 PC groups by ELISpot or histological staining, $CD45^+$/ $CD19^+$, $CD45^+$/ $CD19^-$ and $CD45^-$/$CD19^-$ PCs were sorted. The antibodies used for this surface staining were CD3, CD14, CD16, IgD, CD38, CD27, IgA, CD45, CD19, and DAPI as viability markers. The gating strategy for this sort is also described in Figure 4D. In order to use the cells directly in the mentioned experiments, they were sorted either into 400 µl ELISpot medium or into PBS/ 3% FCS.

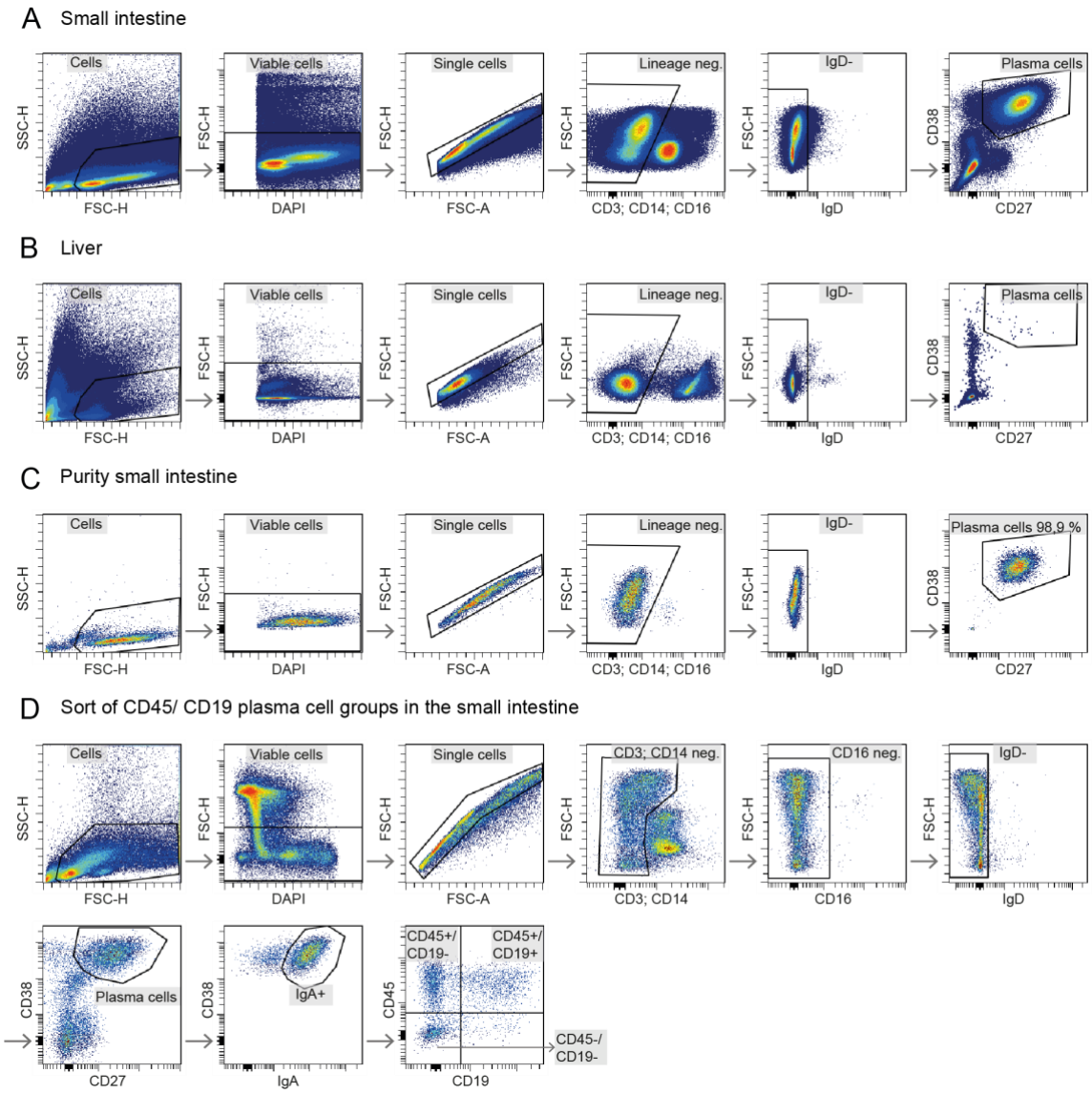

Figure 4: Gating strategy and purity for FACS-sorting For FACS sorting, cells were pre-gated on cells, viable, singles, lineage negative (T-cells, monocytes, macrophages) and IgD negative. PCs were identified as $CD38^{high}$ and $CD27^{+}$. **A:** Representative gating strategy in the small intestine. **B:** Representative gating strategy in the liver. **C:** Representative gating strategy in the small intestine after sort to determine the purity. **D:** Representative gating strategy for different CD45/ CD19 PC groups in the small intestine. FACS: Fluorescence-activated cell sorting; PC: plasma cell.

3.6 Microscopy

3.6.1 Cytocentrifuge preparation

For morphological comparison of the different PC groups, they were first transferred to a glass slide using a Cytospin centrifuge. For this, a cell suspension of 250 µl PBS/ 3% FCS containing 100.000 of the sorted cells was prepared and 250 µl CytoRich was added. The slide was inserted into a Cytofunnel, which was then placed in the Cytospin centrifuge.

The Cytofunnel was filled with the cell suspension and centrifuged at 113 x g for 5 min. For further staining, the slides were removed and air dried.

3.6.2 Hematoxylin and eosin staining

After the slides were air dried, hematoxylin and eosin staining with the H&E fast staining kit was performed. First, the slide rack was placed in a hematoxylin bath for 10 min and then rinsed with tap water for 10 min for blueing. For counterstaining it was placed in the eosin solution for 5 min. After that, it was rinsed with distilled water and dehydrated in increasing concentrations of alcohol. For this, the slide rack was placed in 75%, 95% and 100% ethanol baths for 2 min each. The slides were then cleared in two xylene baths for 5 minutes each. Finally, the sample was mounted in Roti Histokitt and analyzed under the microscope ZEISS Axio Imager.

3.7 ELISpot

To compare IgA antibody production between the different CD45/ CD19 PC groups, an ELISpot assay was performed with the cells sorted as described in chapter 3.5.2. For this, a MultiScreen HTS (0.45µm Hydrophobic High Protein) 96-well plate was first coated with 15 µl of 35% ethanol and then washed two times with 200 µl of PBS. 100 µl of unconjugated purified anti-human IgA at a concentration of 5 µg/ ml was added to the wells and the plate was then incubated at 4°C overnight. The next day, wells were washed twice with 200 µl RPMI/ 10% FCS, to remove unbound antibodies. Subsequently, free binding sites were blocked by incubating the wells with 200 µl RPMI/ 10% FCS in a 37°C Co2 cabinet for two hours. During the incubation, 6000 cells per group were sorted in 1200 µl of ELISpot medium. The ELISpot medium consisted of 16 ml RPMI + 2 ml L-glutamine + 2 ml penicillin/ streptomycin. After sorting, the medium was supplemented with 1% β-mercaptoethanol. The plate was emptied, different numbers of cells were added to the wells, as described in Table 8, and incubated overnight in a 37°C Co2 cabinet. After the incubation, wells were washed twice with 200 µl of distilled water and additionally to that three times with PBS + 0,05% Tween. The wells were then incubated with 100 µl of horseradish peroxidase-labeled goat anti-human IgA at a dilution of

1:1000 in PBS/5% FCS for 2 hours at room temperature. This was followed by another washing step in which the wells were washed four times with PBS + 0,05% Tween and an additional 2 times with PBS. To detect the produced IgA antibodies on the membrane, 20 mg of amino-9-ethylcarbazole (AEC) was dissolved in 2,5 ml of dimethylformamide (DMF) and then diluted 1:20 with 50 mM Na-acetate. Each 1 ml of the solution was supplemented with 1 µl of hydrogen peroxide (H2O2), to catalyze the reaction. 100 µl of this substrate solution was added per well and incubated at room temperature for 3 min. To stop the reaction, wells were washed twice with distilled water. The membrane was removed from the plate and dried for 1 hour in a 37°C incubator. The wells were then punched out onto an adhesive plastic sheet, scanned in a high-resolution scanner and analyzed with the QuPath software (version 0.2.3). All individual spots were manually annotated so that the software could specify the number of spots as well as their mean intensity and their mean area.

Table 8: Number of PCs per well in the ELISpot plate

	All IgA$^+$ PC			**CD45$^+$/ CD19$^+$ PC**			**CD45$^+$/ CD19$^-$ PC**			**CD45$^-$/ CD19$^-$ PC**		
	1	**2**	**3**	**4**	**5**	**6**	**7**	**8**	**9**	**10**	**11**	**12**
A	500	500		500	500		500	500		500	500	
B	250	250		250	250		250	250		250	250	
C	125	125		125	125		125	125		125	125	
D	63	63		63	63		63	63		63	63	
E	32	32		32	32		32	32		32	32	

3.8 BCR bulk sequencing of IgA$^+$ PCs

For BCR bulk sequencing 1000 PCs from human small intestine and liver were FACS sorted into RLT buffer (RNeasy Kit) supplemented with 1% β-mercaptoethanol and stored at -80°C, as described in chapter 3.4.2. The processing (RNA isolation, cDNA synthesis and library preparation) of the samples in preparation for sequencing was carried out by Dr. Lydia Kopplin, Institute for Molecular Medicine. Illumina MiSeq sequencing was then performed by the Genomics Facility of the Interdisciplinary Center for Clinical Research (IZKF) Aachen, and the bioinformatics analysis was performed with the help of Fabio Ticconi, bioinformatician, Institute of Molecular Medicine.

First, RNA was isolated using the RNeasy Plus Micro Kit, according to the manufacturer's protocol. For UMI-tagged BCR-specific cDNA synthesis with template switch, an adapted version of the protocol established by Mamedov et al. (Mamedov et al., 2013) was performed using the Template Switching RT Enzyme Mix (NEB). The prepared cDNA was then purified using the MinElute PCR purification kit as described in the manufactures instruction.

Subsequently, the cDNA was amplified in two PCR steps and in a third amplification, the Illumina adaptors and a barcode at the 3' side were incorporated. The protocol used for the PCR amplifications was a modified version of the two established protocols by Mamedov et al. (Mamedov et al., 2013) and Turchaninova et al. (Turchaninova et al., 2016). A different number of cycles were performed depending on the cDNA concentration. After amplification, PCR products were purified using the QIAquick PCR purification kit after the first PCR and agarose gel electrophoresis with gel extraction (Monarch DNA Gel Extraction Kit) after the second and third PCR for size control.

Finally, with the help of the Genomics Facility (IZKF Aachen), the DNA concentration of the prepared libraries was determined using the Tape Station 42000 (Agilent) and all samples were sequenced using an Illumina MiSeq system (MiSeq Reagent Kit v3).

For analysis, PCR-bias and sequencing errors of the UMI-tagged sequences were corrected using the MIGEC pipeline. The UMI-corrected sequences were then aligned with the MiXCR pipeline using IMGT databases as reference. Clonal groups were identified based on identical IGHV/ IGHJ usage and 85% similarity of their CD3 amino acid sequence. Similarities between different samples were determined by applying the Morisita-Horn Index (MHI), a measure for similarity, with 1 indicating that two samples are identical and 0 indicating a completely different repertoire. Circos plots were created using the R package "circlize" to show possible shared clonotypes and their proportion between different samples. For the diversity analysis of the BCR repertoire, the Shannon and inverse Simpson diversity indices were calculated.

4 Results

4.1 Phenotypic analysis of human B-cells in blood, small intestine and liver

4.1.1 Identification of B-cell subsets by spectral flow cytometry

For the phenotypic characterization of human B-cells in the gut-liver axis, B-cells from the small intestine and liver were analyzed using spectral flow cytometry. In previous work a multiparametric panel of 21 markers has been established to allow an in-depth analysis. Since blood is the most accessible site, human B-cells are currently best analyzed in peripheral blood, so we decided to include PBMCs as a reference tissue in the analysis (Kaminski, Wei, Qian, Rosenberg, & Sanz, 2012). Because the marker based identification of B-cell subsets is inconsistent between different reports (Maecker, McCoy, & Nussenblatt, 2012), we carefully considered the current state of knowledge to devise an appropriate gating strategy (Sanz et al., 2019). B-cells from all three tissues were gated in the same way (Figure 5). Live single cells were identified based forward and sideward scatter profiles and further gating to exclude aggregates and dead cells (Figure 5A). Possible contamination with other cell types of the tissues, such as erythrocytes or hepatocytes, was removed using a SSC-H, SSC-H-B plot (Figure 5A). To accurately identify the B-cell subsets, T-cells ($CD3^+$), macrophages and monocytes ($CD14^+$, $CD16^+$) were excluded from analysis (Figure 5A). Since not all PCs in the intestine express the pan-leukocyte marker CD45 or the B-cell marker CD19 (Landsverk et al., 2017), PCs were identified without these markers, as $CD38^{high}$, $CD27^+$, IgD^- cells (Figure 5B). These could then be further characterized by their isotype expression of IgA, IgM or IgG (Figure 5B). According to the different expression of CD45 and CD19, PCs were furthermore divided into the 3 groups: $CD45^+/CD19^+$, $CD45^+/CD19^-$, $CD45^-/CD19^-$ (Figure 5B). Within the non-PC population, remaining B-cells were identified using the CD45 and CD19 expression (Figure 5C). B-cells were then subdivided into naive and memory phenotypes by analysis of the CD27 expression. The subset of MBCs was further divided into non-switched and switched MBCs. This was done on the basis of differential isotype expression, with all $CD27^+$ cells expressing IgM characterized as non-switched MBCs and IgA or IgG expressing $CD27^+$ cells together as switched MBCs (Figure 5C). Within the $CD27^-$ population, NBCs were identified by IgD and IgM expression (Figure 5C). Since

there are also MBCs that do not express the marker CD27 (Fecteau et al., 2006), $CD27^-$ /IgM^- /IgD^-, but IgA^+ or IgG^+ cells were referred to as switched-non conventional (SNC) memory B-cells (Figure 5C). Finally, PCs and B-cells were grouped together and defined as B-cell lineage for further presentation.

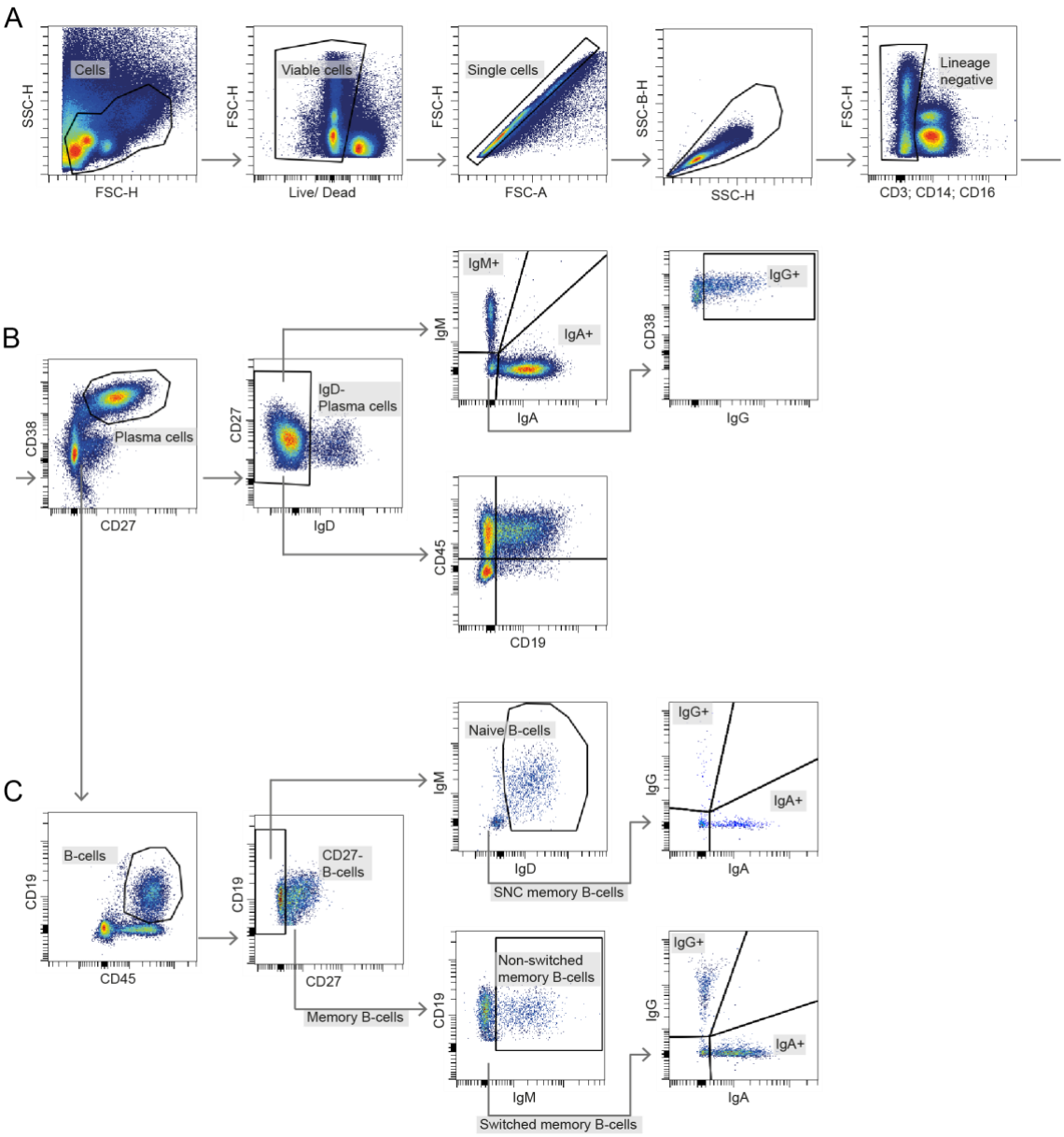

Figure 5: Representative gating strategy to identify different B-cell subsets (intestinal sample as a representative example) **A:** For FACS analysis, cells were pre-gated on cells, viable, singles and lineage negative (T-cells, monocytes, macrophages). In addition, leukocytes were distinguished from other cell types such as erythrocytes and hepatocytes using a SSC-H/ SSC-B-H plot **B:** PCs were identified as $CD38^{high}$/$CD27^+$ and IgD^- cells. These were further categorized based on their isotype and the different expression of CD45 and CD19. **C:** Within the non-PC population, B-cells were gated using $CD45^+$ and $CD19^+$. CD27 was used as the main marker to distinguish MBCs. Based on the isotypes, these were further divided into non-switched MBCs (IgM^+) and switched MBCs (IgA^+ or IgG^+). NBCs were identified as $CD27^-$ and IgM^+/IgD^+ cells. $CD27^-$ cells expressing IgA or IgG were defined as switched-non conventional (SNC) MBCs. PCs: plasma cells; MBCs: memory B-cells; NBCs: naive B-cells.

4.1.2 B-cell subsets are distributed differently in the blood, small intestine and liver

Our results on the distribution of B-cell subsets and their isotype expression in peripheral blood are consistent with previous literature (Blanco et al., 2018; Morbach, Eichhorn, Liese, & Girschick, 2010), validating our staining and gating strategy. The B-cell population in peripheral blood was dominated by NBCs, which accounted for 59.6 ± 9.05%, followed by MBCs, which constituted 33.83 ± 7.91% (Figure 6A). In addition to conventional MBCs, we also found switched-non-conventional MBCs with a frequency of 4.13 ± 1.21%. As expected, plasma blasts were rarely detected (0.98 ± 0.75%) (Figure 6A).

In contrast to blood, PCs dominated the B-cell population in the small intestine with a proportion of 87.58 ± 16.26% (Figure 6A). The remaining B-cells consisted mainly of MBCs and SNC-MBCs, which together accounted for approximately 10% (Figure 6A). Only a few B-cells isolated from the small intestine showed a naive phenotype (2.4 ± 4.66 %) (Figure 6A).

In general, we found fewer B-cells in the liver than in the other two compartments but, interestingly, the distribution of B-cell subsets in the liver differed from that in both, the blood and the small intestine. We noticed a more heterogeneous distribution of NBCs, MBCs and PCs, with NBCs representing the largest subpopulation (32.46 ± 12.79%) (Figure 6A). PCs and MBCs accounted for 19.88 ± 8.038% and 20.57 ± 11.24%, respectively (Figure 6A). The proportion of PCs in the liver was clearly lower than that of PCs in the small intestine, but still greater than in the peripheral blood. MBCs that were not conventional were also observed in the liver, where they accounted for the smallest proportion of B-cells (6.6 ± 3.15%) (Figure 6A).

Upon further characterization of PCs, we found that IgA was the dominant surface isotype in all three tissues (blood: 55.2 ± 10.32%; small intestine: 80.43 ± 7.712; liver: 21.91 ± 9.1%) (Figure 6B). Additionally, IgG accounted for the lowest proportion in all three compartments, with a particularly low fraction in the small intestine (1.51 ± 1.41%) (Figure 6B). In blood and liver, the frequency of IgG^+ PCs was rather similar with approximately 9% in both tissues (Figure 6B).

In line with previous work (Landsverk et al., 2017), we found that compared with blood, not all PCs in the small intestine expressed the markers CD45 or CD19 and that they could be divided into three groups based on their expression: $CD45^+/CD19^+$, $CD45^+/CD19^-$ and $CD45^-/CD19^-$ (Figure 6B). Interestingly, we observed that PCs from the liver, like those from the small intestine, did not all express CD45 or CD19 and could also be divided into the three groups with a similar distribution (Figure 6B).

Subsequently, we analyzed the subset of MBCs in more detail. We found that there were more switched than non-switched MBCs in both the small intestine and the liver (small intestine: 72.54 ± 11.71%; liver: 65.91 ± 17.59%) (Figure 6C). In comparison, switched and non-switched MBCs were approximately equally distributed in blood with a proportion of 54.6 ± 12% and 45.4 ± 12%, respectively (Figure 6C). In the small intestine, the IgA isotype dominated among the switched MBCs (Figure 6C). The distribution between IgA and IgG was approximately equal in the blood, but in contrast, we observed that in the liver, most of the switched MBCs were IgG^+ (Figure 6C). $CD27^-$ MBCs were found in all three organs, again dominated by the IgA isotype in the small intestine (82.23 ± 14.62%) and the IgG isotype in both blood and liver (blood: 62.2 ± 9.53%; liver: 70.03 ± 12.64%) (Figure 6C).

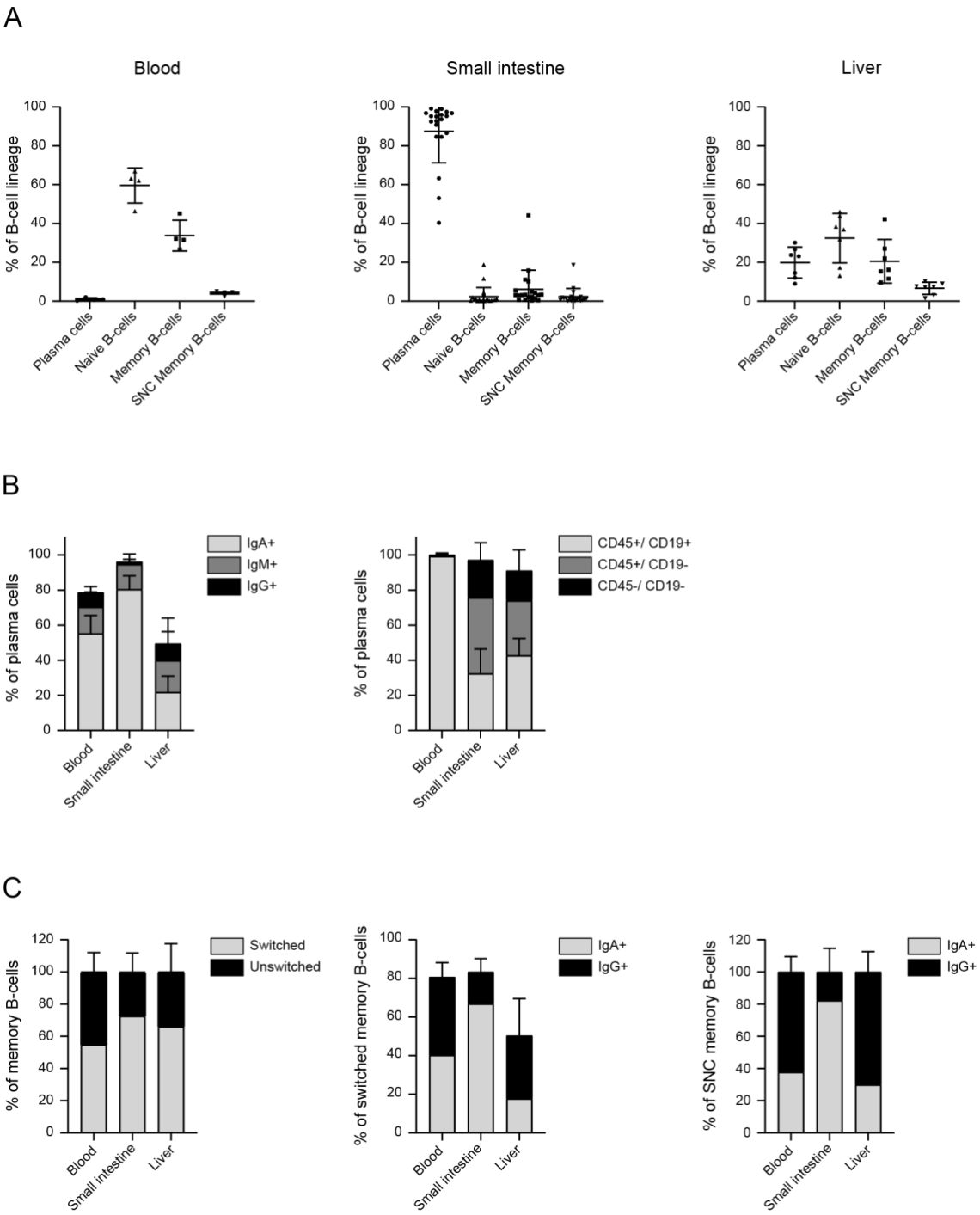

Figure 6: Differences in the B-cell subset distribution and isotype expression in blood, small intestine and liver A: Frequencies of B-cell subsets among total B-cells in blood (left panel), small intestine (middle panel) and liver (right panel). B-cell lineage: PCs and B-cells, gated as shown in Figure 5. **B:** Isotype distribution (left panel) and CD45/ CD19 expression (right panel) of PCs in the three tissues. **C:** Frequencies of switched and non-switched MBCs of total MBCs (left panel). Isotype distribution of switched- (middle panel) and SNC- (right panel) MBCs in blood, small intestine and liver. Data are shown as mean ± SD. PCs: plasma cells; MBCs: memory B-cells; SNC: switched non-conventional.

4.1.3 Dimensionality reduction analysis of B-cells in blood, small intestine and liver

In order to perform a more accurate analysis and visualization of the large number of parameters generated, we decided to apply the Uniform Manifold Approximation and Projection (UMAP) dimensionality reduction algorithm. For this purpose, cells were first pre-gated on B-cell lineage, as shown in Figure 5, and then all samples from one tissue were combined. For the use of the algorithm, we adjusted the number of B-lineage cells in each sample, so that all samples were represented proportionally (Chapter 3.4.3). Using UMAPS, we obtained a good first overview of possible interesting differences in marker expression in the different B-cell subsets of the three tissues. In further analysis steps, we elaborated on these observations.

For phenotypic analysis of B-cells in peripheral blood, we overlaid the manually gated B-cell subsets with the UMAP. Clusters formed by UMAP were mostly congruent with the manually gated subpopulations. NBCs, switched MBCs and PCs were clearly segregated into their own clusters, but non-switched MBCs were clustered together with NBCs, probably due to the similar expression of IgM and IgD (Figure 7A). In addition, cluster sizes differed between PCs, NBCs and MBCs, which was consistent with the distribution of B-cell subsets in blood shown previously (Figure 7A). Different isotype expression within PCs and MBCs also resulted in the formation of clusters (Figure 7A).

The first thing we noticed when plotting the individual markers on the UMAP projection and heat map were the clear differences in the expression of the key markers of the individual B-cell subsets, such as CD45, CD19, CD38, CD27 and the isotypes (Figure 7B-C). Consistent with the literature, we also found that PCs expressed less CD19 and did not express CD20 or BAFFR compared with other B-cell subsets (Glass et al., 2020) (Figure 7B-C). In contrast, all PC subsets appeared to express more Integrin beta 1 and the CCR9 expression was also higher in the PC subpopulations than in the NBCs and MBCs (Figure 7C). Additionally, the expression of the activation marker CD80 appeared to be increased in PCs and switched MBCs compared with NBCs and non-switched MBCs (Figure 7C).

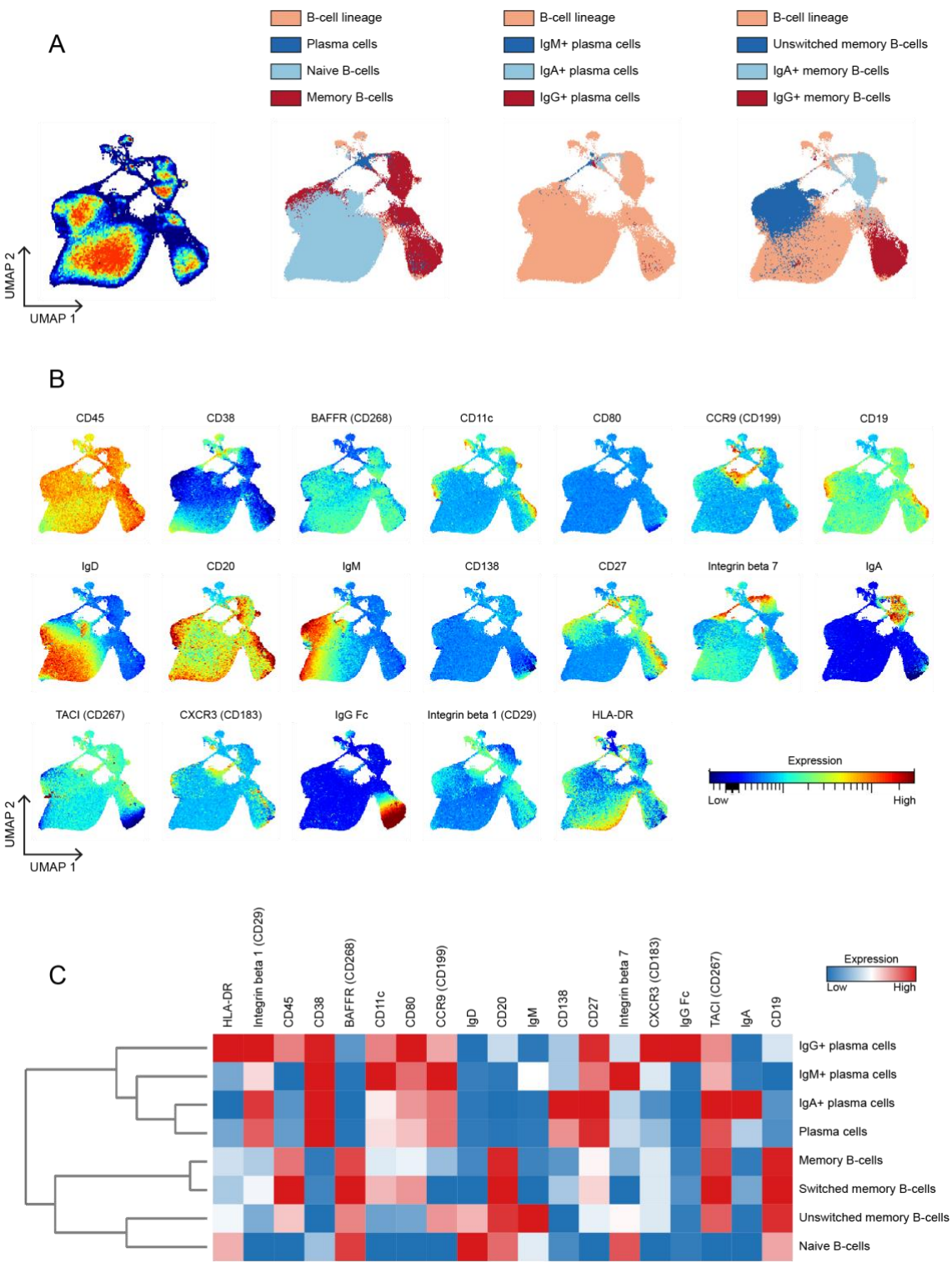

Figure 7: High-dimensional flow cytometry analysis of human B-cells in peripheral blood B-lineage cells from PBMCs of 4 donors were concatenated and visualized using dimensionality reduction. **A:** UMAP projection of B-cell lineage, combining all samples (left panel). Identification of the manually gated B-cell subsets and their isotype expression (gated as shown in Figure 5) by overlaying them with the automatically generated clusters in the UMAP (panel 2-4). **B:** Visualization of the individual marker expression within the UMAP clusters **C:** Heatmap showing the median marker intensities of the B-cell subsets (gated as shown in Figure 5). The dendogram on the left illustrates the similarity between the different subpopulations. UMAP: Uniform Manifold Approximation and Projection.

We then proceeded in the same way with the analysis of B-cells in the small intestine and liver. Again, we detected clustering in UMAPs in both organs that was consistent with our manually gated populations (Figure 8A; Figure 9A). In the small intestine, we could clearly see the separation between PCs and other B-cell subsets (Figure 8A). PCs were further divided into two groups based on their IgA and IgM isotype, including IgG^+ PCs in the IgA cluster (Figure 8A). Interestingly, no clusters were formed based on the different CD45/ CD19 expression. The clusters reflected well the proportions of the different subsets and clearly showed the dominance of IgA^+ PCs in the human small intestine (Figure 8A). The UMAP of the liver samples, did not demonstrate major differences from the other two tissues. PCs, NBCs and MBCs were mostly separated (Figure 9A). Non-switched MBCs were grouped together with the NBCs and the isotypes of switched MBCs formed their own small clusters (Figure 9A). However, the PCs were not subdivided, neither by isotype nor by CD45/CD19 groups (Figure 9A).

Similar to the blood samples, we first detected the high expression of the key markers of each B-cell subset in both organs in the UMAPS as well as in the heatmaps. Especially the expression of CD38 was clearly evident in the PC clusters in both small intestine and liver (Figure 8B; Figure 9B). CD45 and CD19 formed a gradient across the PC clusters of both organs, which was not the case in the peripheral blood B-cells (Figure 8B; Figure 9B). Furthermore, the UMAPs and even more clearly the heatmaps indicated that PCs in both organs did not express CD20 or BAFFR (Figure 8B-C; Figure 9B-C). This was an additional confirmation that the gated population most certainly consisted of PCs. Similar to blood, PCs from both organs appeared to express more Integrin beta 1 and more CCR9 than other B-cell subsets (Figure 8B-C; Figure 9B-C). Interestingly, comparison of the two UMAPS from small intestine and liver showed that more PCs from small intestine expressed CCR9 than PCs from liver (Figure 8B; Figure 9B). As previously noticed in the blood samples, there also seemed to be a difference in the expression of CD80 between the PCs and the other B-cell subsets in the heat map of the small intestine (Figure 8C). However, on the UMAP all clusters displayed the same expression level, so further analysis of these data was performed.

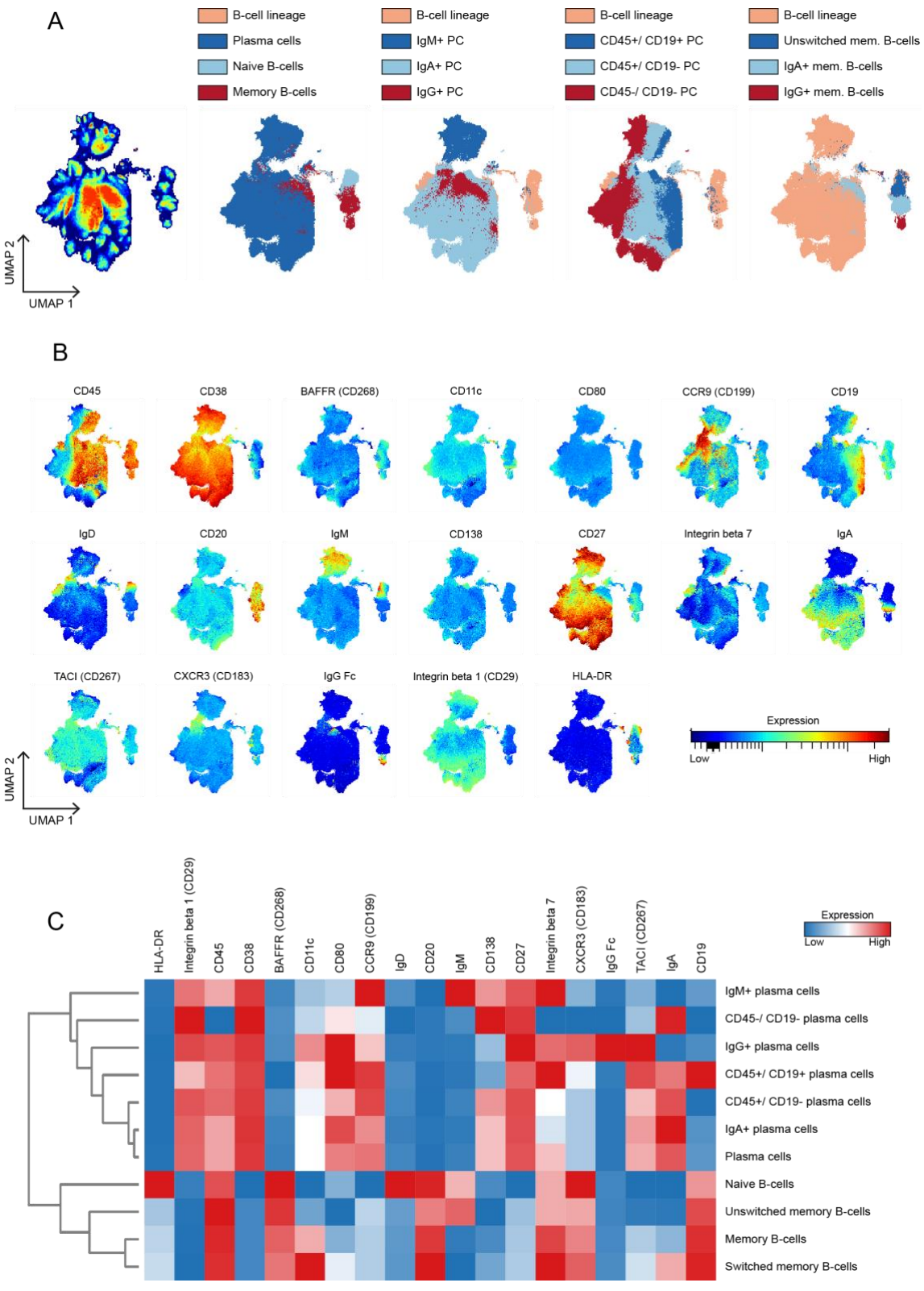

Figure 8: High-dimensional flow cytometry analysis of human B-cells in the small intestine B-lineage cells from small intestine of 22 patients were concatenated and visualized using dimensionality reduction. **A:** UMAP projection of B-cell lineage, combining all samples (left panel). Identification of the manually gated B-cell subsets (gated as shown in Figure 5) by overlaying them with the automatically generated clusters in the UMAP (panel 2-4). **B:** Visualization of the relative surface marker expression within the UMAP clusters **C:** Heatmap showing the median marker intensities of the B-cell subsets (gated as shown in Figure 5). The dendogram on the left illustrates the similarity between the different subpopulations. UMAP: Uniform Manifold Approximation and Projection.

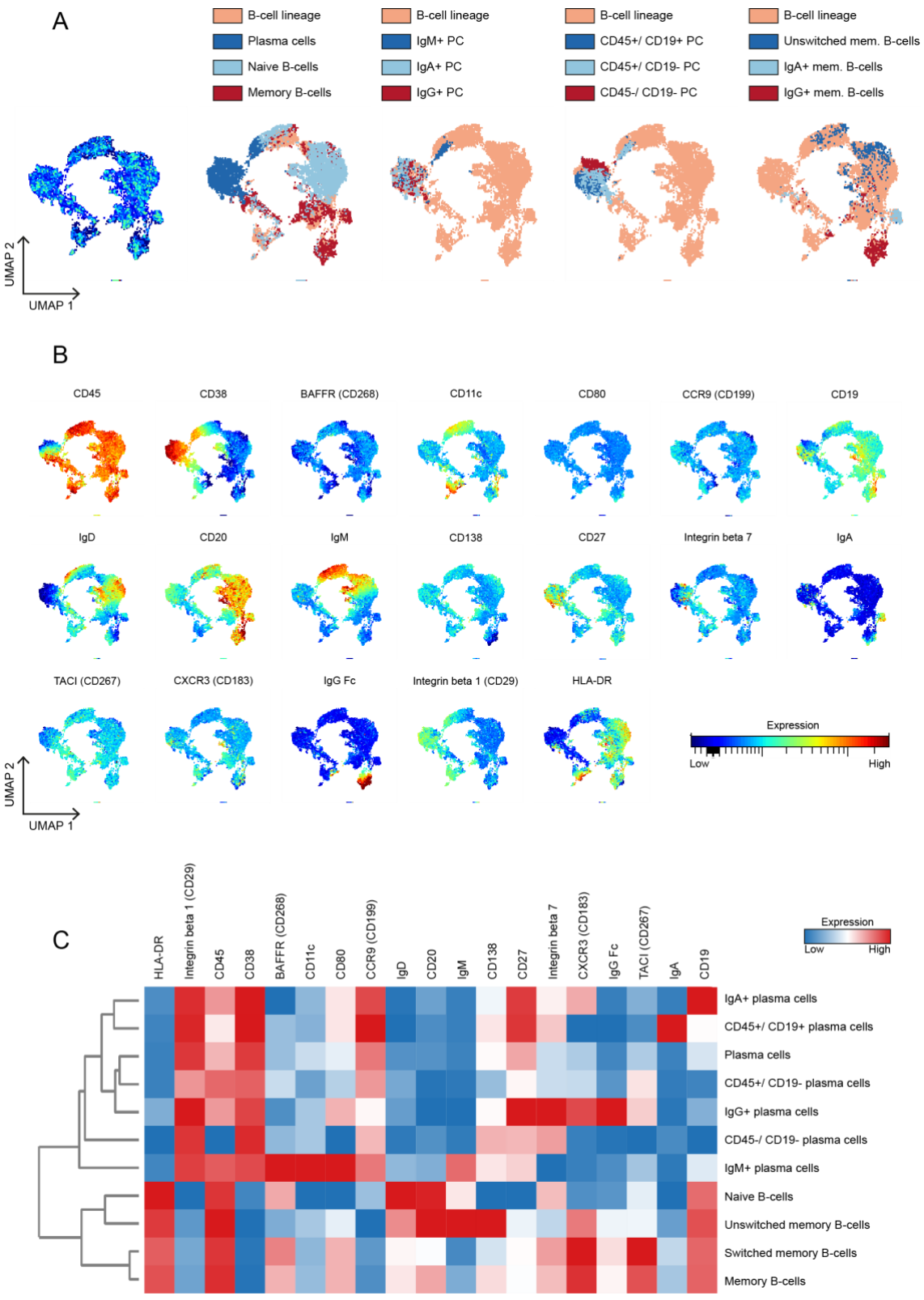

Figure 9: High-dimensional flow cytometry analysis of human B-cells in the liver B-lineage cells from the liver of 7 patients were concatenated and visualized using dimensionality reduction. **A:** UMAP projection of B-cell lineage, combining all samples (left panel). Identification of the manually gated B-cell subsets (gated as shown in Figure 5) by overlaying them with the automatically generated clusters in the UMAP (panel 2-4). **B:** Visualization of the relative surface marker expression within the UMAP clusters **C:** Heatmap showing the median marker intensities of the B-cell subsets (gated as shown in Figure 5). The dendogram on the left illustrates the similarity between the different subpopulations. UMAP: Uniform Manifold Approximation and Projection.

In order to analyze the previously made observations in more detail, we created overlaid contour plots of the respective markers. Using these plots, we were able to see the actual differences in the expression levels additionally to the statistical values. For this purpose, we combined all samples from one tissue and overlaid the PC and the B-cell populations, which were gated as shown in Figure 5. For quantitative analysis, we compared the median fluorescence intensities (MFI) of the mentioned markers within the three populations of PCs, NBCs and MBCs.

First, we confirmed that PCs in all three tissues did not express CD20 and BAFFR compared with the other B-cell subsets (Figure 10A-B) . In addition, we noticed that both NBCs and MBCs in the liver expressed less BAFFR than B-cells in the blood and small intestine (Figure 10A-B). Similar to the CD20 and BAFFR expression, we found that HLA-DR expression was significantly lower in PCs than in other B-cell subsets (Figure 10C). This was most evident in the small intestine and liver samples. In the contour plot of the blood samples, we could observe that some of the PCs expressed HLA-DR, suggesting that these might be circulating, newly formed plasma blasts which we could not detect in the tissue-resident PC populations (Figure 10D). We also found differences in the expression of the homing factors CCR9 and integrin beta 1 between the subsets (Figure 10D-E). Consistent with the previously described function of the chemokine receptor CCR9 in gut-homing of PCs (Pabst et al., 2004), we also observed that PCs from blood and small intestine expressed more CCR9 than NBCs and MBCs (Figure 10D). However, this increased expression was not observed in the liver samples (Figure 10D), suggesting that another marker might be involved in the homing of PCs to liver tissue. Interestingly, we also found that the integrin beta 1 expression was increased in PCs of the three tissues compared with the other B-cell subsets (Figure 10E). This result may indicate that integrin beta 1 could play a more important role in PC migration than in the other B-cell subsets. Analyzing the expression of CD80 and TACI, we noted that these markers were not expressed in all B-cell subsets and tissues (Figure 10F), which was most likely due to inefficient staining. Therefore, these markers were not considered in further analyses.

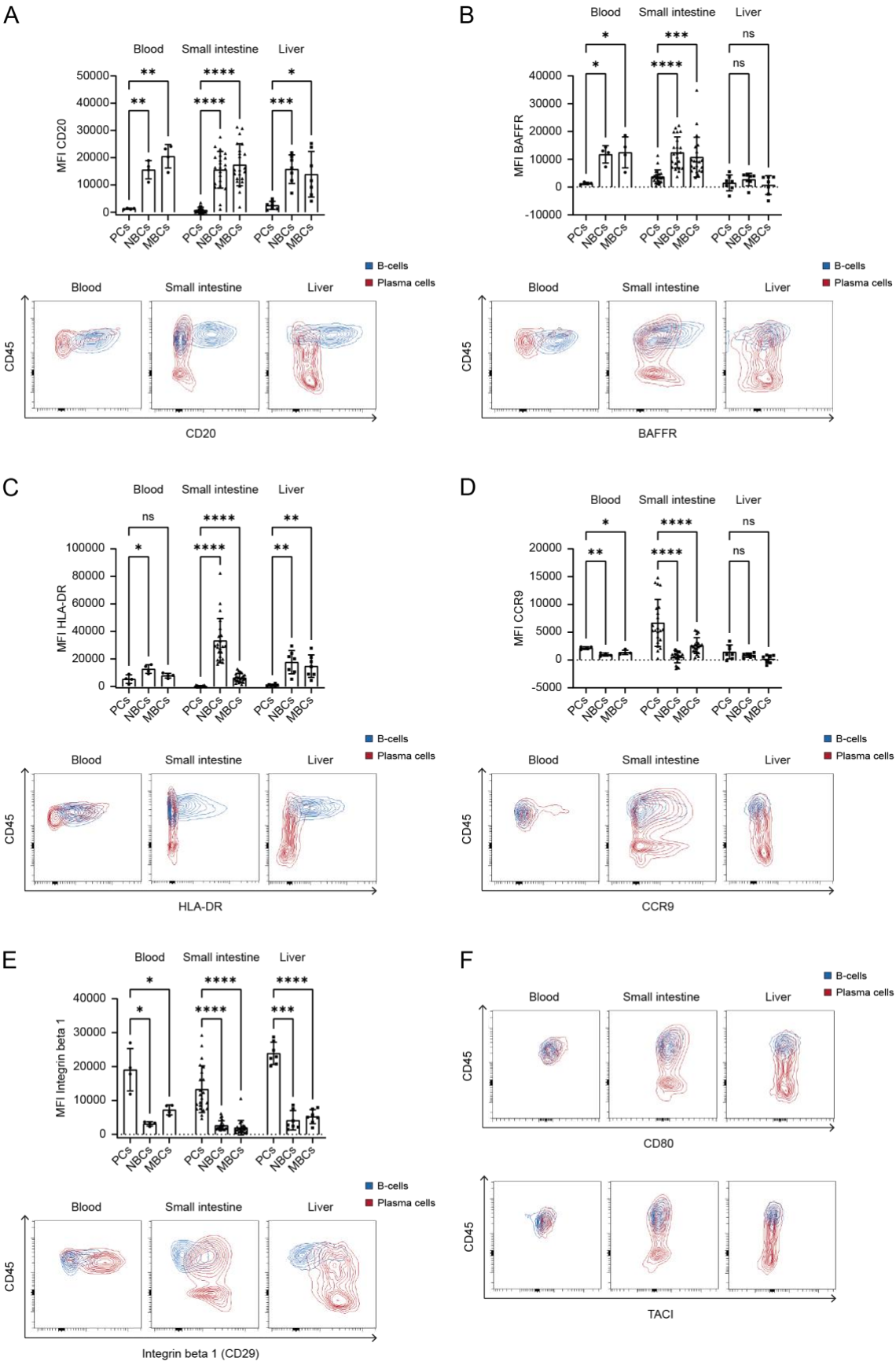

Figure 10: Comparison of surface phenotypic characteristics of PCs and other B-cell subsets in blood, small intestine and liver The expression levels of various markers of PCs, NBCs, and MBCs were analyzed using contour plots and median fluorescence intensity in blood, small intestine and liver. For the contour plots, all samples from one tissue were combined and the PC and B-cell populations (NBCs and MBCs),

gated as shown in Figure 5, were overlaid. Analysis was performed for the markers **A:** CD20, **B:** BAFFR, **C:** HLA-DR, **D:** CCR9, and **E:** Integrin beta 1. **F:** Contour plots of CD80 and TACI revealed that these markers were not expressed in all subsets and tissues, most likely due to inefficient staining, so they were not considered in further analysis. Statistical comparisons were performed using two-way ANOVA with Sidak´s multiple comparison test (*P < 0.05, **P < 0.01, ***P < 0.001, ****P < 0.0001, ns: not significant). Data are shown as mean ± SD. MFI: median fluorescence intensity; PCs: plasma cells; MBCs: memory B-cells; NBCs: naive B-cells.

4.1.4 Phenotypic and functionality analysis of different CD45/ CD19 PC subsets

As previously described, human PCs from the small intestine, but not from the blood, show differential expression of the markers CD45 and CD19. Consistent with previous work (Landsverk et al., 2017), we also observed this differential expression and divided the PC population into three distinct groups: $CD45^+/ CD19^+$, $CD45^+/ CD19^-$, $CD45^-/ CD19^-$ (Figure 11A). Interestingly, we also detected all three CD45/ CD19 PC subsets in human liver (Figure 11A). Unfortunately, due to the small amount of PCs in the liver, it was not possible to FACS-sort the different CD45/ CD19 PC subsets or to perform further analyses on the respective subpopulations. For this reason, we decided to include only PCs of the small intestine in the following analyses. First, we compared the morphological characteristics of the different PC subpopulations (Figure 11B). For this purpose, we performed FACS-sorting of the CD45/ CD19 PC subsets as described in Figure 4, transferred the cell suspensions to glass slides using a CytoSpin centrifuge and stained the cells with hematoxylin and eosin. In morphological comparison, we could not detect any differences between the PC subpopulations (Figure 11B). In addition to phenotypic analysis, we were also interested in the functionality of the respective CD45/ CD19 subsets. Therefore, the IgA production of the sorted CD45/ CD19 groups was compared using an ELISpot assay. Based on the detected spots on the ELISpot membrane, we could determine how many of the added PCs produced IgA. For analysis, the membrane was scanned with a high-resolution scanner and the scans were analyzed using the software QuPath. The individual spots were all manually annotated, so that in addition to the number, we could obtain information on the mean intensity and mean area per spot. This information was of interest to us because it allowed us to determine whether there was a difference in the amount of IgA produced by the PCs between the groups. Based on our analysis, we found that all three subsets contained the same amount of producing cells and that these cells also showed the same amount of IgA production (Figure 11C). These results indicated that there were no morphological, as well as no functional differences, in terms of IgA production, between the groups.

However, we noticed differences in the expression of CD45 and CD19 between the isotype subgroups of PCs from the small intestine (Figure 11D-E). We were able to observe this using an overlaid histogram of the expression of CD45 in the individual isotype subgroups and also in the corresponding contour plots (Figure 11D). We found that IgG$^+$ PCs in the small intestine consisted of a significantly lower proportion of the CD45$^-$/ CD19$^-$ subset compared to the IgM$^+$ PCs (Figure 11D-E). PCs with a CD45$^-$/ CD19$^-$ phenotype are thought to be long-lived PCs in the intestine (Lindeman et al., 2021), so our results suggest that IgG$^+$ PCs contribute to this population to a lesser extent.

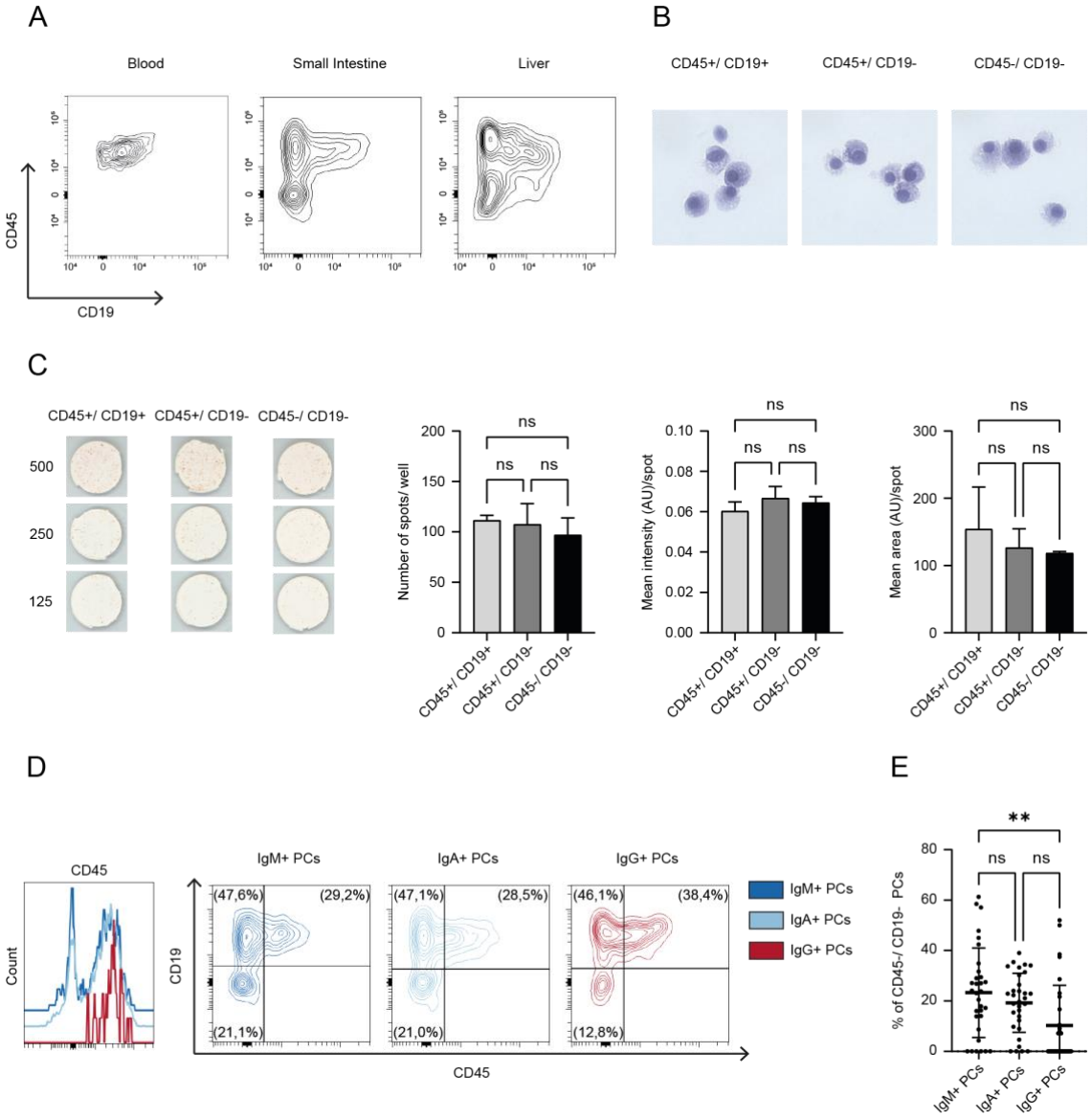

Figure 11: Phenotypic and functionality analysis of the different CD45/ CD19 PC subpopulations **A:** Contour plots of concatenated blood, small intestine and liver samples demonstrate CD45 and CD19 expression of PCs in each organ. **B:** Microscopic images of the different CD45/ CD19 PC subsets from the small intestine sorted by FACS (as described in Figure 4). **C:** Comparison of IgA production in the three CD45/ CD19 PC subsets (FACS-sorted as described inFigure 4) from the small intestine using ELISpot Assay (left panel). Analysis was performed of wells that were filled with 125 IgA$^+$ PCs using the software QuPath.

For the analysis the number of spots per well (left panel), the mean intensity per spot (middle panel) and the mean area per spot (right panel) were compared. **D:** Comparison of CD45 expression of PCs with different isotypes using an overlaid histogram and contour plots combining 20 small intestine samples. **E:** Quantitative analysis of the frequency of the CD45/ CD19 PC subsets in different isotype PC subsets. Statistical comparisons were performed using one-way ANOVA with Tuckey's multiple comparison test (**P < 0.01, ****P < 0.0001, ns: not significant). Data are shown as mean ± SD. PCs: plasma cells; FACS: Fluorescence-activated cell sorting; ELISpot: Enzyme Linked Immuno Spot Assay.

4.1.5 PCs from small intestine and liver differ in phenotypic characteristics

For subsequent analyses, we focused on direct comparison of IgA^+ PCs in the human gut-liver axis. Again, we started with a dimensionality reduction analysis. To determine if there were any phenotypic differences between PCs in the liver and small intestine in general, UMAP analysis was performed for PCs of both organs together (Figure 12A). Since clusters in UMAPs are formed based on the similarity of marker expression, different clusters can be expected to have distinct phenotypic profiles. We noticed that in the UMAP of the combined samples, liver and small intestinal PCs were clustered separately (Figure 12A), suggesting that there should be variations in surface phenotype. Because of the seperate clustering in the UMAP, we then examined the expression of each marker using overlaid histograms of IgA^+ PCs from both organs (Figure 12B). The greatest deviations in histograms we observed were in the expression of IgA, CCR9 and integrin beta 1 (Figure 12B). As shown in the results previously, IgA is a very dominant isotype of gut resident PCs, so the difference in the expression level was not surprising. To confirm the observations of differences in CCR9 and integrin beta 1 expression, we then performed statistical analysis of the MFI of the two markers in IgA^+ PCs (Figure 12C). For additional visualization, we also plotted CCR9 and integrin beta 1 in an overlaid contour plot comparing both organs (Figure 12C). Consistent with the previous results, we found that IgA^+ PCs from the small intestine expressed significantly more CCR9 than PCs from the liver (Figure 12C). Interestingly, the integrin beta 1 expression was significantly higher in IgA^+ PCs from the liver (Figure 12C). However, in comparison, IgA^+ PCs from both organs expressed little integrin beta 7, and there was no difference in this regard (Figure 12C). These results suggest that liver PCs, unlike small intestinal PCs, do not migrate into their tissue because of CCR9 expression, but that integrin beta 1 might play a role in the migration of PCs into the liver.

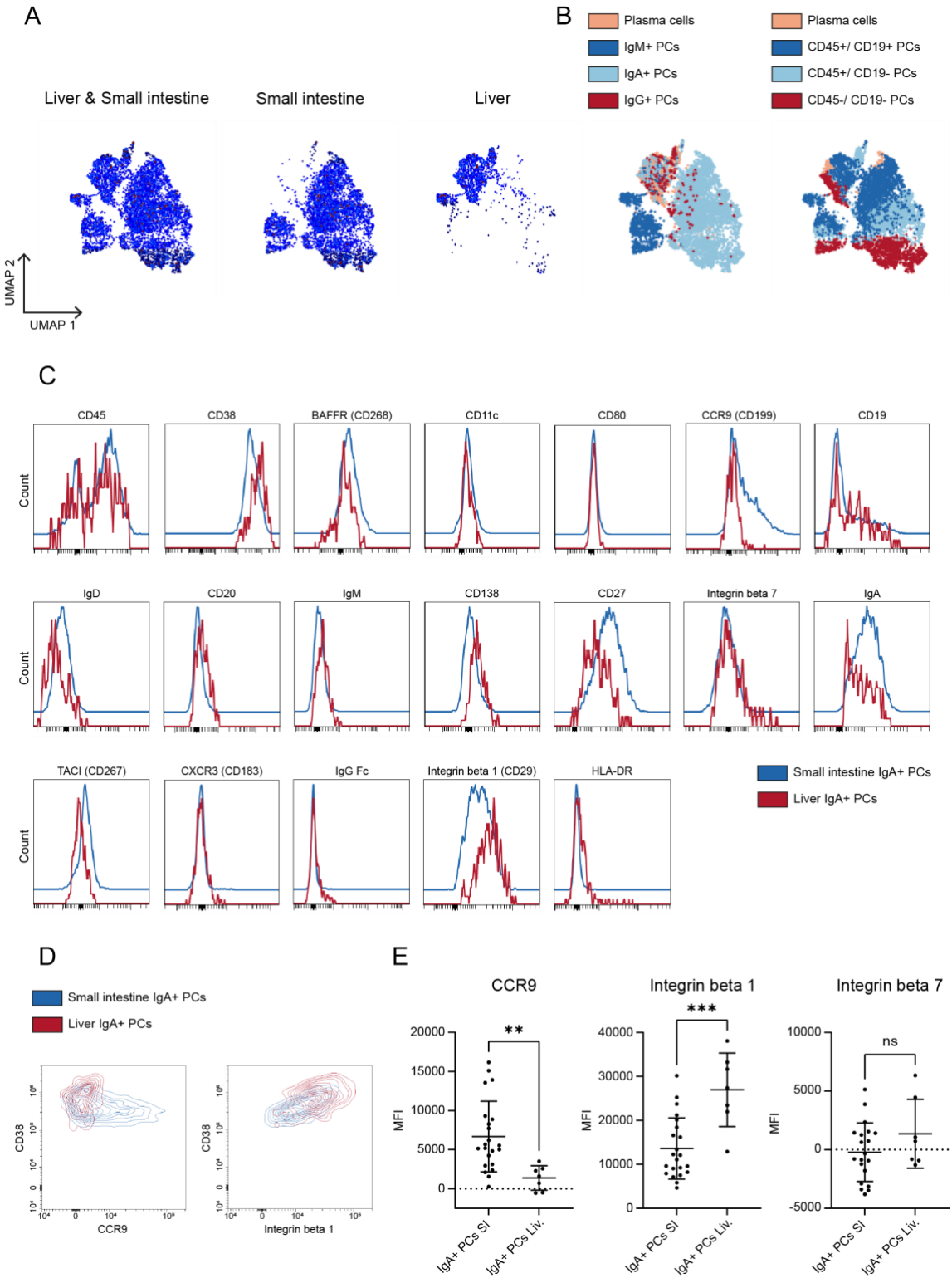

Figure 12: Comparison of the phenotypic characteristics of PCs from small intestine and liver A: UMAP analysis was performed for PCs combing all small intestinal and liver samples. Visualization of the UMAP plots for both organs (left panel) or separately for the respective tissues (middle and right panels). **B:** Identification of manually gated PC subsets (gated as shown in Figure 5) by overlaying them with the automatically generated clusters of the UMAP. **C:** Using overlaid histograms summarizing all samples, expression levels of various markers were compared in IgA$^+$ PCs from both tissues. **D:** Representation of the CCR9 and integrin beta 1 expression in small intestinal and liver IGA$^+$ PCs using overlaid contour plots. **E:** Quantitative analysis of the CCR9, integrin beta 1 and integrin beta 7 expression of IgA$^+$ PCs from both organs. MFI of these markers were compared with unpaired ordinary t-tests (**P <0.01, ***P <0.001, ns:

not significant). UMAP: Uniform Manifold Approximation and Projection; MFI: median fluorescence intensity; PCs: plasma cells; SI: small intestine; Liv.: Liver.

4.2 Comparative analysis of the BCR repertoire in the human gut-liver axis

Each B-cell expresses its own BCR, resulting in a high diversity of BCRs in an individual, known as the BCR repertoire. This repertoire is unique to every individual. Focusing on the comparison of PCs from human small intestine and liver, we were not only interested in phenotyping but also in characterizing the PC repertoire of those organs. From the comparative analysis of the BCR, the diversity and the usage of V- and J-gene segments, we aimed to understand more about the spatial heterogeneity of the PC repertoire in the gut-liver axis.

In addition, previous work suggested that IgA^+ PCs in the liver derived from intestinal Peyer´s patches and that these showed reactivity to commensal bacteria. The antibodies produced in the liver could contribute to the defense against antigens from the gastrointestinal system that enter the liver via the portal circulation (Moro-Sibilot et al., 2016). Therefore, we suspected a clonal relationship between gut and hepatic PCs and investigated this by BCR bulk sequencing of IgA^+ PCs from small intestinal and liver samples of the same individuals.

For BCR sequencing, 1000 PCs from cell suspensions of matched tissues from 5 patients were FACS sorted as described in chapter 3.5.2. After RNA isolation, UMI-tagged BCR-specific cDNA was synthesized, followed by several PCR amplification steps and Illumina library preparation. Libraries were sequenced and then PCR bias and sequencing errors were bioinformatically corrected using the MIGEC pipeline. Thereafter, clonal groups (clonotypes) were defined based on identical usage of IGHV/ IGHJ and 85% similarity of their CDR3.

We first started our analysis by comparing the distribution of PC clonotypes in the small intestine and liver. For this purpose, we ranked the identified clonotypes according to their frequency and displayed the 25 most abundant ones using two different plots (Figure 13A). While one shows the frequency of each clonotype according to its rank, the other displays the cumulative proportion in the total sequenced repertoire (Figure 13A). In both organs, the highest ranked clonotype constituted a large proportion of the

total repertoire (about 12 and 17%, respectively) (Figure 13A). Similarly, we found that the first 20 clonotypes accounted for a large fraction of the liver and small intestine PC repertoire (about 40% and 60%, respectively) (Figure 13A). However, for a direct comparison of the distribution, it should be considered that only 1000 PCs were sorted and sequenced and that the proportion of IgA^+ PCs is lower in the liver than in the small intestine. Thus, the number of BCRs sequenced in both tissues was not exactly the same. Despite this, we observed that the distribution of clonotypes of the PC repertoire in both organs was generally similar.

The BCR genes consist of variable (V), diverse (D), junctional (J) and constant (C) gene segments. To compare the usage of the V and J gene families and to determine whether there are preferences for the gene segments in the two organs, we analyzed the frequency of 13 gene segments (Figure 13B). We observed that the most abundant V segments were IGHV-4 and IGHV-3 (Figure 13B), and the most frequent J gene segment was IGHJ-4 (Figure 13B). In the statistical comparison, we found that PCs from both organs showed the same abundance of V and J gene usage with no significant differences.

Next, we were interested in determining whether the PC repertoire of one organ was more diverse than that of the other. For this, we used the two different diversity indices Shannon and inverse Simpson diversity index, with the higher the value the more diverse the samples (Figure 13C). We found no significant differences in diversity with slight tendencies toward increased diversity in the small intestine (Figure 13C), but again it should be noted that this trend could also be due to the smaller liver sample size. In general, the diversity of the PC repertoire seemed to be the same in both tissues.

Finally, we investigated whether our hypothesis of shared clones between gut and liver samples would be confirmed. We analyzed the similarity of the samples by determining common clonotypes in the samples using the Morisita-Horn similarity index (MHI) (Figure 13D). A value of 1 indicates that 2 samples are composed of exactly the same clones, while a MHI of 0 means that the samples do not share a single clone. In the heatmap showing the MHI of all samples compared, we could already see that there was no similarity between the paired samples (Figure 13D). Plotting the individual MHI values also confirmed this observation, as the MHI between paired samples was close to zero (Figure 13D). Circos plots can be used to obtain even more accurate

representations of possible shared clones, with the thickness of the arcs indicating the proportion and the position in the outer black ring the size of the common clonotype. Although we were able to detect single shared clonotypes in some samples using the circos plots, these were rather small and sporadic and have not been represented in the MHI (Figure 13E). Thus, our results suggested that the PC repertoire in the small intestine and liver, although very similar in terms of distribution and diversity, was distinct with only very few clones in common, suggesting that IgA^+ PCs in the liver and small intestine do not originate from a common source.

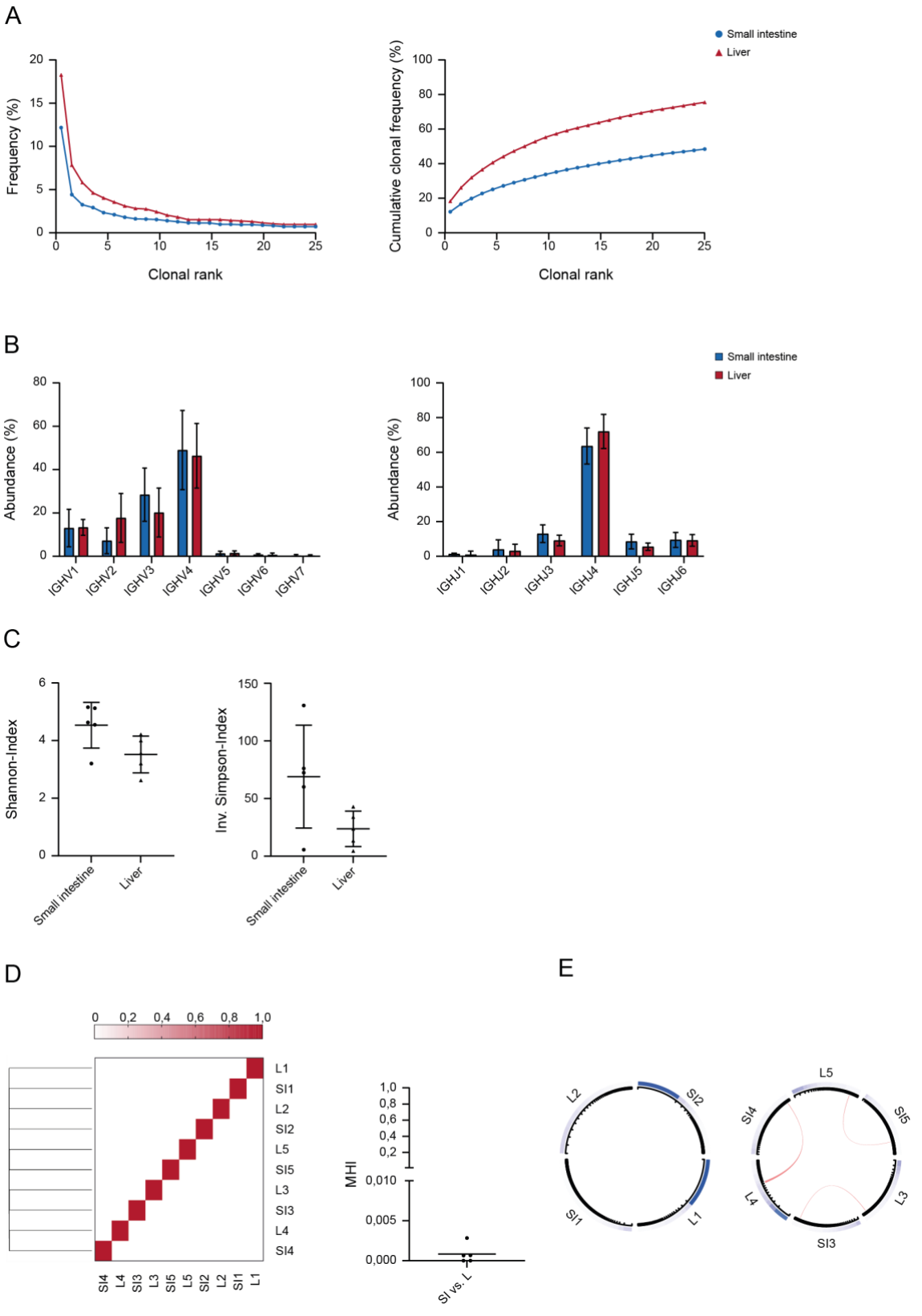

Figure 13: PC repertoires in human small intestine and liver are distinct, despite similarities in clone distribution and diversity The IgA⁺ PC repertoire of human small intestine was compared with that of the liver. For BCR sequencing 1000 PCs of matched tissue samples from 5 patients were FACS sorted (as described in Figure 4) **A:** For the representation of the clonotype distribution, the clonotypes were ranked according to their frequency in the repertoire. Frequency of each ranked clonotype (left panel) and the cumulative proportion of the ranked clonotypes in the repertoire (right panel). Data are shown as mean of the summarized 5 samples per organ. **B:** IGHV and IGHJ-gene family usage of PCs from 5 samples per organ. Statistical comparisons were performed using two way ANOVA with Sidak´s multiple comparison

test. No significant differences were detected. **C:** Comparison of the PC repertoire diversity in small intestine and liver using the Shannon index (left panel) and inverse Simpson index (right panel). Data are shown as mean ± SD. Statistical comparisons were performed using ordinary unpaired t-test. No significant differences were detected. **D:** Similarity of PC repertoires in small intestine and liver was compared using the MHI. The heatmap (left panel) shows the respective values between all samples, with samples being hierarchically clustered using linkage clustering. Representation of individual MHI values between matched liver and small intestine samples using a dot plot. Data are shown as mean ± SD. **E:** Circos plots indicating possible shared clonotypes between the matched small intestine and liver samples. Single shared clonotypes between the matched samples 3-5 are represented by red arcs. The thickness indicates the proportion and the position on the black outer ring indicates the size of each clonotype. BCR: B-cell receptor; MHI: Morisita-Horn index; SI: small intestine; L: liver; PC: plasma cell.

4.3 Analysis of the role of small intestinal B-cells in different stages of NAFLD

NAFLD is a condition in which accumulated fat in the liver leads to inflammation and its development and progression is associated with deregulation of the gut-liver axis (Albillos et al., 2022). It is thought, that dysbiosis and an increased permeability of the intestinal membrane could trigger an inflammatory response in the liver (Jiang et al., 2015). To investigate the possible involvement of B-cells in the gut, we analyzed small intestinal samples from patients diagnosed with NAFLD at different stages (Figure 14). For this purpose, we again performed both phenotypic and BCR repertoire analyses (Figure 14). Based on the pathological NAS of the liver biopsies, we classified the small intestinal samples into three stages of progression of NAFLD (Kleiner et al., 2005). Samples in which the associated liver biopsies revealed a NAS of 0-2 were defined as stage one: NAFL (Figure 14). At a NAS of 3-4, samples were classified into the Borderline NASH group, a stage that represents the transition to the third category: NASH (Figure 14). Samples from patients with a NAS of 5-6 were categorized into the NASH group (Figure 14), which is characterized by severe inflammation in the liver. In addition, we phenotypically compared these groups with other samples from patients without NAFLD.

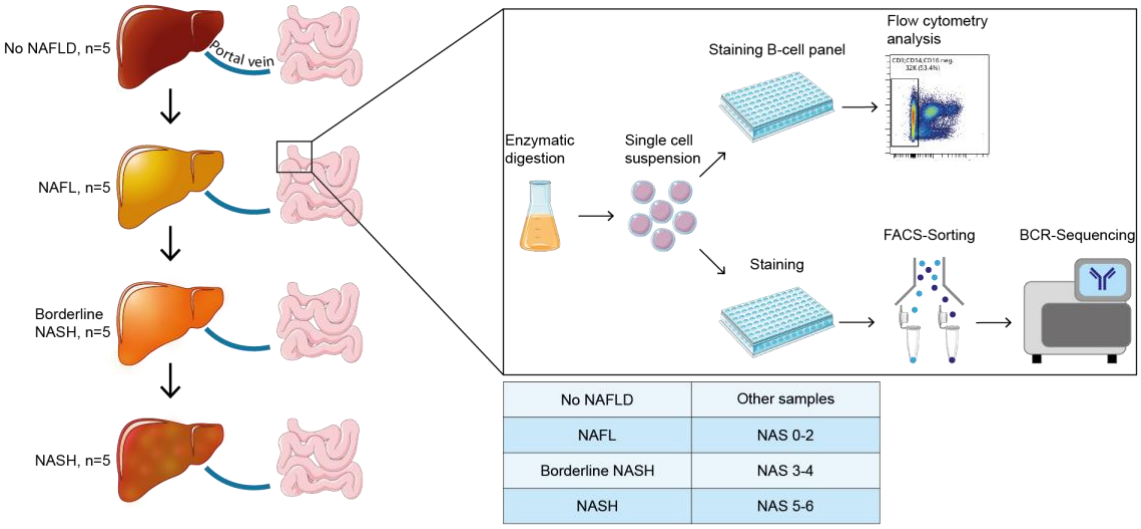

Figure 14: Schematic experimental design for phenotypic and BCR repertoire analysis in patients diagnosed with NAFLD Small intestinal samples from patients diagnosed with NAFLD were retrospectively classified into three stages based on their NAS and compared to other small intestinal samples without NAFLD. For each of the three stages (NAFL, Borderline NASH, NASH) 5 small intestinal samples were examined. Leukocytes were isolated by enzymatic digestion on the same day as surgery and stored at -156°C until further analysis. The cells were defrosted and part of them was used for phenotypic analysis, while the other part of the cells was used for FACS-sorting of PCs (as shown in Figure 4). Subsequently, BCR sequencing of these sorted PCs was performed. BCR: B-cell receptor; NAFLD: non-alcoholic fatty liver-disease; NAS: NAFLD activity score; FACS: Fluorescence-activated cell sorting.

4.3.1 Small intestinal B-cells are phenotypically similar at different stages of NAFLD

First, we examined the general distribution of B-cell subsets and their isotype expression within the different groups (Figure 15A). Comparing the proportion of the B-cell subsets, we didn't find any differences between patients diagnosed with NAFLD and patients without NAFLD or between the different stages of progression (Figure 15A). PCs as well as NBCs and MBCs contributed equally to the B-cell lineage at all stages of NAFLD (Figure 15A). We also did not detect any difference in the isotype or CD45/ CD19 expression of PCs, thus the PC subpopulations remained the same during disease progression (Figure 15B). The same was observed in the analysis of MBCs. Again, there was no difference in the proportion of switched and non-switched MBCs within total MBCs in the different stages (Figure 15C). The expression of the isotypes IgA and IgG in the switched and SNC memory B-cells also did not change (Figure 15C). Thus, we found that the distribution of B-cell subsets and the expression of isotypes remained the same in the comparison of NAFLD patients with patients without NAFLD as well as in disease progression.

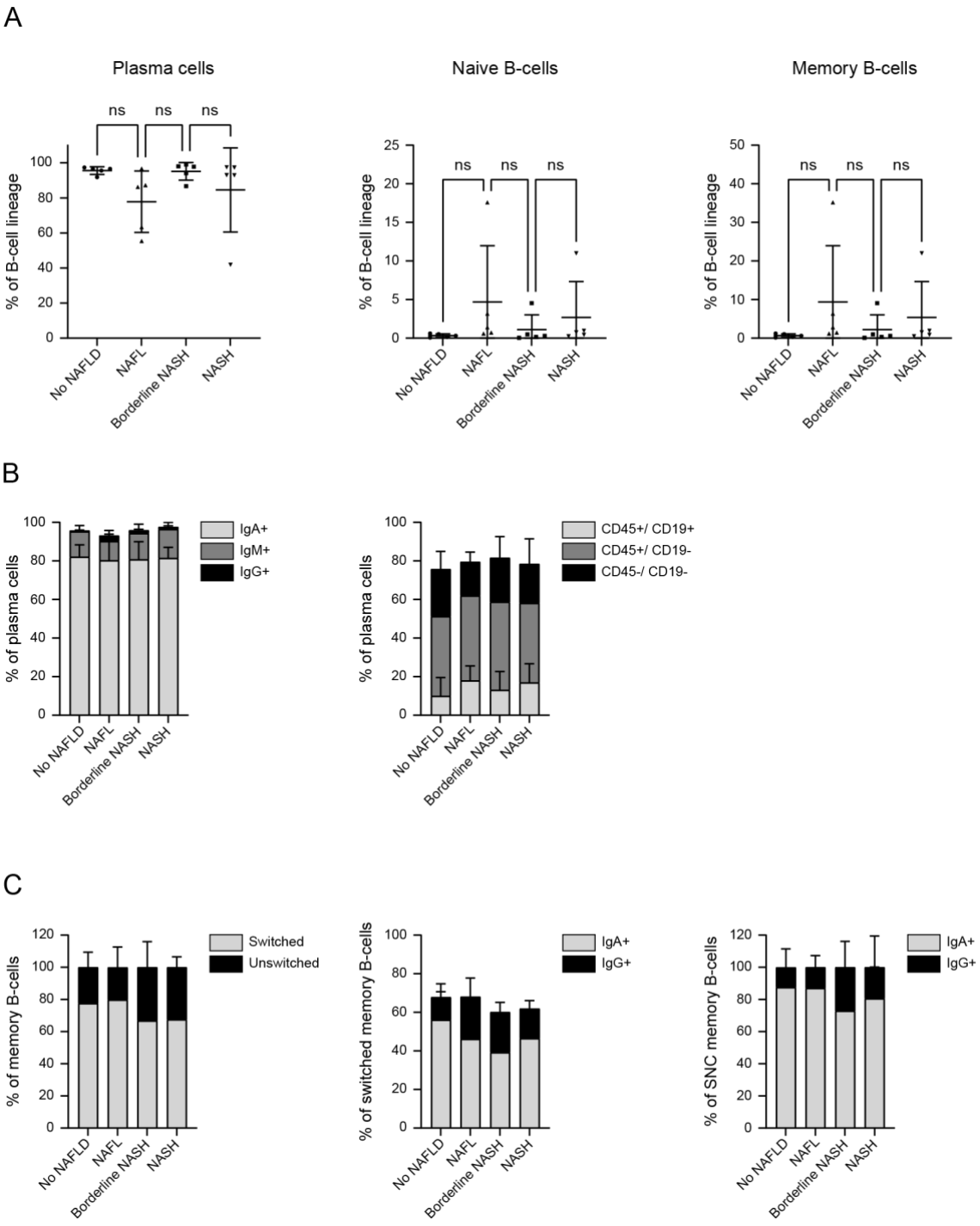

Figure 15: B-cell subset distribution and isotype expression in different stages of NAFLD A: Frequencies of PCs (left panel), NBCs (middle panel) and MBCs (right panel) among the B-cell lineage of small intestinal samples at different stages of NAFLD. **B:** Isotype distribution (left panel) and CD45/ CD19 expression (right panel) of PCs in the different stages of NAFLD. **C:** Frequencies of switched and non-switched MBCs of total MBCs (left panel) and isotype distribution of switched (middle panel) and SNC (right panel) MBCs in the progression of the disease. Data are shown as mean ± SD. Statistical comparisons were performed using one-way ANOVA with Tuckey's multiple comparison test (ns: not significant). NAFLD: non-alcoholic fatty liver disease; NAFL: non-alcoholic fatty liver; NASH: non-alcoholic steatohepatitis; SNC: switched non-conventional; PCs: plasma cells; MBCs: memory B-cells.

Subsequently, we investigated whether we could detect other changes in small intestinal B-cells at different stages of NAFLD, such as in the expression of individual markers. For this purpose, we first performed a dimensionality reduction analysis with UMAP and overlaid the progression groups to detect possible differential clustering (Figure 16A). UMAPs of all groups formed similar clusters in general, but we could still detect small differences, for example, in the overlay of the healthy individuals and the NASH group (Figure 16A). Therefore, we continued with the comparison of the expression of various markers of the B-lineage cells at the different progression stages (Figure 16B). For this purpose, we used overlaid histograms combining all samples of the respective groups and showing the corresponding expression levels (Figure 16B). We found relatively similar expression of all markers in each group, however, the markers CCR9 and IgA appeared to be higher expressed in patients without NAFLD (Figure 16B). In the statistical analysis of the MFI, we could not detect major differences in the expression of the two markers (Figure 16C). To explain the differential clustering we observed in UMAP, we performed many other analyses of marker expression in other B-cell subpopulations such as NBCs and MBCs. However, we did not find any major variations in the expression in this analysis either. Therefore, we assumed that the differences between clusters were likely due to the high variability of human tissue samples and that even small variations, such as in the expression of CCR9 and IgA, could lead to the changes in the clusters. Another explanation for the small differences observed could be that the samples from the NAFLD patients, in contrast to the samples without NAFLD, were first frozen before being stained and analyzed. In general, we found that B-cells from the small intestine of patients with NAFLD did not vary in the phenotype during disease progression.

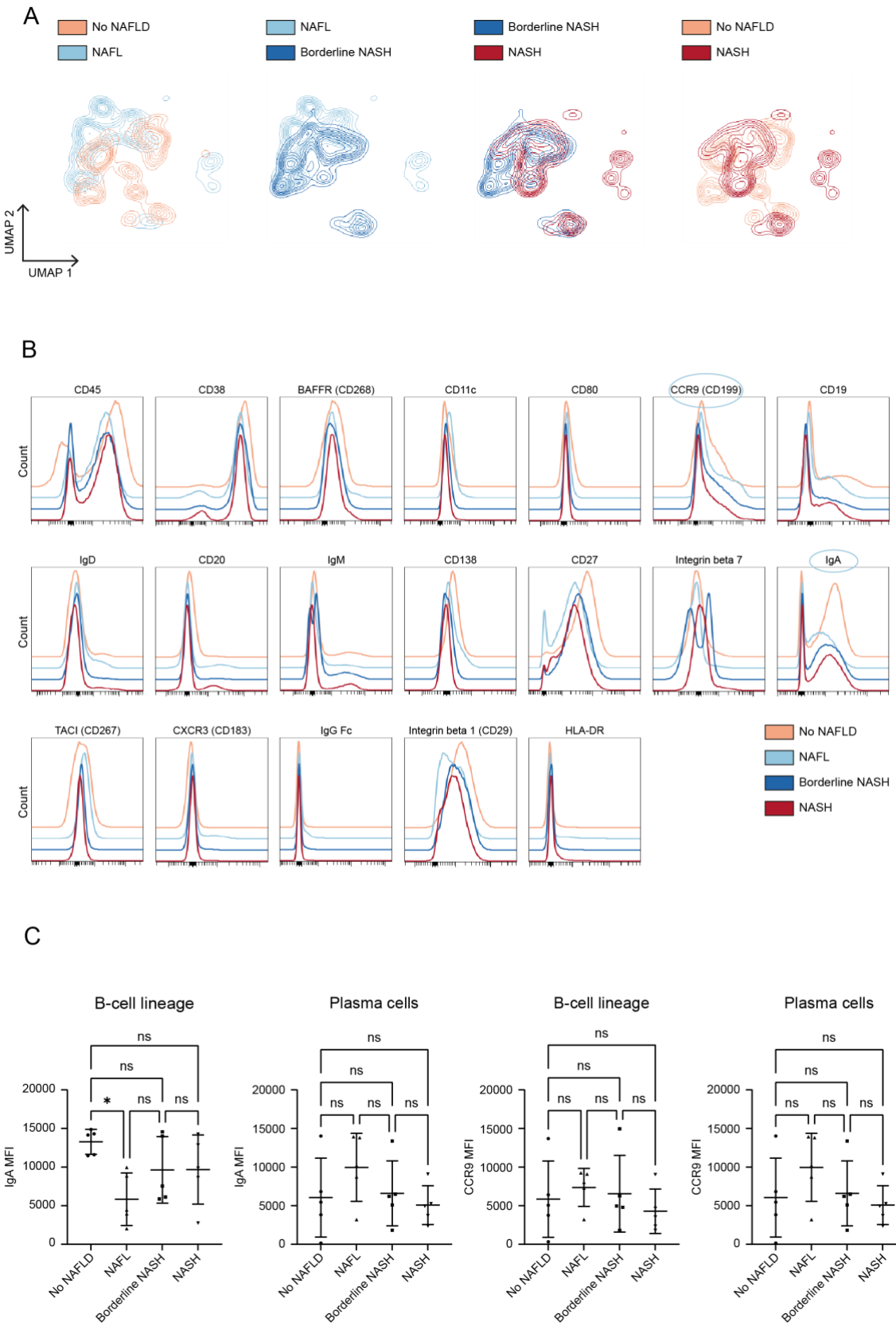

Figure 16: Comparison of surface phenotypic characteristics of small intestinal B-cells at different stages of NAFLD A: UMAP analysis was performed for B-lineage cells, combining all small intestinal samples from patients without and from patients with NAFLD. Overlay of UMAP plots for the different stages of progression: No NAFLD, NAFL, Borderline NASH and NASH. **B:** Overlaid histograms of combined small intestinal samples at different stages of NAFLD showing expression levels of various markers of B-lineage cells. **C:** Quantitative analysis of CCR9 and IgA expression in PCs and B-lineage cells at different stages of progression. MFI of these markers were compared using one-way ANOVA with Tuckey's multiple

comparison test (*P <0.05, ns: not significant). Data are shown as mean ± SD. UMAP: Uniform Manifold Approximation and Projection; MFI: median fluorescence intensity; NAFLD: non-alcoholic fatty liver disease; NAFL: non-alcoholic fatty liver; NASH: non-alcoholic steatohepatitis.

4.3.2 High similarities in the small intestinal PC repertoire at different stages of NAFLD

As previously mentioned, NAFLD is associated with alterations in the intestine, such as increased permeability of the intestinal epithelium and dysbiosis. To investigate whether changes in the microbiota also affect the PC repertoire, we performed BCR bulk sequencing on IgA^+ PCs at different stages of NAFLD. For the analysis of the repertoire in NAFLD, we used the same approach as for the comparison of the repertoire between small intestine and liver. A direct comparison was more accurate in this analysis because all of the samples contained the same amount of cells.

First, we compared the distribution of clonotypes in the PC repertoires of the different groups. We noticed that the top clonotype accounted for about 4-6% of the total sequenced repertoire in all stages of NAFLD (Figure 17A) and frequencies of the other clonotypes were very similar for all groups as well (Figure 17A). We also found that the cumulative proportion of the highest ranked clonotypes was similar in the different stages, with the 50 highest ranked clonotypes accounting for approximately 50% of the total sequenced repertoire (Figure 17A). We noticed only a slight tendency towards a lower cumulative proportion in the more progressive stages (Figure 17A).

Comparing the usage of V and J gene families in the three groups, we observed that the most abundant V gene segment was IGHV-4 and the most abundant J gene segment was IGHJ-4 in these samples as well (Figure 17B). Generally, the family usage of the IGA^+ PCs was very similar at all stages of NAFLD (Figure 17B). However, we observed a trend towards higher frequency of IGHV-4 in more severe disease stages, with a significant difference between NAFL and NASH, along with a lower frequency of IGHV1 and IGHV3 (Figure 17A).

Next, we wanted to investigate whether the diversity of the PC repertoire in the gut changes during the disease progression. Using the Shannon and inverse Simpson diversity indices, we found that although there were no significant differences between the groups, there was again a tendency towards higher diversity in the more progressive stages of NAFLD (Figure 17C). This would also be consistent with the slightly lower

expansion of top clonotypes noted in the cumulative proportion comparison, despite the same number of cells analyzed (Figure 13).

As expected, since all samples were from different individuals, we detected only very few clones shared between samples (Figure 14D). These could be either parts of known public clones (W. Zhang et al., 2017) or might arise during the data analysis due to technical limitations of the method such as ambiguous identification of D segments. In any case the fraction of the shared clonotypes was very small and MHI for the comparison between samples very low (Figure 14D-E).

In conclusion, our results showed that clonality, familial usage and diversity were very similar in the different stages of NAFLD. However, we observed a slight tendency towards increased diversity and altered IGHV-4 usage in the more advanced stages of the disease, which may be related to changes in the gut microbiome.

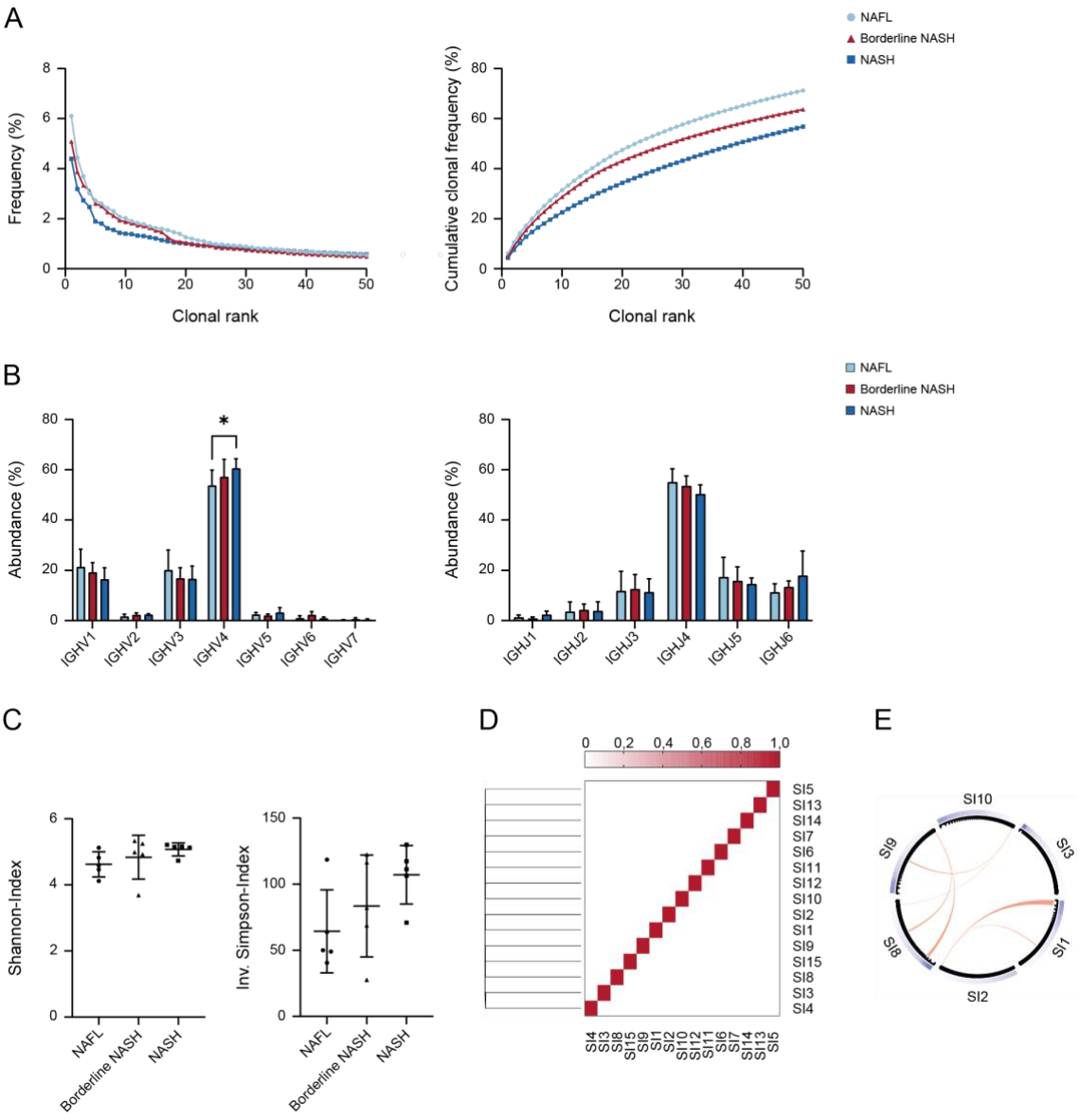

Figure 17: Comparative analysis of the PC repertoire in human small intestine at different stages of NAFLD For analysis, IgA-specific BCR sequencing was performed on 1000 FACS-sorted (Figure 4) PCs of 15 small intestinal samples (5 per group). **A:** For the representation of the clonotype distribution, clonotypes were ranked according to their frequency in the repertoire. Frequency of each ranked clonotype (left panel) and the cumulative proportion of the ranked clonotypes in the repertoire (right panel). Data are shown as mean of 5 summarized samples per group of different NAFLD stages. **B:** IGHV and IGHJ-gene family usage of PCs from 5 samples per group. Statistical comparisons were performed using two way ANOVA with Sidak´s multiple comparison test (*P <0.05). **C:** Comparison of the PC repertoire diversity in the different NAFLD stages using the Shannon index (left panel) and inverse Simpson index (right panel). Data are shown as mean ± SD. Statistical comparisons were performed using one-way ANOVA with Tuckey's multiple comparison test. No significant differences were detected. **D:** Similarity of PC repertoires between all samples was compared using the MHI. The heatmap (left panel) shows the respective MHI values, with samples being hierarchically clustered using linkage clustering. **E:** Circos plots indicating possible shared clonotypes between randomly selected samples. Common clonotypes between samples are represented by red arcs, with thickness indicating the proportion and position on the black outer ring indicating the size of each clonotype. NAFL: non-alcoholic fatty liver; NASH: non-alcoholic steatohepatitis; BCR: B-cell receptor; MHI: Morisita-Horn index; PC: plasma cell.

4.4 Phenotypic characterization of B-cells in ascitic fluid and peripheral blood of cirrhotic patients

Liver cirrhosis is a chronic disease associated not only with spontaneous infections derived from the gut, but also with local and systemic immune dysfunction. For these reasons, we were particularly interested in investigating a possible involvement of B-cells in the development of impaired immunity in patients with liver cirrhosis. Additionally, considering the peritoneal cavity as a link between the gut and the liver, the composition and phenotyping of B-cells in this fluid compartment was also of great interest to us. Therefore, in the next part of the project, we characterized the subpopulations of B-cells in both ascitic fluid and peripheral blood from patients with liver cirrhosis and further compared them with blood samples from healthy donors.

4.4.1 B-cells in ascites and peripheral blood are similar in subset distribution but differ in the expression of certain markers

First, we aimed to analyze B-cells in ascitic fluid in general, and for this purpose, we compared B-cell distribution, isotype expression and other B-cell marker expression from ascitic fluid with paired blood samples from cirrhotic patients. Using a similar approach to the previous analysis, we used dimensionality reduction analysis to obtain an initial overview of the two compartments (Figure 18A). Applying UMAPS, we observed almost no differences in clustering between ascites and blood samples, suggesting that B-cells of the two compartments were highly similar (Figure 18A). Overlaying the manually gated B-cell subsets (gated as shown in Figure 5), we noticed that the clustering of UMAPs strongly overlapped with the previously determined populations (Figure 18B). Regarding the proportions of the B-cell subsets, we found that PCs, MBCs and SNC MBCs constituted the same proportion of the B-cell lineage in ascites and blood (Figure 18C). However, we observed that the proportion of NBCs was significantly lower in the ascitic fluid (Figure 18C). Apart from that, we did not detect any differences between blood and ascites samples in further analysis of MBC subpopulations or the isotype expression of PCs, MBCs and SNC MBCs (Figure 18D).

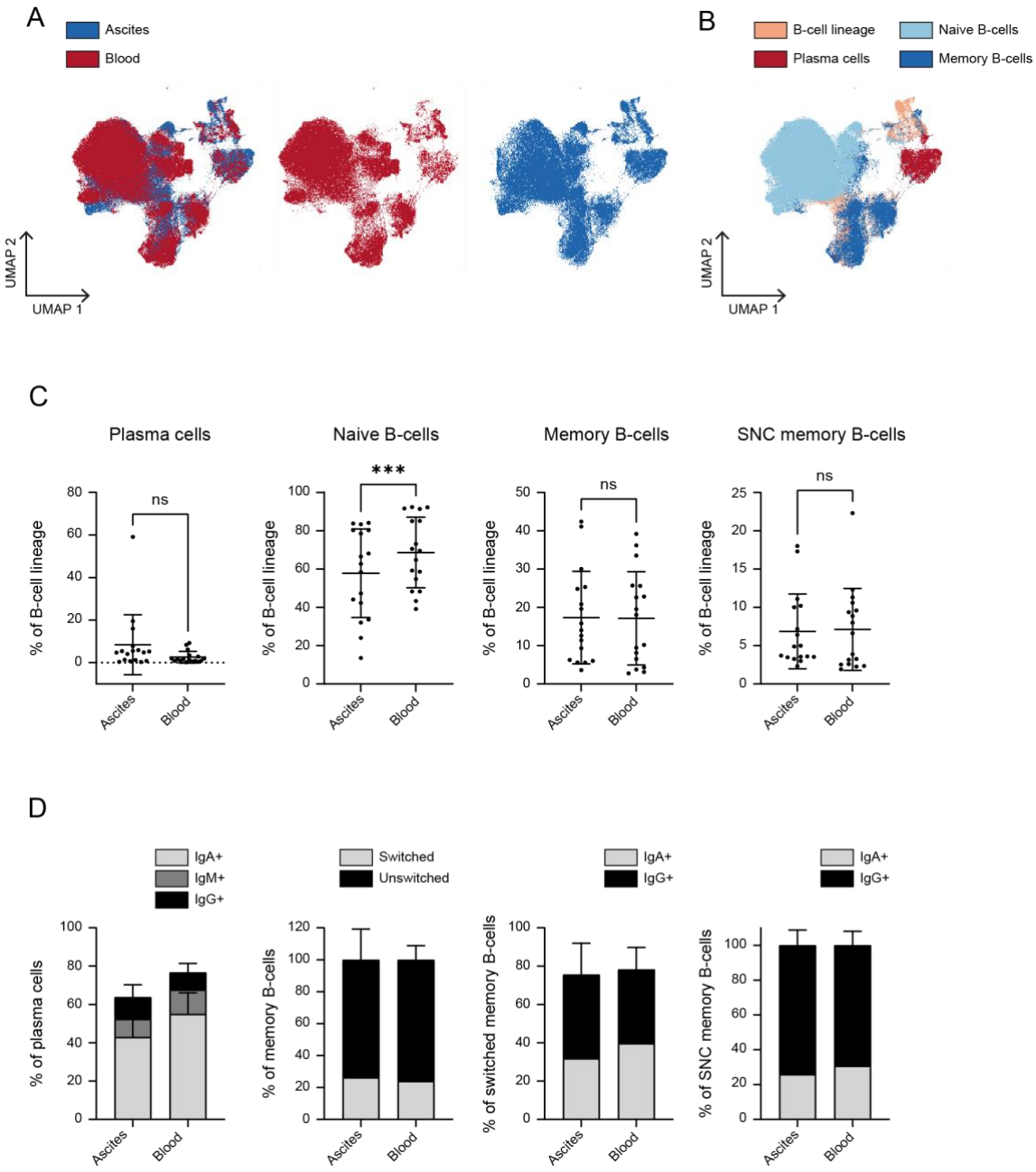

Figure 18: Comparison of the B-cell subset distribution and isotype expression in ascites and peripheral blood of cirrhotic patients A: UMAP analysis was performed for B-lineage cells combining all paired ascites and peripheral blood samples of cirrhotic patients. Visualization of UMAP plots for both compartments (left panel) or separately for the respective one (middle and right panel). **B:** Identification of manually gated B-cell subsets (gated as shown in Figure 5) by overlaying them with the automatically generated clusters of the UMAP. **C:** Comparison of the frequencies of PCs (left panel), NBCs (middle left panel), MBCs (middle right panel) and SNC-memory B-cells (right panel) among the B-cell lineage in ascites and blood samples. **D:** Comparison of the frequency of switched and non-switched MBCs among total MBCs (middle left panel) and different isotypes among PCs (left panel), switched MBCs (middle right panel) and SNC MBCs (right panel) in ascites and peripheral blood of patients with liver cirrhosis. Data are shown as mean ± SD. Statistical comparisons were performed using ordinary paired t-tests (***P <0.001; ns: not significant). UMAP: Uniform Manifold Approximation and Projection; NBCs: naive B-cells; SNC: switched non-conventional; MBCs: memory B-cells; PCs: plasma cells.

We then additionally compared the expression profile in the ascites and blood samples. Using overlaid histograms combining all samples (Figure 19A), we noted differences particularly in BAFFR, IgD and IgM expression, as peripheral blood B-cells appeared to express these markers at higher levels than ascitic B-cells (Figure 19A). Using overlaid contour plots and MFI, we performed further analysis on these observations (Figure 19B-C). This confirmed our finding of significantly lower expression of the survival factor BAFF-Receptor in ascites samples than in blood samples in both NBCs and MBCs (Figure 19B). As shown in the previous results (Figure 10B), PCs did not express BAFFR, therefore we could not detect any difference between ascites and blood in this B-cell subset (Figure 19B). The different expression of this marker in both NBCs and MBCs was also evident in the contour plots (Figure 19B). In addition to the finding that the B-cell compartment in ascites contained fewer NBCs, we also found that these NBCs expressed not only less BAFFR but also less IgD and IgM than their blood counterpart (Figure 19C). However, unlike in the different expression of BAFFR, we could not detect the difference of IgD and IgM expression very clearly in the contour plots (Figure 19C). Thus, our results suggest that the B-cell subsets in ascites and blood are in general very similar, but that there are still differences, for instance in the proportion of NBCs and in the expression of individual markers.

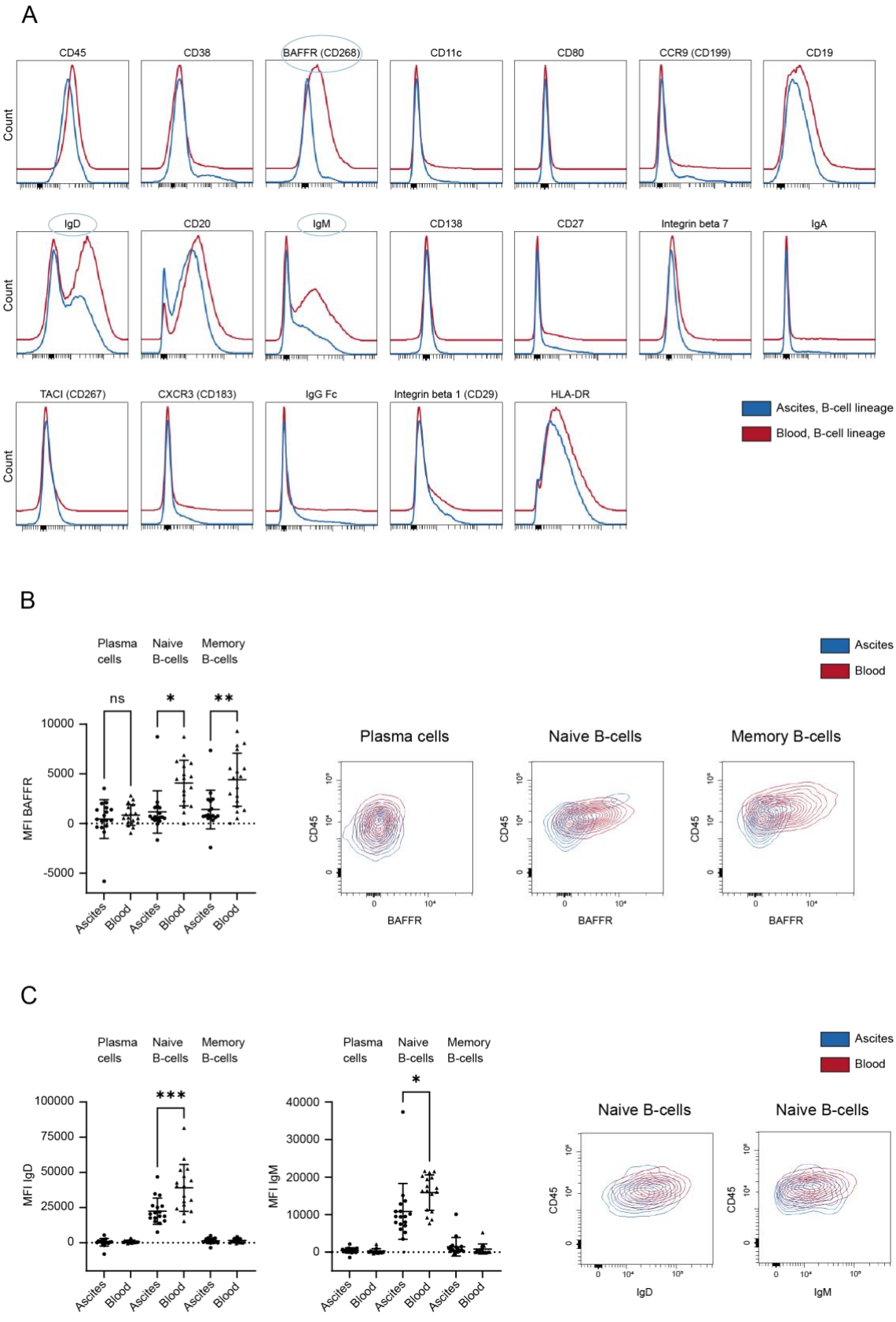

Figure 19: Comparison of surface phenotypic characteristics of B-cells in paired ascites and peripheral blood samples A: Overlaid histograms of combined ascites and blood samples from cirrhotic patients used to compare the expression levels of various markers of B-lineage cells. **B:** Quantitative analysis of BAFFR expression of PCs, NBCs and MBCs in comparison of ascites and blood samples. Representation of BAFFR expression in the respective B-cell subsets of the two compartments, using overlaid contour plots. **C:** Comparison of IgD and IgM expression of PCs, NBCs and MBCs in ascites and blood samples. Representation of IgD and IgM expression of NBCs in both compartments using overlaid contour plots.

Statistical analysis was performed using one-way repeated measures ANOVA with Sidak´s multiple comparison test (B) or paired ordinary t-test (C). Dara are shown as mean ± SD. UMAP: Uniform Manifold Approximation and Projection; MFI: median fluorescence intensity; PCs: plasma cells; NBCs: naive B-cells; MBCs: memory B-cells.

4.4.2 Altered phenotypic characteristics in B-cells from ascites and peripheral blood of cirrhotic patients compared with healthy blood donors

After comparing B-cells in ascites and blood from cirrhotic patients, we were interested in investigating possible changes in the distribution or phenotypic characteristics in comparison to healthy blood donors. The demographic, clinical and laboratory characteristics of the included cirrhotic patients are shown in Table 9. The study comprised 18 patients with liver cirrhosis, 13 of them were male, and their mean age was 62 ± 9.3 years. Most patients developed cirrhosis due to alcohol consumption. Other causes included NASH, hemochromatosis and sclerosing cholangitis. The mean MELD score of the patient group was 17 ± 8.6, and at the time of sample collection, the Child-Pugh score was B in 12 patients and C in the other 7 patients. In addition, 4 of the patients developed acute-on-chronic liver failure, and 5 patients underwent liver transplantation or died in the 90 days after sample collection. The study included 4 healthy controls from anonymous blood donors about whom we do not know further data. The remaining laboratory parameters are listed in the Table 9.

Table 9: Demographic, clinical and laboratory characteristics of the cirrhotic patient population

Liver cirrhosis (n=18)		**Ascites**		**Blood**	
Age (years)	62 ± 9.3	Cell count	388.1 ± 331.8	Sodium	128.7 ± 27.6
Male/ Female	13/ 5	Polymorpho-nuclear Leukocytes	38.5	C-reactive protein	20.3 ± 13.5
Etiology: Alcohol/ Others	11/ 7	Protein	2 ± 1.3	Protein	6.2 ± 1.3
Child Pugh (B/C)	12/ 6	Albumin	1.1 ± 0.7	Creatinine	1.5 ± 0.8

MELD	17 ± 8.6		Albumin	3.2 ± 0.6
ACLF (yes/ no)	4/ 14		Bilirubin	4.2 ± 7.8
LTX/ Death within 90 days (yes/no)	5/ 13		INR	1.5 ± 0.4
SAAG	2.1 ± 0.5		ALT	33.9 ± 27.7
			AST	65 ± 57.6
			Leukocytes	6.1 ± 3.1
			Platelets	118.3 ± 43.7

In line with previous work (Cardoso et al., 2021) we detected changes in the proportions of NBCs and MBCs (Figure 20). We found a lower proportion of MBCs in the peripheral blood as well as in the ascitic fluid of cirrhotic patients compared to healthy blood donors (Figure 20A). Interestingly, the ratio of switched and non-switched MBCs to total MBCs also changed in these patients (Figure 20A). In healthy blood donors, the ratio of these two subpopulations was about 1:1 (Figure 20A). In patients with cirrhosis, the proportion of switched MBCs was nearly 80 %, whereas the proportion of non-switched MBCs decreased to levels of roughly 20 % (Figure 20A). Again, we were able to detect this in both the blood and ascites of the patients (Figure 20A). However, the isotype expression of switched MBCs remained the same (Figure 20A). Examining the individual marker expressions, we noticed differences in the survival factor BAFF receptor (Figure 20B). We found that BAFFR expression not only differed between ascites and blood samples (Figure 19), but also observed that MBCs in blood from cirrhotic patients expressed less BAFFR than those from healthy blood donors (Figure 20B). Analyzing this expression in more detail, we noticed differences between switched and non-switched MBCs, in particular that the switched MBCs showed this lower expression significantly, whereas only a slight change was observed in the non-switched MBCs (Figure 20B).

Using UMAP and an overlaid histogram of MBCs, we were able to demonstrate this difference in expression more clearly (Figure 20B). Since switched but not non-switched MBCs can survive without BAFFR signaling (Scholz et al., 2008; Smulski & Eibel, 2018), the change in MBC subpopulation distribution might be caused by a lower BAFFR expression. To exclude other variations in marker expression, we additionally examined the integrins and chemokine receptors that were included in our B-cell staining panel. However, we did not detect differences in the expression of the markers CXCR3, integrin beta 7, integrin beta 1 or CCR9 in MBCs from healthy and diseased persons (Figure 20C).

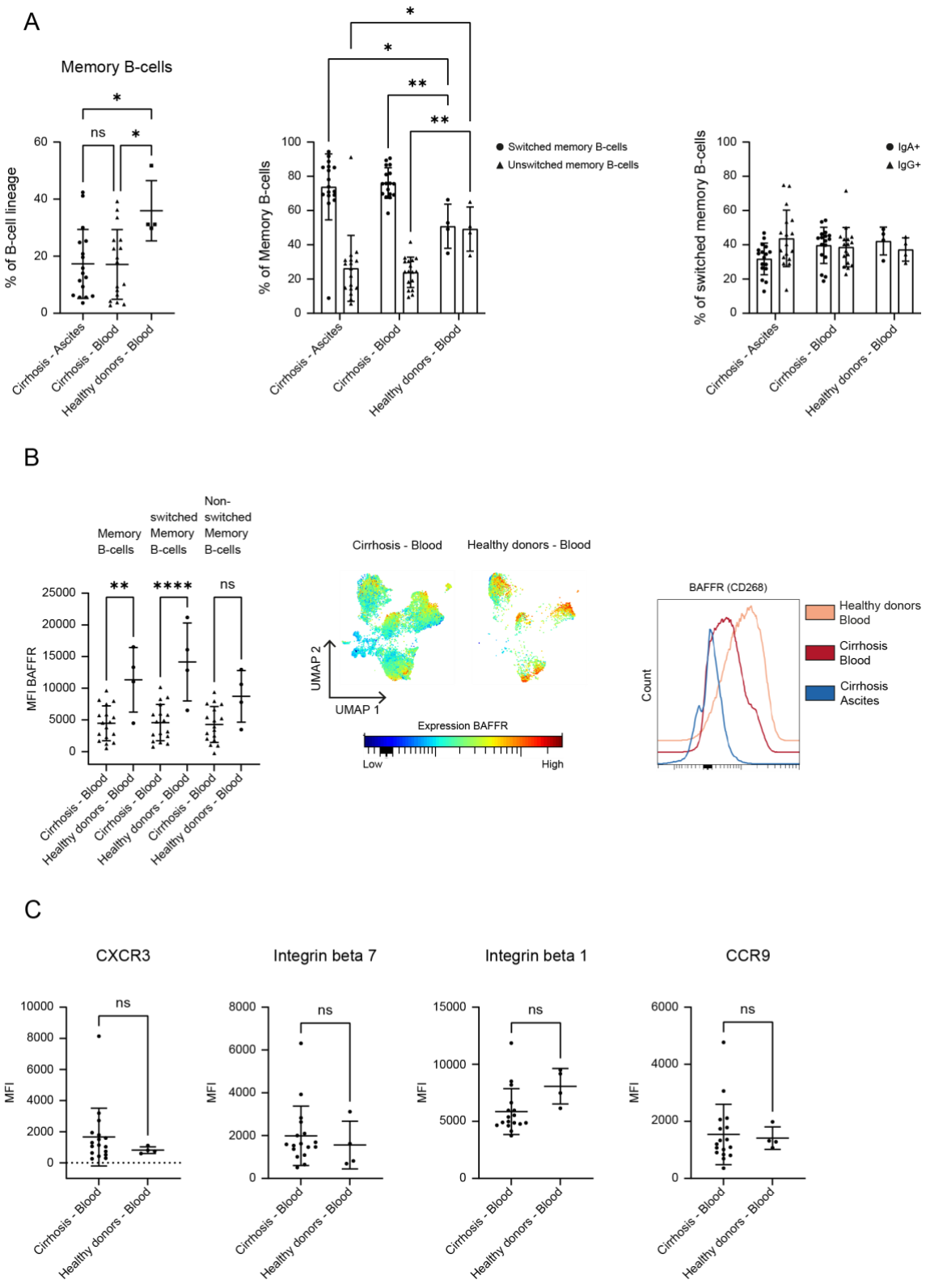

Figure 20: Altered phenotypic characteristics of MBCs in ascites and blood of cirrhotic patients **A:** Analysis of the distribution of MBCs and their subpopulations. Frequency of MBCs among the B-cell lineage of healthy blood donors compared with blood and ascites from cirrhotic patients (left panel). Comparison of the proportion of switched and non-switched MBCs to total MBCs (middle panel) and of the isotype expression of switched MBCs (right panel) in the respective groups. **B:** Analysis of the MFI of BAFFR in MBCs, switched MBCs and non-switched MBCs from blood of healthy donors and cirrhotic patients. Visualization of the differential BAFFR expression using UMAP and an overlaid histogram of MBCs summarizing all samples. **C:** Comparison of the MFI of CXCR3, integrin beta 7, integrin beta 1 and CCR9 in blood of healthy donors and cirrhotic patients. Statistical comparisons were performed using one-

way ANOVA with Tuckey's multiple comparison test (A-B), two-way ANOVA with Sidak´s multiple comparison test (A, middle panel) or ordinary unpaired t-test (C) (*P < 0.05, **P < 0.01, ***P < 0.001, ****P < 0.0001, ns: not significant). Data are shown as mean ± SD. MFI: median fluorescence intensity; UMAP: Uniform Manifold Approximation and Projection; MBCs: memory B-cells.

Compared to MBCs, we did not observed any changes in the proportion of PCs and NBCs in the blood of cirrhotic patients (Figure 21A). The isotype subpopulations of PCs were also equally distributed (Figure 21A). However, we found that NBCs in cirrhosis also demonstrated significantly lower BAFFR expression (Figure 21B). Thus, our results showed that the subset of MBCs in particular was altered in cirrhosis, both in blood and ascites. Not only the distribution of this B-cell subset and its subpopulations, but also the expression of the marker BAFFR were affected. Although the proportion of NBCs remained the same in cirrhotic patients, this subset also showed significantly lower expression of BAFFR.

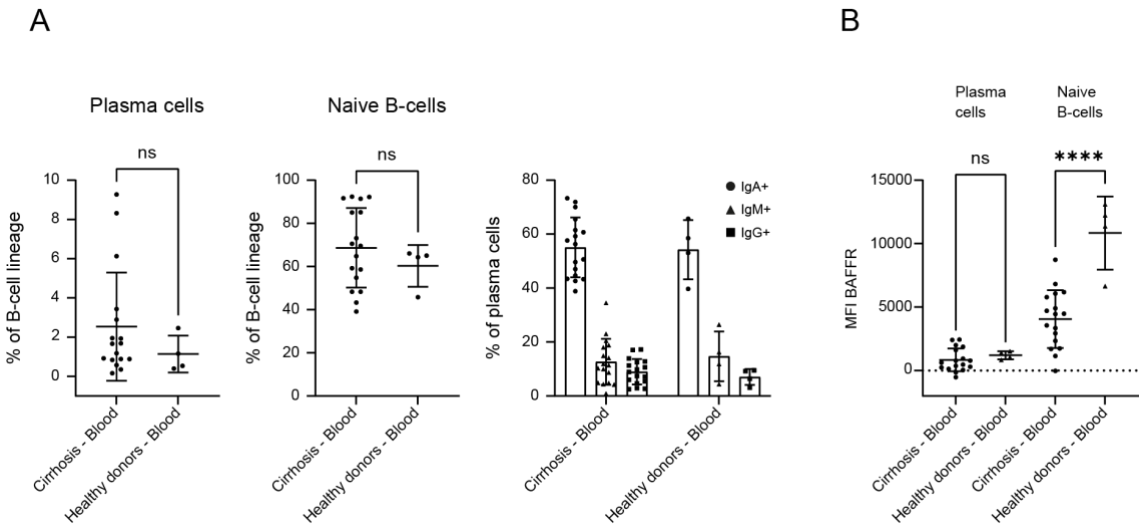

Figure 21: B-cell subset distribution and BAFFR expression of PCs and NBCs in cirrhotic patients **A:** Frequency of PCs and NBCs among the B-cell lineage of healthy blood donors compared with blood from cirrhotic patients (left and middle panel). Comparison of the frequency of the different PC isotype subpopulation in both groups (right panel). **B:** Analysis of the MFI of BAFFR in PCs and NBCs from blood of healthy donors and cirrhotic patients. Statistical comparisons were performed using ordinary unpaired t-tests (****P < 0.0001, ns: not significant). Data are shown as mean ± SD. MFI: median fluorescence intensity; PCs: plasma cells; NBCs: naive B-cells.

4.4.3 Increased alterations in the distribution of B-cell subsets in cirrhotic patients with a poor prognosis.

After examining the differences in B-cell phenotype between healthy and cirrhotic subjects, we were now interested in determining whether we would observe further

changes in cirrhotic patients under different conditions. Therefore, we investigated the distribution of B-cell subsets and their marker expression in blood of cirrhotic patients in combination with different laboratory parameters, etiologies and prognoses. Interestingly, we found an increase in some of the previously observed changes in cirrhotic patients who received liver transplantation (LTX) or died (DTH) within 90 days after obtaining the samples. Analyzing the distribution of B-cell subsets, we found a further decrease in the proportion of MBCs in patients with LTX or DTH compared with patients without LTX or DTH (Figure 22A). In addition, the subset of NBCs was also affected in these patients (Figure 22A). We observed that although the proportion of NBCs in the blood of healthy donors and cirrhotic patients without poor prognosis was the same, it increased significantly in cirrhotic patients who received LTX or died (to about 90% compared with about 60% in healthy blood) (Figure 22A). As previously seen (Figure 20), MBCs in the blood of patients consisted of more switched MBCs compared with blood from healthy individuals, however, this proportion did not change further with a worse clinical outcome (Figure 22A). We also did not notice any differences in the proportion of PCs in the respective conditions (Figure 22A). Based on the analysis of overlaid histograms, we could not detect major variations in the expression of individual markers in NBCs or MBCs (Figure 22B). Only the expression of BAFFR appeared to be lower in both B-cell subsets of cirrhotic patients with poor prognosis (Figure 22B). However, this observation could not be confirmed by statistical analysis (Figure 22C). In conclusion, our results in this part of the study demonstrate that the previously reported changes in the distribution of B-cell subsets increased in individuals who received LTX or died as a result of the condition.

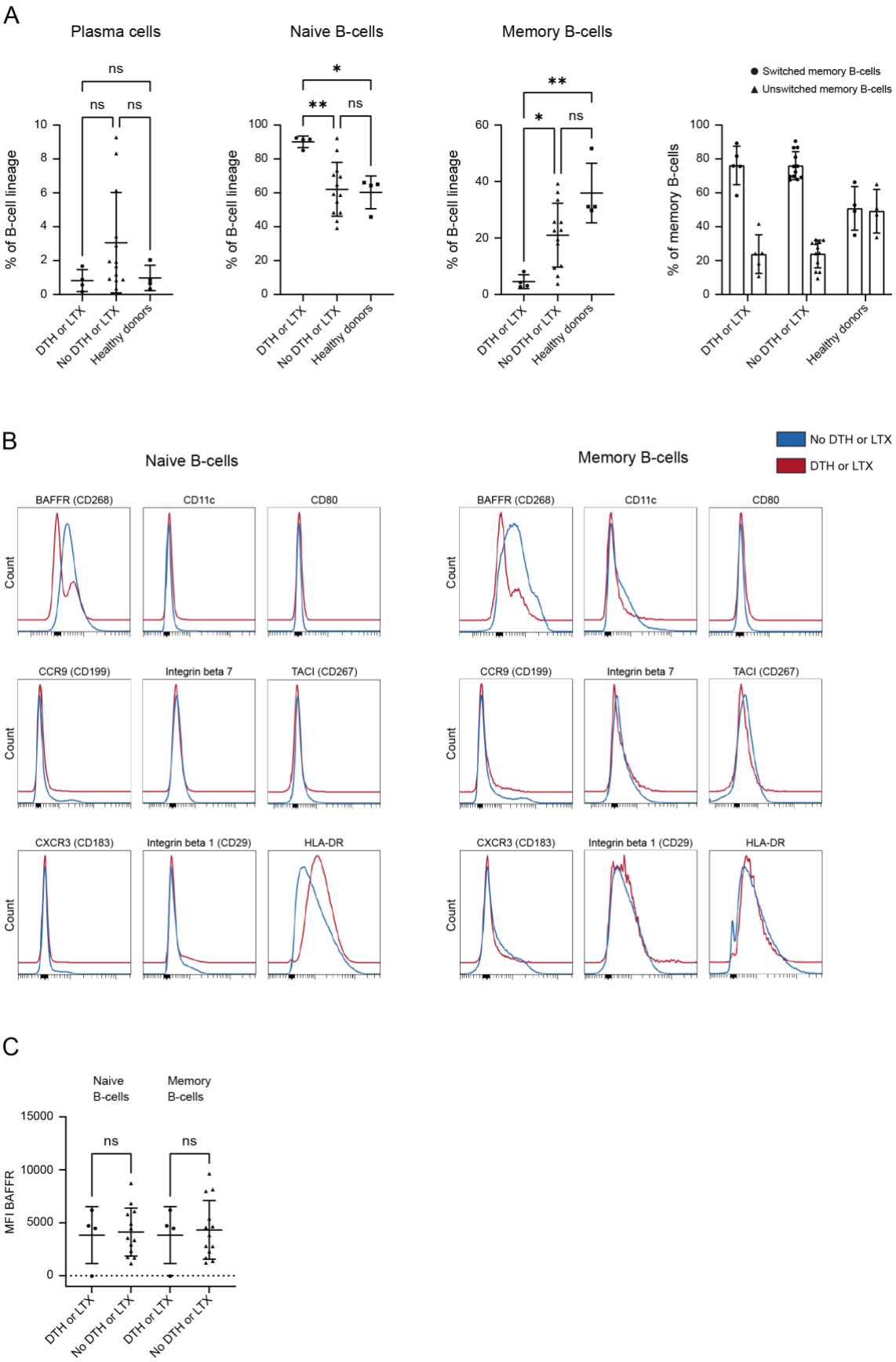

Figure 22: Phenotypic analysis of B-cells from cirrhotic patients with different prognoses Comparison of phenotypic characteristics of cirrhotic patients who received LTX or died within 90 days after sampling with patients who did not. **A:** Frequency of PCs, NBCs and MBCs among the B-cell lineage in blood from healthy donors compared with cirrhotic patients with or without LTX or DTH. Distribution of switched

MBCs and non-switched MBCs among total MBCs in the different outcomes. **B:** Representation of the expression of various markers in NBCs and MBCs in the two different groups of cirrhotic patients using overlaid histograms combining all samples of each group. **C:** Comparison of the MFI of BAFFR in NBCs and MBCs from blood of cirrhotic patients with or without LTX or DTH. Data are shown as mean ± SD. Statistical comparisons were performed using one-way ANOVA with Tuckey´s multiple comparison test (A) or ordinary unpaired t-test (C) (*P<0.05, **P<0.01, ns: not significant). DTH: death; LTX: liver transplantation; MFI: median fluorescence intensity; PCs: plasma cells; NBCs: naive B-cells; MBCs: memory B-cells.

5 Discussion

The involvement of B-cells in the coordination of intestinal immunity is an active field of research. Although it is known that the gut and the liver form a functional unit and that liver immunity is involved in protective immune responses against enteropathogens, knowledge about the B-cell compartment of the human liver is still limited. A better understanding of hepatic B-cells and the relation to their intestinal counterparts is essential to better understand pathomechanisms and therapeutic options of many liver diseases. In this work, we sought to characterize B-cells within the human gut-liver axis using phenotypic and repertoire analyses and to gain a better understanding of their involvement in diseases associated with the gut-liver axis.

5.1 Phenotypic differences of B-cells in the gut-liver axis

The several subsets of B-cells are responsible for different functions during the immune response. Therefore, differences in their distribution in the organs reflect distinct functions of the humoral immunity in these regions. B-cells in peripheral blood mainly comprise NBCs and MBCs that circulate between secondary lymphoid tissues to encounter their specific antigen and induce an immune response. In the intestine, by contrast, the B-cell compartment consists mainly of PCs localized in the lamina propria, continuously producing antibodies and thereby performing an effector function to maintain homeostasis. Our findings that NBCs were the main subset in the peripheral blood, whereas PCs represented the main subpopulation in the small intestine, are therefore consistent with the current understanding of B-cells in these sites and are in line with previous work (Nair et al., 2016). Our results also demonstrate that the subset distribution within the B-cell compartment of the liver was different from that of the other two sites, supporting the concept of a tissue-specific B-cell response. The distribution of B-cells in the liver was much more heterogeneous, with NBCs represented the major subpopulation while both MBCs and PCs were also highly abundant with a similar proportion of approximately 20 %. Thus, the functions of B-cells in the liver could involve, first, encountering gut-derived antigens and subsequently initiating an immune response by NBCs and MBCs, and second, an effector function

through the production of antibodies by PCs. Even though our results showed that PCs constituted a much higher proportion in the liver than in the blood, they are inconsistent with the B-cell distribution in human liver demonstrated by Moro-Sibilot et al. in which PCs accounted for approximately 60-70% of the hepatic B-cell compartment (Moro-Sibilot et al., 2016). Although the selected patient population and the method of cell sampling using an enzymatic digestion process were comparable to our study, there were significant differences in the chosen gating strategy. In contrast to our approach, the authors initially pre-gated on $CD45^+$ cells and defined PCs simply as $CD19^+$/ $CD20^-$ cells. This approach could be an explanation for the different distribution of B-cell populations found in the human liver. Another study using single-cell RNA sequencing observed a tissue-specific B-cell distribution as well, but in contrast to our data and the data of Moro-Sibilot et al., described that MBCs constituted the main subset in the liver (J. Zhao et al., 2020). In this study, however, the authors examined liver perfusions instead of liver tissue, which could lead to divergent results. Altogether, understanding of the exact composition of B-cells in the human liver is very limited, and varying sampling and analytical methods make it challenging to obtain consistent results. Therefore, our thorough analysis of the B-cell distribution based on surface expression represents an important contribution to the understanding of the hepatic B-cell population in humans.

Since the proportion of PCs in the liver differed clearly from the low fraction of PCs in the blood, we were interested not only in the general distribution of the B-cell subsets but also in a more detailed characterization of the hepatic PC population. In both the small intestine and blood, the dominant PC isotype is known to be IgA, and based on the expression of specific gut homing factors such as CCR10 and integrin beta 7, circulating IgA^+ PCs are thought to originate from mucosal immune responses (Mei et al., 2009). Given that liver-resident PCs also expressed mainly IgA in our studies, it could be assumed that these also originate from mucosal immune responses and circulate from the gut to the liver via the portal vein. However, it is important to consider that IgG expression is downregulated on the membrane of mature PCs, in contrast to IgA and IgM expression (Pinto et al., 2013). Because previous work using single-cell RNA sequencing showed that liver PCs were mainly composed of IgG^+ cells (Domínguez Conde et al., 2022), this may be one reason why only about 50% of liver PCs displayed

surface isotype expression in our results. Thus, considering the previous studies, the dominant isotype of the PC subset in the liver could be IgG rather than IgA, but this would be shown differently in surface phenotyping due to the downregulation of IgG.

The immunological memory that is characteristic for the adaptive immune system includes not only MBCs but also long-lived PCs that are localized in the bone marrow and continuously produce antibodies to maintain the necessary immunoglobulin blood titer (Halliley et al., 2015). A recent study has suggested that these long-lived PCs are not restricted to the bone marrow, but are also found in the intestine. PCs in the intestine identified by the markers CD38 and CD27 could be subdivided into three subgroups using the markers CD45 and CD19. The study demonstrated that the population of $CD45^+/CD19^+$ PCs was constantly exchanged, $CD45^+/CD19^-$PCs represented an intermediate stage, and $CD45^-/CD19^-$ PCs constituted long-lived PCs that could survive for decades in the gut. This assumption was made by examining recipient and donor B-cells after pancreaticoduodenal transplantation, which revealed that the recipient $CD45^-/CD19^-$ PC population consisted mainly of donor cells even after one year, with almost no replacement (Landsverk et al., 2017). Consistent with the previous data, we also detected three different CD45/CD19 populations in the intestine. Using an ELISpot assay, our data additionally indicated that the three populations were similar with respect to their spot-forming capacity, i.e. were likely to produce and secrete similar amounts of IgA. This would be in contrast to the study by Landsverk et al., which noted that in vitro cultured $CD45^+/ CD19^-$ and $CD45^-/CD19^-$ PCs were producing less IgA than the $CD45^+/ CD19^+$ subpopulation. However, we performed the ELISpot experiment on only one sample, so it should be repeated for confirmation. Also in agreement with the above study, we found that the suspected long-lived PCs in the gut consisted mainly of IgA^+ cells and that very few $CD45^-$ PCs were represented within the IgG^+ PC subset. This result contrasts with studies on long-lived PCs in bone marrow, which mainly comprise IgG^+ PCs (Halliley et al., 2015). Thus, the functions of long-lived PC populations might differ depending on the tissue.

Interestingly, we were able to detect these three different PC populations not only in the intestine but also in the liver in similar proportions. Since the PCs detected in the liver exhibited other similar PC-specific expression patterns as their counterparts in the intestine and blood, such as no expression of CD20, BAFFR and HLAR-DR, it can be

assumed that this population indeed consisted of PCs. Whether and to what extent this includes long-lived PCs would require further investigation, but the assumption would be consistent with that of Domínguez Conde et al. who found an increased expression of integrin alpha 8 in PCs from both jejunum and liver, which was previously associated with bone marrow PCs and therefore may be associated with long-lived PCs. Therefore, this group suggested that in addition to the bone marrow and possibly the intestine, the liver could also harbor long-lived PCs (Domínguez Conde et al., 2022). In our study, it was unfortunately not possible to perform further analyses of these different PC populations besides the phenotypic analyses, as the small number of PCs in the liver samples did not allow proper FACS sorting into the respective groups.

We further found that PCs from all three sites showed a higher expression of integrin beta 1 (CD29) than NBCs and MBCs. Integrin beta 1 expression in B-cells has previously been described mainly in the context of PC migration to the bone marrow, both in healthy individuals and in diseases such as multiple myeloma (Benet, Jing, & Fooksman, 2021; Hathi et al., 2022). In addition, Andreani et al. have recently shown that integrin beta 1 could be involved in the differentiation of marginal zone B-cells and PCs. By depleting integrin beta 1 on mature $CD21^+$ B-cells in mice, the authors observed that the absence of this protein impaired the T-cell independent differentiation of PCs, which was associated with lower levels of specific serum antibodies and reduced amounts of PCs in the spleen (Andreani, Ramamoorthy, Fässler, & Grosschedl, 2023). In a similar approach to our study, Nair et al. also investigated the surface expression of individual factors known to be involved in mucosal homing by immunophenotyping analysis of human B-cells using mass cytometry. Their analysis revealed that PCs express integrin beta 1 in both peripheral blood and intestine, whereas this was not the case for other B-cell subsets (Nair et al., 2016). Our results extend this observation by showing that not only blood and intestinal PCs but also hepatic PCs express integrin beta 1. However, further studies are needed to investigate the function of this expression and to determine whether this is a general characteristic of PCs that is independent of the region or a tissue-specific expression.

By direct comparison of intestinal and hepatic PCs, we further observed a different expression pattern of factors that might be involved in the migration and homing. Consistent with the role of CCR9 in the migration of PCs into the intestinal mucosa (Pabst

et al., 2004), our results showed increased CCR9 expression on intestinal PCs compared with other B-cell subsets. In addition, circulating PCs also exhibited increased expression of CCR9, in agreement with the previously mentioned association between circulating PCs and mucosal immune responses (Mei et al., 2009). Interestingly, we were unable to detect this level of expression in hepatic PCs and found CCR9 expression to be significantly lower in hepatic PCs compared with intestinal PCs. In contrast, the previously observed expression of integrin beta 1 appeared to be clearly higher on hepatic PCs than on intestinal PCs. The liver parenchyma consists mainly of hepatocytes, which also express high levels of integrin beta 1 (Speicher et al., 2014). This expression appears to be essential for the interaction of hepatocytes with the extracellular matrix, as this matrix is composed of numerous ligands of integrin beta 1 , such as collagen, fibronectin and laminin (Baiocchini et al., 2016). Reduced or absent expression of integrin beta 1 by knockout in mice was found to lead to severe impairment of liver regeneration in response to injury (Speicher et al., 2014). In addition, Guo et al. recently investigated the recruitment of monocytes to the liver during the progression of NASH and showed that extracellular vesicles loaded with integrin beta 1 were released by hepatocytes as a result of lipotoxic stress to mediate monocyte adhesion. Thus, they suggested that integrin beta 1 might play an important role in monocyte recruitment to the liver during the disease progression (Guo et al., 2019). For these reasons, the higher expression of integrin beta 1 on hepatic PCs might also be indicative for a possible role in the migration and retention of PCs in the liver tissue. Since PCs can accumulate in various liver diseases and promote their progression towards acute-on-chronic liver failure (Y. Zhao et al., 2022), the investigation of the mechanisms involved in PC migration and retention in liver tissues is of significant interest.

Based on the observed differential distribution of B-cell subsets in the blood, intestine and liver as well as the varying expression of individual markers, our phenotypic analysis results indicate that liver resident B-cells represent a tissue-specific population. The expression of different homing factors in PCs supports this assumption and implies that hepatic PCs do not migrate from the intestine to the liver via the systemic circulation in order to re-migrate to the lamina propria, but rather represent a distinct population specific to liver tissue possibly carrying out their own functions.

Regarding PCs and IgA in the gut-liver axis it should be considered that bile is one of the major links between the two organs and also harbors a considerable amount of both monomeric and polymeric IgA. However, the question of the source of this biliary IgA is still not fully understood. Unlike in rats, in which about 90% of biliary IgA is derived from plasma clearance, human hepatocytes do not express pIgR, so only a small proportion of biliary IgA derives from plasma (Brown & Kloppel, 1989). It is suggested that the majority of biliary IgA is produced locally by PCs, which are found within the mucosa of the accessory glands of bile ducts. The immunoglobulins produced are transported into the bile by endocytic vesicular transport through epithelial cells (Nagura et al., 1983). Since the concentration of IgA in the bile of the gallbladder is higher than in hepatic bile, it can be assumed that there is additional secretion of IgA during the storage in the gallbladder (Vuitton, Seilles, Claude, Sava, & Delacroix, 1985). As our results show that the human liver harbors only a small fraction of PCs, the question remains whether this fraction is sufficient for the local production. Further investigation is needed to clarify the source of biliary IgA, focusing on whether more PCs are present in the mucosa of extrahepatic bile ducts or whether there is other, possibly extrahepatic, IgA production.

While studies on human samples can lead to interesting new insights, they also come with some limitations that need to be considered when interpreting the results. First, the number of samples we analyzed was limited due to their accessibility, so a larger sample size should be considered to confirm the observed results. Second, in preparation for flow cytometry analysis, we performed enzymatic digestion of the tissue to generate single cell suspensions. This digestion could destroy individual surface expressed markers that are then no longer properly detected in the analysis (Autengruber, Gereke, Hansen, Hennig, & Bruder, 2012), as it may have been the case for the CD138 and CD80 markers in our study. The liver is a highly perfused organ, so in comparative studies with mouse samples, perfusion of the liver is usually performed prior to preparation in order to avoid contamination with blood cells (Shi et al., 2020). The liver samples we obtained were relatively small pieces located in the periphery of the organ and accordingly did not contain large blood vessels, so we were not able to perform perfusion in this way. Instead, we cut the liver samples into very small pieces and washed them thoroughly with PBS before digestion. Nevertheless, in this case, contamination with PBMCs cannot be completely excluded. Finally, it should be noted

that the analysis was performed on samples taken from diseased individuals. In our study, care was taken to ensure that the liver sections examined were taken from a region unaffected by pathology to represent a healthy condition as possible.

5.2 B-cell clones in the gut-liver axis are restricted to the respective tissue

To further complete the characterization of hepatic and intestinal PCs, we additionally performed BCR sequencing of IgA^+ PCs from both organs of an individual. First, we noted that the largest clonotype in gut and liver accounted for a very high proportion of the total analyzed repertoire (approximately 12 and 17%, respectively). This high percentage has not been demonstrated in previous studies of the BCR repertoire in the human intestine (W. Zhang et al., 2017), although another study examining the clonal distribution of B-cell clones throughout the body also found that the expansion of the largest clone was significantly greater in tissues compared with blood. This could result from the sampling procedure, in which only localized cells of a specific tissue region are analyzed. However, the clonal distribution and expansion in distinct tissues has not yet been well defined and requires more investigation (Meng et al., 2017). Further analysis revealed that IgA^+ PCs from liver and intestine both showed preferential family usage of IGHV-4 and IGHJ-4. This is only partially consistent with previous findings of IgHV-3 being the predominant gene segment of PCs in the human gut (Scheid et al., 2023). Apart from the difference in the most frequently used gene segment, the distribution of the usage of the other genes within the IgHV gene family appears similar, with IgHV-3 and IgHV-4 being the most abundant. For the usage of the IgHJ gene segments, we found the same distribution as previously described in the literature, with a clear dominance of the IgHJ-4 gene (Benckert et al., 2011). The reason for the different predominance in the IGHV family usage is not yet apparent to us and would need further clarification.

We then aimed to address the question of a possible clonal relationship between PCs from the human liver and intestine, based on the suggestion that hepatic PCs originate from the GALT and are able to recognize intestinal antigens (Moro-Sibilot et al., 2016). In our results, using MHI and Circos plots, we found that the hepatic and intestinal PC repertoire was distinct within an individual and had very few common clones, suggesting that the IgA^+ PCs in the liver and small intestine do not originate from the same source.

Thus, our results are in line with the study by Domínguez Conde et al., who performed single cell RNA-sequencing on 16 tissues, including liver, from 12 donors. They found common clones shared between different tissues within the individuals. Regarding PCs these clones were restricted to the liver, spleen or bone marrow and therefore no clonal sharing between the liver and the intestinal organs was observed (Domínguez Conde et al., 2022). Other studies investigating the clonal distribution of B-cells have mainly used DNA from whole tissue as a source for next-generation sequencing, thus including all B-cells without prior sorting for PCs. Therefore, the results of the following studies are only partially comparable to ours. For instance, a study by Meng et al. who performed next-generation sequencing of the heavy chain of BCRs in 8 different tissues from 6 organ donors revealed that regarding the distribution of B-cell clones there appeared to be a relationship between highly perfused organs such as blood, bone marrow, lung and spleen, and between the different sections of the gastrointestinal tract, comprising the jejunum, ileum and colon (Meng et al., 2017). Although their study did not include liver samples, they found that the distribution of B-cell clones was restricted to the intestinal compartment and that there was no clonal sharing with other tissues. However, Chung et al. have shown that diseases related to the gut-liver axis may affect and reverse this restriction of B-cell clones. Using BCR sequencing of whole tissue samples obtained from biopsies, they found that in patients with primary sclerosing cholangitis and inflammatory bowel disease, a substantial proportion of B-cell clones, 8.3% on average, were shared between gut and liver samples. Based on this finding, the authors suggested that disease-specific antigens are shared within the gut-liver axis, and B-cells derived from a common clonal origin are capable of recognizing them in both organs (Chung et al., 2018). Of some concern, however, is that the control samples used in the study were almost absent of B-cells in both organs, making it impossible to compare the results with a healthy control. In comparison with the results described herein, it should also be considered that their definition of a B-cell clonotype was different from ours, which is in agreement with the previous studies mentioned above.

Our analysis of BCR sequencing in human tissue also has some limitations. This includes that only a low number of cells could be sorted and analyzed due to the limited number of PCs in human liver samples. In addition, the proportion of IgA^+ PCs in liver and intestine was not identical among the sorted cells, and since we used only IgA-specific

primer, this resulted in different numbers of sequenced cells in the two organs. However, if we would have used the smallest sample for downsampling, we would have lost too much data for a proper analysis.

Taken together, both flow cytometry analysis, which revealed different phenotypic characteristics of hepatic PCs, and sequencing of the BCR repertoire, which identified a distinct repertoire without clonal sharing, suggest that the human liver harbors a small but tissue-specific PC population. Further studies regarding the migration of PCs into this tissue and their functionality could be of critical interest, as hepatic PCs may be involved in the progression of various liver diseases.

5.3 Phenotypic and repertoire properties of intestinal B-cells remain similar in different stages of NAFLD

As described previously, it is well established that alterations in the gut-liver axis, such as dysbiosis and intestinal barrier impairment, as well as in the hepatic B-cell compartment, may be involved in the development and progression of NAFLD (Boursier et al., 2016; Bruzzì et al., 2018). In this regard, Barrow et al. demonstrated that changes in the microbiota can lead to the accumulation and activation of intrahepatic B-cells, which could result in an aggravation of the disease state. They demonstrated this by performing fecal transplantations from NAFLD patients and healthy subjects to recipient mice. The mice that received fecal transplants from diseased individuals exhibited more pronounced liver inflammation involving hepatic B-cells with increased intracellular expression of TNF-α and IL-6, indicating a proinflammatory function of these cells (Barrow et al., 2021). In addition, it was shown that intestinal inflammation may be present in NAFLD patients in association with dysbiosis. Based on immunohistochemical studies of duodenal mucosa, a decrease in both $CD4^+$ and $CD8^+$ T-cells was observed in diseased patients compared to healthy subjects. This was also associated with increased expression of TNF-α and IL-6 measured by qPCR, which may be related with intestinal inflammation (Jiang et al., 2015). To investigate the relation between the involvement of B-cells described by Barrow et al. and the intestinal inflammation observed by Jiang et al., we extended our phenotypic analyses to intestinal B-cells from NAFLD patients at different stages. In our analysis, however, we did not detect any changes in the

composition of the individual B-cell subsets between patients without NAFLD and patients with NAFLD or between different stages of the progression. The proportions of PCs, MBCs and NBCs remained the same at all disease stages, and the expression of immunoglobulins within these subgroups did not differ. Thereby, we did not detect an increase in IgG^+ PCs that is often observed in intestinal inflammation (Boland et al., 2020).

Using an adoptive transfer model, Hu et al. further showed that T-cells from mesenteric lymph nodes (MLN) of NAFLD donor mice accumulated more frequently in the livers of NAFLD recipient mice than T-cells from other organs such as spleen, bone marrow and thymus. This recruitment was reported to occur through hepatic upregulation of CCL5 and an increased expression of its receptor CCR3 on T- and B-cells, as demonstrated by real-time PCR. In addition, the authors noted an increased expression of CCR9 on MLN T- and B-cells (Hu et al., 2016). A more detailed phenotypic examination of intestinal B-cells in our study did not reveal altered expression of homing factors. However, compared with the above study, our study included human intestinal samples and not mouse samples, and furthermore, our panel did not include the marker of interest CCR3. Therefore, it is difficult to compare the results with our study, but we did not detect altered expression patterns of any marker or the increased expression of CCR9 mentioned above. In contrast to the changes in B-cell properties detected in the peripheral blood of late stage NAFLD patients (Waller et al., 2022), our phenotypic analysis did not reveal altered B-cell properties in the intestine of NAFLD patients. However, it is important to note that we performed only phenotypic analysis and did not examine proinflammatory characteristics or carry out functional analysis. Since Hu et al. found changes in the expression of homing factors on MLN lymphocytes but also no differences in lymphocyte distribution, our analysis is not sufficient to rule out the possible involvement of intestinal B-cells in NAFLD.

In addition, since NAFLD is associated with alterations in the gut microbiota, which in turn may have an effect on the intestinal BCR repertoire (Li et al., 2020), we were interested in whether we would detect changes in the intestinal IgA^+ PC repertoire in patients with NAFLD at different stages. Our sequencing analysis did not reveal major differences in the repertoire at the respective stages. We noted only a tendency toward higher diversity at later stages and a small difference in the usage of IGHV genes, with

preferential usage of IGHV-4 increasing with disease progression. This preferential usage of the IGHV-4 gene has been described previously in the context of Crohn's disease (Bashford-Rogers et al., 2019). However, we did not detect a clonal expansion as described in acute-on-chronic liver failure (Yan et al., 2019) or in other inflammatory conditions in the gut such as Crohn's disease (Bashford-Rogers et al., 2019).

To conclude, our analysis did not reveal major changes in the phenotype or repertoire of intestinal B-cells in patients with NAFLD, but due to the lack of further studies, we cannot exclude their involvement in the development or progression of the disease. However, because human samples generally exhibit very high variability, the small sample size, again due to difficult accessibility, could affect the results. In addition, variability may have been further increased because, although all samples were freshly prepared, further analyses for flow cytometry and repertoire were performed partly on previously frozen samples and partly directly after enzymatic digestion. Finally, the BCR repertoire analysis was performed on a relatively small number of PCs, which should also be taken into account in the interpretation of the data.

5.4 Altered distribution of B-cell subsets and reduced BAFF-R expression in the blood and ascites of cirrhotic patients

The previously described immune dysfunction associated with cirrhosis negatively impacts the disease progression and also affects the B-cell compartment, which could contribute to vaccine hyposensitivity and susceptibility to bacterial infections in patients with cirrhosis (McCashland, Preheim, & Gentry, 2000). Another common complication of the disease is ascites, which mainly results from portal hypertension due to remodeling of the liver parenchyma. Since it is already known that the distribution of circulating B-cell subsets changes during liver cirrhosis (Doi et al., 2012), we were interested in describing these changes in more detail through our in-depth phenotypic analysis. Furthermore, most analyses only examine B-cells in the peripheral blood, so that by including ascites samples we could extend these observations to another anatomical region affected by the disease.

Although B-cells in the mouse peritoneal cavity have been characterized in detail (Wang et al., 2015), these analyses are still missing for their human counterpart. As the peritoneal B-cell compartment in mice is largely composed of innate-like B1-cells, and their existence in humans has not yet been fully clarified (Descatoire et al., 2011), the results observed in mice cannot be directly applied to humans. Romanelli et al. have already analyzed the lymphocyte subsets and cytokines in ascitic fluid, however, this study focused mainly on the distribution of individual T-cell subsets and did not include markers required for the analysis of the B-cell compartment (Romanelli et al., 2020). Our results describing the distribution of B-cells in ascites compared to blood, which appeared to be highly similar except for a slightly smaller subset of NBCs, therefore provide new information about B-cells in the human peritoneal cavity during liver cirrhosis.

As previously described by Doi et al. we also observed that the distribution of B-cell subsets differed between healthy donors and patients with liver cirrhosis. We found a significant decrease in the proportion of MBCs and in particular in that of non-switched MBCs, so that the relative percentage of switched MBCs increased. These observations are therefore consistent with the above study, which also revealed a decrease in MBCs and especially IgM^+ MBCs by flow cytometry, independent of the presence of hepatitis C virus infection or hepatocellular carcinoma in cirrhotic patients (Doi et al., 2012). Thus, our analysis may contribute to previous observations that this alteration occurs not only in the blood of patients but also in the ascitic fluid. In addition, the authors showed in their study that circulating B-cells in cirrhotic patients exhibit lower CD70 expression as well as TNFβ and IgG production after CD40/ TLR9 activation, suggesting a hyporesponsive state of these cells. However, the reason for the decrease of the MBC subset proportion and the hyporesponsive reaction is not yet understood. Doi et al. suggest that the decrease may be caused by an enhanced differentiation of MBCs into PCs. This assumption was based on the observation of hyperimmunoglobulinemia in cirrhotic patients and the finding that $CD27^+$ B-cells showed increased activation-induced cytidine deaminase mRNA expression, which could indicate their differentiation into PCs (Doi et al., 2018). We were not able to detect an increased proportion of PCs in our data, so our results would not support this assumption. In contrast to the above study, the authors further reported that circulating

$CD27^+$ B-cells exhibited increased TLR9 expression and were more reactive to stimulation, resulting in their differentiation into PCs. Given the inconsistent findings of the different studies, the cause of the drastic decline in MBCs is not yet understood, and more research is needed to answer this question.

Of interest, an increase in serum immunoglobulins has been observed in many different chronic liver diseases, such as alcohol-related liver disease (Inamine & Schnabl, 2018), NAFLD (McPherson et al., 2014) or viral hepatitis (Lin, Sun, Mao, & Chen, 2016). In addition, the level of immunoglobulins seems to correlate with the extent of fibrosis and thus with the progression of the disease (McPherson et al., 2014). Various explanations for this increase exist, however, the cause and origin of the antibody production is still unclear. For example, Liu et al. assume that the formation of portacaval shunts in portal hypertension leads to a bypassing of the liver and thus to an increased serum level of antigens and endotoxins derived from the intestine. These would then result in a general activation of PCs with enhanced antibody production (W. T. Liu et al., 2015). In our data, we did not find an increase in PCs or an altered expression pattern in the blood of cirrhotic patients. However, we did not examine secondary lymphoid tissues, which would be needed in order to support this theory. Another source could be the transition of intestinally produced antibodies into the bloodstream in the state of cirrhosis. Howell et al. showed that dimeric IgA in particular increases and that the ratio of dimeric to monomeric IgA shifts in cirrhotic patients. They suggest that this is caused by portal hypertension-induced intestinal leakage with increased translocation of intestinal IgA (Howell et al., 2023). While our observation cannot rule out translocation of produced IgA, our work in patients with NAFLD, which is also associated with increased intestinal permeability, showed no differences in the proportion of B-cell subsets or their expression patterns. However, our group did not enroll patients who had already progressed from NASH into cirrhosis. We identified only a small hepatic PC population in our liver samples. Since an accumulation of PCs in the liver have been demonstrated in conditions such as autoimmune hepatitis (Beer & Dienes, 2021), it would be of great interest to examine liver samples from chronically diseased patients to evaluate a possible hepatic source of antibody production.

Our multiparametric analysis allowed us to further investigate the expression of particular markers along with the distribution of B-cell subsets. We detected decreased

BAFF-R expression on both NBCs and MBCs not only in the blood but also in the ascites of the patients. Interestingly, switched MBCs in particular appeared to express less BAFFR on their surface. The finding of Scholz et al. that switched MBCs do not depend on BAFF signaling for survival compared to non-switched MBCs (Scholz et al., 2008) could explain our observation that mainly non-switched MBCs are affected by the decreased expression, resulting in a lower proportion. The fact that only the non-switched MBCs expressing BAFFR would survive could also explain the marked difference between BAFFR expression on switched and non-switched MBCs. A reduced BAFFR expression on circulating B-cells, which was also associated with a lower frequency of MBCs similar to our results, was previously described in patients with hepatocellular carcinoma (HCC) (Khlaiphuengsin et al., 2020). However, in contrast to cirrhotic patients, the proportion of both non-switched and switched MBCs as well as of PCs were reduced. Since this study examined HCC patients, the results are not directly comparable to ours, but in combination with the observations of Khlaiphuengsin et al., our results indicate that reduced BAFFR expression may be a cause for the changes in the B-cell subset distribution. In both the HCC patients as well as in cirrhotic patients, an increased BAFF concentration could be detected in the blood (Doi et al., 2018; Khlaiphuengsin et al., 2020). Whether this increased BAFF concentration is a cause for the decreased expression of its receptor, for example by induced downregulation, or a consequence of the reduced expression, as a compensatory increase, needs to be clarified in further analyses. Another reason for the observed lower BAFFR expression on B-cells could be, that BAFFR bound to BAFF could no more be captured by the used conjugated antibodies and therefore not detectable by flow cytometry, as described by Smulski et al. (Smulski et al., 2017). Under this assumption, the increased BAFF concentration in the blood of cirrhotic patients would lead to increased binding to its receptor, which would result in the failure to detect the bound BAFFR in the analysis. However, this assumption could not explain the decreased proportion of MBCs in the course of the disease. Further studies are essential to clarify the exact cause of this reduced expression and its impact on the distribution of the B-cell subset.

Including the clinical data of the patients into the analysis, we found no correlation between MBC reduction and clinical laboratory parameters such as creatinine, albumin, CRP, INR, ALT and AST. Also, the cause of liver cirrhosis, for instance, whether it was

induced by alcohol or not, showed no differences in the B-cell subset alterations or BAFFR expression. This is in agreement with the results of Doi et al., who also found that the cirrhosis-related changes in the B-cell subsets were independent of etiology (Doi et al., 2018). However, we further found that a poorer prognosis was associated with an aggravation of the observed changes, with an even greater decrease of the MBC subset and, in addition, an increase of the NBC proportion. This observation is consistent with the study by Doi et al. who also observed a further decline in peripheral $CD27^+$ B-cells in advanced stages of liver cirrhosis (Doi et al., 2018). In contrast, Cardoso et al. found an initial decline in $CD27^+$ MBCs that increased, along with the proportion of PCs in patients with more advanced disease stages (Cardoso et al., 2021). Thus, the observations during disease progression also appear to differ greatly between studies.

Our work therefore provides new insights into B-cell abnormalities in patients with liver cirrhosis and extends previous observations to another anatomic region affected by the disease. It should be noted, however, that our analysis included only 18 patients and 4 healthy controls. Further investigations with a larger sample size are needed to confirm the findings and clarify the reasons for the lower BAFFR expression and the reduced proportion of MBCs.

5.4.1 Outlook for possible future approaches

Another explanation besides the already mentioned hypotheses for this decrease could be the regulatory shedding of the receptor described by Smulski et al.. Their study showed that the BAFF receptor is processed in a regulated manner by the ADAM proteases ADAM 10 and ADAM 17. This processing usually occurs only upon ligand binding and only in cells that co-express TACI. However, they further demonstrated that activation of protein kinase C can also lead to activation of ADAM 17, resulting in processing of the receptor without ligand binding (Smulski et al., 2017). Patients with liver cirrhosis (Doi et al., 2018) as well as patients with NASH (Miyake et al., 2013), a disease also associated with fibrosis, showed an elevation of BAFF levels in their blood. In addition to the conditions already discussed, an increase in serum BAFF concentration is also observed in other diseases, such as the autoimmune induced systemic lupus erythematosus (Salazar-Camarena et al., 2016) and the multisystemic inflammatory

syndrome associated with COVID-19 (Klocperk et al., 2023). Interestingly, in both of these cases, the increased BAFF level also correlates with a lower expression of BAFF-R on B-cells. The exact reasons for the increased BAFF concentrations and the reduced BAFF-R expression are still not understood.

One suggestion might be that the amount of BAFF-producing cells such as monocytes and dendritic cells as well as their BAFF expression may be increased in the context of systemic inflammation, which is for instance associated with liver cirrhosis. This increased amount of circulating BAFF could result in increased binding and thus processing of the BAFFR. Another hypothesis could be that in the context of fibrosis or inflammation, activation of ADAM proteases might lead to increased, less regulatory shedding of the BAFFR, resulting in reduced BAFF signaling with impaired B-cell survival. The increased BAFF levels could thus be interpreted as a compensatory mechanism due to the lower proportion of MBCs.

To investigate these hypotheses, BAFF levels could be measured by ELISA and analyzed in relation to the alterations in the B-cell compartment. Moreover, the mRNA expression of ADAM 10 and ADAM 17 could be examined in B-cells of the diseased patients by PCR analysis. In addition, studies of the soluble BAFFR in the serum of patients could provide information on whether the decreased BAFFR expression is caused by the processing of ADAM proteases. These investigations could provide information about the impairment of the immune response in cirrhotic patients and possibly serve as a basis for future therapeutic approaches.

7 References

Albillos, A., Martin-Mateos, R., Van der Merwe, S., Wiest, R., Jalan, R., & Álvarez-Mon, M. (2022). Cirrhosis-associated immune dysfunction. *Nat Rev Gastroenterol Hepatol, 19*(2), 112-134. doi:10.1038/s41575-021-00520-7

Almeida, J., Polvorosa, M. A., Gonzalez-Quintela, A., Madruga, I., Marcos, M., Pérez-Nieto, M. A., . . . Laso, F. J. (2015). Altered Distribution of Peripheral Blood Maturation-Associated B-Cell Subsets in Chronic Alcoholism. *Alcohol Clin Exp Res, 39*(8), 1476-1484. doi:10.1111/acer.12783

Andreani, V., Ramamoorthy, S., Fässler, R., & Grosschedl, R. (2023). Integrin β1 regulates marginal zone B cell differentiation and PI3K signaling. *J Exp Med, 220*(1). doi:10.1084/jem.20220342

Andy Coenen, A. P. (Producer). https://pair-code.github.io/understanding-umap/.

Arrese, M., Cabrera, D., Kalergis, A. M., & Feldstein, A. E. (2016). Innate Immunity and Inflammation in NAFLD/NASH. *Dig Dis Sci, 61*(5), 1294-1303. doi:10.1007/s10620-016-4049-x

Autengruber, A., Gereke, M., Hansen, G., Hennig, C., & Bruder, D. (2012). Impact of enzymatic tissue disintegration on the level of surface molecule expression and immune cell function. *Eur J Microbiol Immunol (Bp), 2*(2), 112-120. doi:10.1556/EuJMI.2.2012.2.3

Baiocchini, A., Montaldo, C., Conigliaro, A., Grimaldi, A., Correani, V., Mura, F., . . . Mancone, C. (2016). Extracellular Matrix Molecular Remodeling in Human Liver Fibrosis Evolution. *PLoS One, 11*(3), e0151736. doi:10.1371/journal.pone.0151736

Barrow, F., Khan, S., Fredrickson, G., Wang, H., Dietsche, K., Parthiban, P., . . . Revelo, X. S. (2021). Microbiota-Driven Activation of Intrahepatic B Cells Aggravates NASH Through Innate and Adaptive Signaling. *Hepatology, 74*(2), 704-722. doi:10.1002/hep.31755

Bashford-Rogers, R. J. M., Bergamaschi, L., McKinney, E. F., Pombal, D. C., Mescia, F., Lee, J. C., . . . Smith, K. G. C. (2019). Analysis of the B cell receptor repertoire in six immune-mediated diseases. *Nature, 574*(7776), 122-126. doi:10.1038/s41586-019-1595-3

Beer, A., & Dienes, H. P. (2021). Autoimmune hepatitis-is histology conclusive? *Ann Transl Med, 9*(8), 733. doi:10.21037/atm-20-5084

Benckert, J., Schmolka, N., Kreschel, C., Zoller, M. J., Sturm, A., Wiedenmann, B., & Wardemann, H. (2011). The majority of intestinal IgA+ and IgG+ plasmablasts in the human gut are antigen-specific. *J Clin Invest, 121*(5), 1946-1955. doi:10.1172/jci44447

Benet, Z., Jing, Z., & Fooksman, D. R. (2021). Plasma cell dynamics in the bone marrow niche. *Cell Rep, 34*(6), 108733. doi:10.1016/j.celrep.2021.108733

Blanco, E., Pérez-Andrés, M., Arriba-Méndez, S., Contreras-Sanfeliciano, T., Criado, I., Pelak, O., . . . Orfao, A. (2018). Age-associated distribution of normal B-cell and plasma cell subsets in peripheral blood. *J Allergy Clin Immunol, 141*(6), 2208-2219.e2216. doi:10.1016/j.jaci.2018.02.017

Boland, B. S., He, Z., Tsai, M. S., Olvera, J. G., Omilusik, K. D., Duong, H. G., . . . Chang, J. T. (2020). Heterogeneity and clonal relationships of adaptive immune cells in ulcerative colitis revealed by single-cell analyses. *Sci Immunol, 5*(50). doi:10.1126/sciimmunol.abb4432

Boursier, J., Mueller, O., Barret, M., Machado, M., Fizanne, L., Araujo-Perez, F., . . . Diehl, A. M. (2016). The severity of nonalcoholic fatty liver disease is associated with gut dysbiosis and shift in the metabolic function of the gut microbiota. *Hepatology, 63*(3), 764-775. doi:10.1002/hep.28356

Brandtzaeg, P., & Johansen, F. E. (2005). Mucosal B cells: phenotypic characteristics, transcriptional regulation, and homing properties. *Immunol Rev, 206*, 32-63. doi:10.1111/j.0105-2896.2005.00283.x

Brown, W. R., & Kloppel, T. M. (1989). The liver and IgA: immunological, cell biological and clinical implications. *Hepatology, 9*(5), 763-784. doi:10.1002/hep.1840090518

Bruneau, A., Hundertmark, J., Guillot, A., & Tacke, F. (2021). Molecular and Cellular Mediators of the Gut-Liver Axis in the Progression of Liver Diseases. *Front Med (Lausanne), 8*, 725390. doi:10.3389/fmed.2021.725390

Bruzzì, S., Sutti, S., Giudici, G., Burlone, M. E., Ramavath, N. N., Toscani, A., . . . Albano, E. (2018). B2-Lymphocyte responses to oxidative stress-derived antigens contribute to the evolution of nonalcoholic fatty liver disease (NAFLD). *Free Radic Biol Med, 124*, 249-259. doi:10.1016/j.freeradbiomed.2018.06.015

Brynjolfsson, S. F., Persson Berg, L., Olsen Ekerhult, T., Rimkute, I., Wick, M. J., Mårtensson, I. L., & Grimsholm, O. (2018). Long-Lived Plasma Cells in Mice and Men. *Front Immunol, 9*, 2673. doi:10.3389/fimmu.2018.02673

Calis, J. J., & Rosenberg, B. R. (2014). Characterizing immune repertoires by high throughput sequencing: strategies and applications. *Trends Immunol, 35*(12), 581-590. doi:10.1016/j.it.2014.09.004

Caraux, A., Klein, B., Paiva, B., Bret, C., Schmitz, A., Fuhler, G. M., . . . Perez-Andres, M. (2010). Circulating human B and plasma cells. Age-associated changes in counts and detailed characterization of circulating normal CD138- and CD138+ plasma cells. *Haematologica, 95*(6), 1016-1020. doi:10.3324/haematol.2009.018689

Cardoso, C. C., Matiollo, C., Pereira, C. H. J., Fonseca, J. S., Alves, H. E. L., Silva, O. M. D., . . . Santos-Silva, M. C. (2021). B-cell compartment abnormalities are associated with ACLF and mortality in patients with liver cirrhosis. *Clin Res Hepatol Gastroenterol, 45*(4), 101698. doi:10.1016/j.clinre.2021.101698

Chen, K., Magri, G., Grasset, E. K., & Cerutti, A. (2020). Rethinking mucosal antibody responses: IgM, IgG and IgD join IgA. *Nat Rev Immunol, 20*(7), 427-441. doi:10.1038/s41577-019-0261-1

Chung, B. K., Henriksen, E. K. K., Jørgensen, K. K., Karlsen, T. H., Hirschfield, G. M., & Liaskou, E. (2018). Gut and Liver B Cells of Common Clonal Origin in Primary Sclerosing Cholangitis-Inflammatory Bowel Disease. *Hepatol Commun, 2*(8), 956-967. doi:10.1002/hep4.1200

Colonna-Romano, G., Bulati, M., Aquino, A., Pellicanò, M., Vitello, S., Lio, D., . . . Caruso, C. (2009). A double-negative (IgD-CD27-) B cell population is increased in the peripheral blood of elderly people. *Mech Ageing Dev, 130*(10), 681-690. doi:10.1016/j.mad.2009.08.003

Cooper, M. D., & Alder, M. N. (2006). The evolution of adaptive immune systems. *Cell, 124*(4), 815-822. doi:10.1016/j.cell.2006.02.001

Craven, L., Rahman, A., Nair Parvathy, S., Beaton, M., Silverman, J., Qumosani, K., . . . Silverman, M. (2020). Allogenic Fecal Microbiota Transplantation in Patients With Nonalcoholic Fatty Liver Disease Improves Abnormal Small Intestinal Permeability: A Randomized Control Trial. *Am J Gastroenterol, 115*(7), 1055-1065. doi:10.14309/ajg.0000000000000661

De Silva, N. S., & Klein, U. (2015). Dynamics of B cells in germinal centres. *Nat Rev Immunol, 15*(3), 137-148. doi:10.1038/nri3804

Delmonte, O. M., Schuetz, C., & Notarangelo, L. D. (2018). RAG Deficiency: Two Genes, Many Diseases. *J Clin Immunol, 38*(6), 646-655. doi:10.1007/s10875-018-0537-4

den Braanker, H., Bongenaar, M., & Lubberts, E. (2021). How to Prepare Spectral Flow Cytometry Datasets for High Dimensional Data Analysis: A Practical Workflow. *Front Immunol, 12*, 768113. doi:10.3389/fimmu.2021.768113

Descatoire, M., Weill, J. C., Reynaud, C. A., & Weller, S. (2011). A human equivalent of mouse B-1 cells? *J Exp Med, 208*(13), 2563-2564. doi:10.1084/jem.20112232

Di Noia, J. M., & Neuberger, M. S. (2007). Molecular mechanisms of antibody somatic hypermutation. *Annu Rev Biochem, 76*, 1-22. doi:10.1146/annurev.biochem.76.061705.090740

Doi, H., Hayashi, E., Arai, J., Tojo, M., Morikawa, K., Eguchi, J., . . . Yoshida, H. (2018). Enhanced B-cell differentiation driven by advanced cirrhosis resulting in hyperglobulinemia. *J Gastroenterol Hepatol*. doi:10.1111/jgh.14123

Doi, H., Iyer, T. K., Carpenter, E., Li, H., Chang, K. M., Vonderheide, R. H., & Kaplan, D. E. (2012). Dysfunctional B-cell activation in cirrhosis resulting from hepatitis C infection associated with disappearance of CD27-positive B-cell population. *Hepatology, 55*(3), 709-719. doi:10.1002/hep.24689

Domínguez Conde, C., Xu, C., Jarvis, L. B., Rainbow, D. B., Wells, S. B., Gomes, T., . . . Teichmann, S. A. (2022). Cross-tissue immune cell analysis reveals tissue-specific features in humans. *Science, 376*(6594), eabl5197. doi:10.1126/science.abl5197

Fecteau, J. F., Côté, G., & Néron, S. (2006). A new memory CD27-IgG+ B cell population in peripheral blood expressing VH genes with low frequency of somatic mutation. *J Immunol, 177*(6), 3728-3736. doi:10.4049/jimmunol.177.6.3728

Ferguson, S. E., Han, S., Kelsoe, G., & Thompson, C. B. (1996). CD28 is required for germinal center formation. *J Immunol, 156*(12), 4576-4581.

Fianchi, F., Liguori, A., Gasbarrini, A., Grieco, A., & Miele, L. (2021). Nonalcoholic Fatty Liver Disease (NAFLD) as Model of Gut-Liver Axis Interaction: From Pathophysiology to Potential Target of Treatment for Personalized Therapy. *Int J Mol Sci, 22*(12). doi:10.3390/ijms22126485

Friedman, S. L., Neuschwander-Tetri, B. A., Rinella, M., & Sanyal, A. J. (2018). Mechanisms of NAFLD development and therapeutic strategies. *Nat Med, 24*(7), 908-922. doi:10.1038/s41591-018-0104-9

Gardner, D., Jeffery, L. E., & Sansom, D. M. (2014). Understanding the CD28/CTLA-4 (CD152) pathway and its implications for costimulatory blockade. *Am J Transplant, 14*(9), 1985-1991. doi:10.1111/ajt.12834

Georgiou, G., Ippolito, G. C., Beausang, J., Busse, C. E., Wardemann, H., & Quake, S. R. (2014). The promise and challenge of high-throughput sequencing of the antibody repertoire. *Nat Biotechnol, 32*(2), 158-168. doi:10.1038/nbt.2782

Ginès, P., Krag, A., Abraldes, J. G., Solà, E., Fabrellas, N., & Kamath, P. S. (2021). Liver cirrhosis. *Lancet, 398*(10308), 1359-1376. doi:10.1016/s0140-6736(21)01374-x

Glass, D. R., Tsai, A. G., Oliveria, J. P., Hartmann, F. J., Kimmey, S. C., Calderon, A. A., . . . Bendall, S. C. (2020). An Integrated Multi-omic Single-Cell Atlas of Human B Cell Identity. *Immunity, 53*(1), 217-232.e215. doi:10.1016/j.immuni.2020.06.013

Golinski, M. L., Demeules, M., Derambure, C., Riou, G., Maho-Vaillant, M., Boyer, O., . . . Calbo, S. (2020). CD11c(+) B Cells Are Mainly Memory Cells, Precursors of

Antibody Secreting Cells in Healthy Donors. *Front Immunol, 11*, 32. doi:10.3389/fimmu.2020.00032

Gorfu, G., Rivera-Nieves, J., & Ley, K. (2009). Role of beta7 integrins in intestinal lymphocyte homing and retention. *Curr Mol Med, 9*(7), 836-850. doi:10.2174/156652409789105525

Guo, Q., Furuta, K., Lucien, F., Gutierrez Sanchez, L. H., Hirsova, P., Krishnan, A., . . . Ibrahim, S. H. (2019). Integrin β(1)-enriched extracellular vesicles mediate monocyte adhesion and promote liver inflammation in murine NASH. *J Hepatol, 71*(6), 1193-1205. doi:10.1016/j.jhep.2019.07.019

Halliley, J. L., Tipton, C. M., Liesveld, J., Rosenberg, A. F., Darce, J., Gregoretti, I. V., . . . Lee, F. E. (2015). Long-Lived Plasma Cells Are Contained within the CD19(-)CD38(hi)CD138(+) Subset in Human Bone Marrow. *Immunity, 43*(1), 132-145. doi:10.1016/j.immuni.2015.06.016

Hathi, D., Chanswangphuwana, C., Cho, N., Fontana, F., Maji, D., Ritchey, J., . . . Shokeen, M. (2022). Ablation of VLA4 in multiple myeloma cells redirects tumor spread and prolongs survival. *Sci Rep, 12*(1), 30. doi:10.1038/s41598-021-03748-0

Helmink, B. A., & Sleckman, B. P. (2012). The response to and repair of RAG-mediated DNA double-strand breaks. *Annu Rev Immunol, 30*, 175-202. doi:10.1146/annurev-immunol-030409-101320

Hosomi, S., Oshitani, N., Kamata, N., Sogawa, M., Okazaki, H., Tanigawa, T., . . . Arakawa, T. (2011). Increased numbers of immature plasma cells in peripheral blood specifically overexpress chemokine receptor CXCR3 and CXCR4 in patients with ulcerative colitis. *Clin Exp Immunol, 163*(2), 215-224. doi:10.1111/j.1365-2249.2010.04290.x

Howell, J., Van, H., Pham, M. D., Sawhney, R., Li, F., Bhat, P., . . . Anderson, D. (2023). A novel point-of-care test for cirrhosis based on dimeric to monomeric IgA ratio in blood: a pilot cohort study. *Hepatol Commun, 7*(4). doi:10.1097/hc9.0000000000000106

Hu, Y., Zhang, H., Li, J., Cong, X., Chen, Y., He, G., . . . Liu, Y. (2016). Gut-derived lymphocyte recruitment to liver and induce liver injury in non-alcoholic fatty liver disease mouse model. *J Gastroenterol Hepatol, 31*(3), 676-684. doi:10.1111/jgh.13183

Inamine, T., & Schnabl, B. (2018). Immunoglobulin A and liver diseases. *J Gastroenterol, 53*(6), 691-700. doi:10.1007/s00535-017-1400-8

Jiang, W., Wu, N., Wang, X., Chi, Y., Zhang, Y., Qiu, X., . . . Liu, Y. (2015). Dysbiosis gut microbiota associated with inflammation and impaired mucosal immune function in intestine of humans with non-alcoholic fatty liver disease. *Sci Rep, 5*, 8096. doi:10.1038/srep08096

Kaminski, D. A., Wei, C., Qian, Y., Rosenberg, A. F., & Sanz, I. (2012). Advances in human B cell phenotypic profiling. *Front Immunol, 3*, 302. doi:10.3389/fimmu.2012.00302

Khlaiphuengsin, A., Chuaypen, N., Sodsai, P., Buranapraditkun, S., Boonpiyathad, T., Hirankarn, N., & Tangkijvanich, P. (2020). Decreased of BAFF-R expression and B cells maturation in patients with hepatitis B virus-related hepatocellular carcinoma. *World J Gastroenterol, 26*(20), 2645-2656. doi:10.3748/wjg.v26.i20.2645

Kleiner, D. E., Brunt, E. M., Van Natta, M., Behling, C., Contos, M. J., Cummings, O. W., . . . Sanyal, A. J. (2005). Design and validation of a histological scoring system for

nonalcoholic fatty liver disease. *Hepatology, 41*(6), 1313-1321. doi:10.1002/hep.20701

Klocperk, A., Bloomfield, M., Parackova, Z., Aillot, L., Fremuth, J., Sasek, L., . . . Sediva, A. (2023). B cell phenotype and serum levels of interferons, BAFF, and APRIL in multisystem inflammatory syndrome in children associated with COVID-19 (MIS-C). *Mol Cell Pediatr, 10*(1), 15. doi:10.1186/s40348-023-00169-z

Lacotte, S., Brun, S., Muller, S., & Dumortier, H. (2009). CXCR3, inflammation, and autoimmune diseases. *Ann N Y Acad Sci, 1173*, 310-317. doi:10.1111/j.1749-6632.2009.04813.x

Landsverk, O. J., Snir, O., Casado, R. B., Richter, L., Mold, J. E., Réu, P., . . . Jahnsen, F. L. (2017). Antibody-secreting plasma cells persist for decades in human intestine. *J Exp Med, 214*(2), 309-317. doi:10.1084/jem.20161590

LeBien, T. W., & Tedder, T. F. (2008). B lymphocytes: how they develop and function. *Blood, 112*(5), 1570-1580. doi:10.1182/blood-2008-02-078071

Li, H., Limenitakis, J. P., Greiff, V., Yilmaz, B., Schären, O., Urbaniak, C., . . . Macpherson, A. J. (2020). Mucosal or systemic microbiota exposures shape the B cell repertoire. *Nature, 584*(7820), 274-278. doi:10.1038/s41586-020-2564-6

Lin, S., Sun, Q., Mao, W., & Chen, Y. (2016). Serum Immunoglobulin A (IgA) Level Is a Potential Biomarker Indicating Cirrhosis during Chronic Hepatitis B Infection. *Gastroenterol Res Pract, 2016*, 2495073. doi:10.1155/2016/2495073

Lindeman, I., Zhou, C., Eggesbø, L. M., Miao, Z., Polak, J., Lundin, K. E. A., . . . Sollid, L. M. (2021). Longevity, clonal relationship, and transcriptional program of celiac disease-specific plasma cells. *J Exp Med, 218*(2). doi:10.1084/jem.20200852

Liu, M., Silva-Sanchez, A., Randall, T. D., & Meza-Perez, S. (2021). Specialized immune responses in the peritoneal cavity and omentum. *J Leukoc Biol, 109*(4), 717-729. doi:10.1002/jlb.5mir0720-271rr

Liu, W. T., Jing, Y. Y., Han, Z. P., Li, X. N., Liu, Y., Lai, F. B., . . . Wei, L. X. (2015). The injured liver induces hyperimmunoglobulinemia by failing to dispose of antigens and endotoxins in the portal system. *PLoS One, 10*(3), e0122739. doi:10.1371/journal.pone.0122739

Loder, F., Mutschler, B., Ray, R. J., Paige, C. J., Sideras, P., Torres, R., . . . Carsetti, R. (1999). B cell development in the spleen takes place in discrete steps and is determined by the quality of B cell receptor-derived signals. *J Exp Med, 190*(1), 75-89. doi:10.1084/jem.190.1.75

Maecker, H. T., McCoy, J. P., & Nussenblatt, R. (2012). Standardizing immunophenotyping for the Human Immunology Project. *Nat Rev Immunol, 12*(3), 191-200. doi:10.1038/nri3158

Mamedov, I. Z., Britanova, O. V., Zvyagin, I. V., Turchaninova, M. A., Bolotin, D. A., Putintseva, E. V., . . . Chudakov, D. M. (2013). Preparing unbiased T-cell receptor and antibody cDNA libraries for the deep next generation sequencing profiling. *Front Immunol, 4*, 456. doi:10.3389/fimmu.2013.00456

Martín-Mateos, R., & Albillos, A. (2021). The Role of the Gut-Liver Axis in Metabolic Dysfunction-Associated Fatty Liver Disease. *Front Immunol, 12*, 660179. doi:10.3389/fimmu.2021.660179

Martin-Mateos, R., Alvarez-Mon, M., & Albillos, A. (2019). Dysfunctional Immune Response in Acute-on-Chronic Liver Failure: It Takes Two to Tango. *Front Immunol, 10*, 973. doi:10.3389/fimmu.2019.00973

Mattos, A. A., Wiltgen, D., Jotz, R. F., Dornelles, C. M. R., Fernandes, M. V., & Mattos Â, Z. (2020). Spontaneous bacterial peritonitis and extraperitoneal infections in

patients with cirrhosis. *Ann Hepatol, 19*(5), 451-457. doi:10.1016/j.aohep.2020.04.010

McCashland, T. M., Preheim, L. C., & Gentry, M. J. (2000). Pneumococcal vaccine response in cirrhosis and liver transplantation. *J Infect Dis, 181*(2), 757-760. doi:10.1086/315245

McPherson, S., Henderson, E., Burt, A. D., Day, C. P., & Anstee, Q. M. (2014). Serum immunoglobulin levels predict fibrosis in patients with non-alcoholic fatty liver disease. *J Hepatol, 60*(5), 1055-1062. doi:10.1016/j.jhep.2014.01.010

Mei, H. E., Yoshida, T., Sime, W., Hiepe, F., Thiele, K., Manz, R. A., . . . Dörner, T. (2009). Blood-borne human plasma cells in steady state are derived from mucosal immune responses. *Blood, 113*(11), 2461-2469. doi:10.1182/blood-2008-04-153544

Meng, W., Zhang, B., Schwartz, G. W., Rosenfeld, A. M., Ren, D., Thome, J. J. C., . . . Luning Prak, E. T. (2017). An atlas of B-cell clonal distribution in the human body. *Nat Biotechnol, 35*(9), 879-884. doi:10.1038/nbt.3942

Mesin, L., Schiepers, A., Ersching, J., Barbulescu, A., Cavazzoni, C. B., Angelini, A., . . . Victora, G. D. (2020). Restricted Clonality and Limited Germinal Center Reentry Characterize Memory B Cell Reactivation by Boosting. *Cell, 180*(1), 92-106.e111. doi:10.1016/j.cell.2019.11.032

Miele, L., Valenza, V., La Torre, G., Montalto, M., Cammarota, G., Ricci, R., . . . Grieco, A. (2009). Increased intestinal permeability and tight junction alterations in nonalcoholic fatty liver disease. *Hepatology, 49*(6), 1877-1887. doi:10.1002/hep.22848

Miyake, T., Abe, M., Tokumoto, Y., Hirooka, M., Furukawa, S., Kumagi, T., . . . Onji, M. (2013). B cell-activating factor is associated with the histological severity of nonalcoholic fatty liver disease. *Hepatol Int, 7*(2), 539-547. doi:10.1007/s12072-012-9345-8

Mizuochi, T., Ito, M., Saito, K., Kasai, M., Kunimura, T., Morohoshi, T., . . . Yamaguchi, K. (2010). Possible recruitment of peripheral blood CXCR3+ CD27+ CD19+ B cells to the liver of chronic hepatitis C patients. *J Interferon Cytokine Res, 30*(4), 243-252. doi:10.1089/jir.2009.0047

Morbach, H., Eichhorn, E. M., Liese, J. G., & Girschick, H. J. (2010). Reference values for B cell subpopulations from infancy to adulthood. *Clin Exp Immunol, 162*(2), 271-279. doi:10.1111/j.1365-2249.2010.04206.x

Mörbe, U. M., Jørgensen, P. B., Fenton, T. M., von Burg, N., Riis, L. B., Spencer, J., & Agace, W. W. (2021). Human gut-associated lymphoid tissues (GALT); diversity, structure, and function. *Mucosal Immunol, 14*(4), 793-802. doi:10.1038/s41385-021-00389-4

Moro-Sibilot, L., Blanc, P., Taillardet, M., Bardel, E., Couillault, C., Boschetti, G., . . . Dubois, B. (2016). Mouse and Human Liver Contain Immunoglobulin A-Secreting Cells Originating From Peyer's Patches and Directed Against Intestinal Antigens. *Gastroenterology, 151*(2), 311-323. doi:10.1053/j.gastro.2016.04.014

Muller, W. A. (2002). Leukocyte-endothelial cell interactions in the inflammatory response. *Lab Invest, 82*(5), 521-533. doi:10.1038/labinvest.3780446

Nagura, H., Tsutsumi, Y., Hasegawa, H., Watanabe, K., Nakane, P. K., & Brown, W. R. (1983). IgA plasma cells in biliary mucosa: a likely source of locally synthesized IgA in human hepatic bile. *Clin Exp Immunol, 54*(3), 671-680.

Nair, N., Newell, E. W., Vollmers, C., Quake, S. R., Morton, J. M., Davis, M. M., . . . Greenberg, H. B. (2016). High-dimensional immune profiling of total and

rotavirus VP6-specific intestinal and circulating B cells by mass cytometry. *Mucosal Immunol, 9*(1), 68-82. doi:10.1038/mi.2015.36

Noor, M. T., & Manoria, P. (2017). Immune Dysfunction in Cirrhosis. *J Clin Transl Hepatol, 5*(1), 50-58. doi:10.14218/jcth.2016.00056

Nutt, S. L., Hodgkin, P. D., Tarlinton, D. M., & Corcoran, L. M. (2015). The generation of antibody-secreting plasma cells. *Nat Rev Immunol, 15*(3), 160-171. doi:10.1038/nri3795

Okabe, Y. (2024). Development and organization of omental milky spots. *Immunol Rev, 324*(1), 68-77. doi:10.1111/imr.13337

Pabst, O., Hornef, M. W., Schaap, F. G., Cerovic, V., Clavel, T., & Bruns, T. (2023). Gut-liver axis: barriers and functional circuits. *Nat Rev Gastroenterol Hepatol*. doi:10.1038/s41575-023-00771-6

Pabst, O., Ohl, L., Wendland, M., Wurbel, M. A., Kremmer, E., Malissen, B., & Förster, R. (2004). Chemokine receptor CCR9 contributes to the localization of plasma cells to the small intestine. *J Exp Med, 199*(3), 411-416. doi:10.1084/jem.20030996

Parthasarathy, G., Revelo, X., & Malhi, H. (2020). Pathogenesis of Nonalcoholic Steatohepatitis: An Overview. *Hepatol Commun, 4*(4), 478-492. doi:10.1002/hep4.1479

Patel, A. M., Liu, Y. S., Davies, S. P., Brown, R. M., Kelly, D. A., Scheel-Toellner, D., . . . Stamataki, Z. (2021). The Role of B Cells in Adult and Paediatric Liver Injury. *Front Immunol, 12*, 729143. doi:10.3389/fimmu.2021.729143

Pinto, D., Montani, E., Bolli, M., Garavaglia, G., Sallusto, F., Lanzavecchia, A., & Jarrossay, D. (2013). A functional BCR in human IgA and IgM plasma cells. *Blood, 121*(20), 4110-4114. doi:10.1182/blood-2012-09-459289

Polyzos, S. A., Kountouras, J., & Mantzoros, C. S. (2019). Obesity and nonalcoholic fatty liver disease: From pathophysiology to therapeutics. *Metabolism, 92*, 82-97. doi:10.1016/j.metabol.2018.11.014

Robinson, J. P. (2022). Flow cytometry: past and future. *Biotechniques, 72*(4), 159-169. doi:10.2144/btn-2022-0005

Robinson, M. W., Harmon, C., & O'Farrelly, C. (2016). Liver immunology and its role in inflammation and homeostasis. *Cell Mol Immunol, 13*(3), 267-276. doi:10.1038/cmi.2016.3

Romanelli, R. G., Vitiello, G., Gitto, S., Giudizi, M. G., Biagiotti, R., Carraresi, A., . . . Almerigogna, F. (2020). Characterization of lymphocyte subsets in ascitic fluid and peripheral blood of decompensated cirrhotic patients with chronic hepatitis C and alcoholic liver disease: A pivotal study. *Int J Immunopathol Pharmacol, 34*, 2058738420929587. doi:10.1177/2058738420929587

Salazar-Camarena, D. C., Ortiz-Lazareno, P. C., Cruz, A., Oregon-Romero, E., Machado-Contreras, J. R., Muñoz-Valle, J. F., . . . Palafox-Sánchez, C. A. (2016). Association of BAFF, APRIL serum levels, BAFF-R, TACI and BCMA expression on peripheral B-cell subsets with clinical manifestations in systemic lupus erythematosus. *Lupus, 25*(6), 582-592. doi:10.1177/0961203315608254

Sanders, C. K., & Mourant, J. R. (2013). Advantages of full spectrum flow cytometry. *J Biomed Opt, 18*(3), 037004. doi:10.1117/1.Jbo.18.3.037004

Sanz, I., Wei, C., Jenks, S. A., Cashman, K. S., Tipton, C., Woodruff, M. C., . . . Lee, F. E. (2019). Challenges and Opportunities for Consistent Classification of Human B Cell and Plasma Cell Populations. *Front Immunol, 10*, 2458. doi:10.3389/fimmu.2019.02458

Scheid, J. F., Eraslan, B., Hudak, A., Brown, E. M., Sergio, D., Delorey, T. M., . . . Xavier, R. J. (2023). Remodeling of colon plasma cell repertoire within ulcerative colitis patients. *J Exp Med, 220*(4). doi:10.1084/jem.20220538

Scholz, J. L., Crowley, J. E., Tomayko, M. M., Steinel, N., O'Neill, P. J., Quinn, W. J., 3rd, . . . Cancro, M. P. (2008). BLyS inhibition eliminates primary B cells but leaves natural and acquired humoral immunity intact. *Proc Natl Acad Sci U S A, 105*(40), 15517-15522. doi:10.1073/pnas.0807841105

Shalapour, S., Lin, X. J., Bastian, I. N., Brain, J., Burt, A. D., Aksenov, A. A., . . . Karin, M. (2017). Inflammation-induced IgA+ cells dismantle anti-liver cancer immunity. *Nature, 551*(7680), 340-345. doi:10.1038/nature24302

Shi, W., Wang, Y., Zhang, C., Jin, H., Zeng, Z., Wei, L., . . . Sun, G. (2020). Isolation and purification of immune cells from the liver. *Int Immunopharmacol, 85*, 106632. doi:10.1016/j.intimp.2020.106632

Smulski, C. R., & Eibel, H. (2018). BAFF and BAFF-Receptor in B Cell Selection and Survival. *Front Immunol, 9*, 2285. doi:10.3389/fimmu.2018.02285

Smulski, C. R., Kury, P., Seidel, L. M., Staiger, H. S., Edinger, A. K., Willen, L., . . . Eibel, H. (2017). BAFF- and TACI-Dependent Processing of BAFFR by ADAM Proteases Regulates the Survival of B Cells. *Cell Rep, 18*(9), 2189-2202. doi:10.1016/j.celrep.2017.02.005

Speicher, T., Siegenthaler, B., Bogorad, R. L., Ruppert, R., Petzold, T., Padrissa-Altes, S., . . . Werner, S. (2014). Knockdown and knockout of β1-integrin in hepatocytes impairs liver regeneration through inhibition of growth factor signalling. *Nat Commun, 5*, 3862. doi:10.1038/ncomms4862

Spencer, J., & Bemark, M. (2023). Human intestinal B cells in inflammatory diseases. *Nat Rev Gastroenterol Hepatol, 20*(4), 254-265. doi:10.1038/s41575-023-00755-6

Spencer, J., & Sollid, L. M. (2016). The human intestinal B-cell response. *Mucosal Immunol, 9*(5), 1113-1124. doi:10.1038/mi.2016.59

Stebegg, M., Kumar, S. D., Silva-Cayetano, A., Fonseca, V. R., Linterman, M. A., & Graca, L. (2018). Regulation of the Germinal Center Response. *Front Immunol, 9*, 2469. doi:10.3389/fimmu.2018.02469

Suchanek, O., & Clatworthy, M. R. (2023). Homeostatic role of B-1 cells in tissue immunity. *Front Immunol, 14*, 1106294. doi:10.3389/fimmu.2023.1106294

Tilg, H., Adolph, T. E., & Trauner, M. (2022). Gut-liver axis: Pathophysiological concepts and clinical implications. *Cell Metab, 34*(11), 1700-1718. doi:10.1016/j.cmet.2022.09.017

Tripathi, A., Debelius, J., Brenner, D. A., Karin, M., Loomba, R., Schnabl, B., & Knight, R. (2018). The gut-liver axis and the intersection with the microbiome. *Nat Rev Gastroenterol Hepatol, 15*(7), 397-411. doi:10.1038/s41575-018-0011-z

Tsochatzis, E. A., Bosch, J., & Burroughs, A. K. (2014). Liver cirrhosis. *Lancet, 383*(9930), 1749-1761. doi:10.1016/s0140-6736(14)60121-5

Turchaninova, M. A., Davydov, A., Britanova, O. V., Shugay, M., Bikos, V., Egorov, E. S., . . . Chudakov, D. M. (2016). High-quality full-length immunoglobulin profiling with unique molecular barcoding. *Nat Protoc, 11*(9), 1599-1616. doi:10.1038/nprot.2016.093

van Best, N., Rolle-Kampczyk, U., Schaap, F. G., Basic, M., Olde Damink, S. W. M., Bleich, A., . . . Hornef, M. W. (2020). Bile acids drive the newborn's gut microbiota maturation. *Nat Commun, 11*(1), 3692. doi:10.1038/s41467-020-17183-8

Vrieze, A., Van Nood, E., Holleman, F., Salojärvi, J., Kootte, R. S., Bartelsman, J. F., . . . Nieuwdorp, M. (2012). Transfer of intestinal microbiota from lean donors increases insulin sensitivity in individuals with metabolic syndrome. *Gastroenterology, 143*(4), 913-916.e917. doi:10.1053/j.gastro.2012.06.031

Vuitton, D. A., Seilles, E., Claude, P., Sava, P., & Delacroix, D. L. (1985). Gall bladder: the predominant source of bile IgA in man? *Clin Exp Immunol, 62*(1), 185-192.

Waller, K. J., Saihi, H., Li, W., Brindley, J. H., De Jong, A., Syn, W. K., . . . Alazawi, W. (2022). Single-cell phenotypes of peripheral blood immune cells in early and late stages of non-alcoholic fatty liver disease. *Clin Mol Hepatol*. doi:10.3350/cmh.2022.0205

Wang, H., Lin, J. X., Li, P., Skinner, J., Leonard, W. J., & Morse, H. C., 3rd. (2015). New insights into heterogeneity of peritoneal B-1a cells. *Ann N Y Acad Sci, 1362*(1), 68-76. doi:10.1111/nyas.12791

Weisel, N. M., Weisel, F. J., Farber, D. L., Borghesi, L. A., Shen, Y., Ma, W., . . . Shlomchik, M. J. (2020). Comprehensive analyses of B-cell compartments across the human body reveal novel subsets and a gut-resident memory phenotype. *Blood, 136*(24), 2774-2785. doi:10.1182/blood.2019002782

Wu, Z., Xu, J., Tan, J., Song, Y., Liu, L., Zhang, F., . . . Liu, Y. (2019). Mesenteric adipose tissue B lymphocytes promote local and hepatic inflammation in non-alcoholic fatty liver disease mice. *J Cell Mol Med, 23*(5), 3375-3385. doi:10.1111/jcmm.14232

Yan, Q., Wang, L., Lai, L., Liu, S., Chen, H., Zhang, J., . . . Sui, W. (2019). Next generation sequencing reveals novel alterations in B-cell heavy chain receptor repertoires associated with acute-on-chronic liver failure. *Int J Mol Med, 43*(1), 243-255. doi:10.3892/ijmm.2018.3946

Zhang, F., Jiang, W. W., Li, X., Qiu, X. Y., Wu, Z., Chi, Y. J., . . . Liu, Y. L. (2016). Role of intrahepatic B cells in non-alcoholic fatty liver disease by secreting pro-inflammatory cytokines and regulating intrahepatic T cells. *J Dig Dis, 17*(7), 464-474. doi:10.1111/1751-2980.12362

Zhang, W., Feng, Q., Wang, C., Zeng, X., Du, Y., Lin, L., . . . Liu, X. (2017). Characterization of the B Cell Receptor Repertoire in the Intestinal Mucosa and of Tumor-Infiltrating Lymphocytes in Colorectal Adenoma and Carcinoma. *J Immunol, 198*(9), 3719-3728. doi:10.4049/jimmunol.1602039

Zhao, J., Zhang, S., Liu, Y., He, X., Qu, M., Xu, G., . . . Zhang, Z. (2020). Single-cell RNA sequencing reveals the heterogeneity of liver-resident immune cells in human. *Cell Discov, 6*, 22. doi:10.1038/s41421-020-0157-z

Zhao, Y., He, W., Wang, C., Cui, N., Yang, C., You, Z., . . . Chen, X. (2022). Characterization of intrahepatic B cells in acute-on-chronic liver failure. *Front Immunol, 13*, 1041176. doi:10.3389/fimmu.2022.1041176

Zhou, W. C., Zhang, Q. B., & Qiao, L. (2014). Pathogenesis of liver cirrhosis. *World J Gastroenterol, 20*(23), 7312-7324. doi:10.3748/wjg.v20.i23.7312

Zhou, Y., Zhang, Y., Han, J., Yang, M., Zhu, J., & Jin, T. (2020). Transitional B cells involved in autoimmunity and their impact on neuroimmunological diseases. *J Transl Med, 18*(1), 131. doi:10.1186/s12967-020-02289-w

8 Appendix

8.1 List of Abbreviations

%	Percent
°C	Degree Celsius
7AAD	7-Aminoactinomycin D
ADAM	A disintegrin and metalloproteinase
AID	Activation-induced cytidine deaminase
ALT	Alanine Aminotransferase
ANOVA	Analysis of variance
APC	Antigen-presenting cell
APRIL	A proliferation-inducing ligand
AST	Aspartate Aminotransferase
BAFF	B-cell activating factor
BAFFR	B-cell activating factor receptor
BCMA	B-cell maturation factor
BCR	B-cell receptor
C	Constant gene
CCL	CC-type motif chemokine ligand
CCR	CC-type motif chemokine receptor
CD	Cluster of differentiation
cDNA	Complementary DNA
CDR	Complementarity-determining region
CRP	C-reactive protein
CTLA-4	Cytotoxic T-lymphocyte-associated protein 4
CXCR	CXC-type motif chemokine receptor
DAMPs	Damage-associated molecular pattern
DAPI	4´,6-diamidino-2-phenylindole
DNA	Deoxyribonucleic acid
DTH	Death
EDTA	Ethylenediaminetetraacetic acid
ELISA	Enzyme-linked Immunosorbent Assay
ELISpot	Enzyme Linked Immuno Spot Assay
FACS	Fluorescence activated cell sorting
FCS	Foetal calf serum

FlowSOM	Flow Cytometry Self-Organizing Map
FXR	Farnesoid X receptor
g	Gram
GALT	Gut-associated lymphoid tissue
GC	Germinal center
H&E	Hematoxylin and eosin
HBSS	Hanks balanced salt solution
HCC	Hepatocellular carcinoma
HLA-DR	Human Leukocyte Antigen - DR-Isotype
h-SNE	Hierarchical stochastic neighbor embedding
Ig	Immunoglobulin
IGH	Immunoglobulin heavy chain
IL	Interleukin
INR	International Normalized Ratio
IZKF	Interdisziplinäres Zentrum für Klinische Forschung
LTX	Liver transplant
M	Molar
MAdCAM-1	Mucosal Addressin Cell Adhesion Molecule-1
MBC	Memory B-cell
MELD	Model for End-Stage Liver Disease
MFI	Median fluorescence intensity
MHC II	Major histocompatibility complex class II
MHI	Morosita Horn Index
MIGEC	Molecular identifier guided correction
min	Minutes
Ml	Millilitre
MLN	Mesenteric lymph node
mm	Millimeter
mRNA	messenger RNA
NAFLD	Non-alcoholic fatty liver disease
NAS	NAFLD activity score
NASH	Non-alcoholic steatohepaitis
NBC	Naive B-cell
ns	Not significant
PAMPs	Pathogen-associated molecular patterns
PBMCs	Peripheral blood mononuclear cells

PBS	Phosphate buffered saline
PC	Plasma cell
PCR	Polymerase chain reaction
PIGR	Polymeric immunoglobulin receptor
RAG	Recombination activation gene
RBC	Red blood cell
RNA	Ribonucleic acid
rpm	Revolutions per minute
SCFA	Short-chain fatty acid
SD	Standard deviation
sec	Second
Seq	Sequencing
SNC	Switched-non conventional
SPADE	Spanning-tree Progression Analysis of Density-normalized Events
TACI	Transmembrane activator calcium modulator and cyclophilin ligand interactor
TCR	T-cell receptor
Th-cell	T-helper cell
TLR	Toll-like receptor
TNF- α	Tumor necrosis factor alpha
t-SNE	T-distributed stochastic neighbor embedding
UMAP	Uniform manifold approximation and projection
UMI	Unique molecular identifier
VCAM-1	Vascular cell adhesion molecule 1
VDJ	Variable- (V-), diversity- (D-) and joining- (J-) DNA segment
VLA-4	Very late antigen-4
µ	Micro

8.2 List of Figures

8.3 List of Tables

9 Danksagung

Zum Abschluss dieser Arbeit möchte ich mich bei allen bedanken, die mich während meiner Promotionszeit begleitet und unterstützt haben.

Mein besonderer Dank gilt meinem Doktorvater, Prof. Dr. rer. nat. Oliver Pabst, für die stets unterstützende Betreuung und die Offenheit, mit der er mir, als Laboranfängerin, begegnet ist. Durch seine stetige Bereitschaft, meine Fragen zu beantworten und mich bei theoretischen, aber auch praktischen Herausforderungen zu unterstützen, habe ich in dieser Zeit unglaublich viel lernen können. Besonders schätze ich seine Geduld, mir selbst die komplexesten Zusammenhänge verständlich zu machen, und die Möglichkeit, unter seiner Anleitung tief in die experimentelle Forschung einzutauchen.

Mein Dank gilt auch dem gesamten Team des Instituts, das mir von Anfang an das Gefühl gegeben hat, willkommen zu sein. Aufgrund der wertschätzenden und familiären Atmosphäre bin ich immer sehr gerne ins Labor gekommen und das hat meine Arbeit stark bereichert. Ein besonderer Dank geht an Christina Petrick, Nathalie Steinke und Silke Vaßen, die mir geduldig die Grundlagen der Laborarbeit vermittelt, mich bei der Probengewinnung unterstützt und mir schließlich ihr Vertrauen im Umgang mit deren sensiblen und behüteten Geräten geschenkt haben. Ebenso danke ich Dr. Ana Izcue für ihre wissenschaftliche Expertise, die die Basis dieses Projekts gelegt hat, sowie für ihre Erklärungen bei der Analyse von FACS-Daten. Zudem wäre ohne die wertvolle Erfahrung und Unterstützung von Dr. Lydia Kopplin bei der Sequenzierung, sowie der bioinformatischen Expertise von Fabio Ticconi dieser Teil des Projekts nicht möglich gewesen. Darüber hinaus möchte ich denjenigen danken, die außerhalb des Instituts zu diesem Projekt beigetragen haben. Prof. Dr. Neumann danke ich für die Möglichkeit der Probengewinnung, und Prof. Bruns sowie Dr. Oluwatomi Ibidapo-ob dafür, dass sie uns großzügig Proben zur Verfügung gestellt haben, die die Ausweitung des Projekts ermöglichten.

Ein herzliches Dankeschön gilt schließlich meiner Familie, meinen Freunden und meinem Freund. Sie haben sich als die besten Zuhörer erwiesen, mich stets unterstützt und mir bei jedem Schritt der letzten Jahre liebevoll zur Seite gestanden.

10 Erklärung zur Datenaufbewahrung

Erklärung § 5 Abs. 1 zur Datenaufbewahrung

Hiermit erkläre ich, dass die dieser Dissertation zu Grunde liegenden Originaldaten im Institut für Molekulare Medizin des Universitätsklinikums Aachen hinterlegt sind.

11 Erklärung über den Eigenanteil

Eidesstattliche Erklärung gemäß § 5 Abs. (1) und § 11 Abs. (3) 12. der Promotionsordnung

Hiermit erkläre ich, Monika Schütz an Eides statt, dass ich folgende in der von mir selbstständig erstellten Dissertation „B-cell phenotypes and BCR clonality in the human gut-liver axis: a tissue-specific analysis“ dargestellten Ergebnisse erhoben habe. Bei der Durchführung der Arbeit hatte ich folgende Hilfestellungen, die in der Danksagung angegeben sind.

	Monika Schütz	Prof. Dr. Oliver Pabst	Dr. Ana Izcue	Dr. Lydia Kopplin	Fabio Ticconi	Nathalie Steincke/ Silke Vaßen/ Christina Petrick	Prof. Dr. Tony Bruns	Dr. Oluwatomi Ibidapo-ob	Prof. Dr. Ulf Peter Neu-mann	Summe (%)
Studien-überwachung		80	10				10			100
Studiendesign		60	30				10			100
Probengewinnung (Blut, Darm, Leber, Aszites)	20					20		20	40	100
Zellisolierung (Blut, Darm, Leber, Aszites)	60					20		20		100
Durchführung der Experimente zur Phänotypisierung	100									100
Datenauswertung Phänotypisierung	100									100
Durchführung der Experimente zur Sequenzierung	20			80						100
Datenauswertung Sequenzierung	30				70					100
Bereitstellung von Materialien		100								100
Interpretation der Datenauswertung	60	30	10							100